Numerical Modelling of Bladder Filling and Prostate Positioning in Modern Radiotherapy

Jarema Krywonos

Ph.D. Thesis   2011

Numerical Modelling of Bladder Filling and Prostate Positioning in Modern Radiotherapy

Jarema Krywonos

A thesis submitted in partial fulfilment of the requirement of the Liverpool John Moores University for the degree of Doctor of Philosophy

Engineering, Technology and Maritime Operations, Liverpool John Moores University

February 2011

THE FOLLOWING HAVE NOT BEEN COPIED ON INSTRUCTION FROM THE UNIVERSITY

Acknowledgments

Jarema Krywonos

ABSTRACT

The human bladder is an important organ within the pelvic system of the human body. It routinely collects urine excreted by the kidneys prior to disposal via urination causing significant variation in the shape and volume of the bladder. The mechanics of the filling process directly affects the function of the bladder and its interaction with the surrounding organs, in particular the position of the prostate that can influence the diagnosis and planning of radiotherapy treatments of prostate cancer. The success of prostate radiotherapy depends on the delivery of high doses of radiation to a defined tissue volume with a high degree of positional accuracy. A detailed study is required to establish the volume and shape change of the bladder during the course of the radiotherapy treatment, over a long period of time, and to develop an effective modelling tool to simulate this complex mechanical process to provide guidance to diagnosis and treatment planning.

In this work, systematic data of the bladder dimension are presented based on measurement of Computed Tomography (CT) images of a group of 10 patients with prostate cancer, over the course of radiotherapy treatment. A method of measuring the bladder wall distance in the anterior–posterior (AP), superior–inferior (SI) and left–right (LR) directions is implemented. Systematic data obtained from scanned images taken on the transaxial, sagittal and coronal planes are analysed and compared to assess the potential influence of the scanning sequence on the shape and size of the bladder. The variation of the bladder dimensions, volume and shape were analysed between different arms for the same subject and the upper limit of bladder volume variation were determined. The relationship between some key dimensional parameters (such as wall distance and aspect ratio) with the volume change is established. Key systematic results of prostatic displacement are determined, and inter subject difference of prostate positional change is analysed. The process of bladder filling and potential inter and intra subject difference and their influence on the diagnosis and planning process are discussed.

A systematic numerical modelling method based on MR images has been developed to simulate the mechanics of bladder filling and its effects on the position of the prostate. A new approach for constructing detailed three dimensional (3D) Finite Element (FE) models that were specific to each patient were developed using multiple magnetic resonance (MR) images taken in three different planes (transaxial, sagittal, and coronal). Detailed sensitivity studies have been performed in comparing the 2-D and 3-D model, mesh size, materials models and parameters. The overall model of bladder deformation was compared with repeated images of the filled bladder that were obtained using computed tomography (CT) to validate the FE models. FE bladder deformation was found to be comparable to repeated CT images of the same patient, thus validating the FE models and the approach used in this work. The relationship between bladder deformation and its volume change has been established. The numerical results showed that the bladder dimensions increased linearly with its volume and the predicted coefficients is comparable to some published clinical results. The movement of the prostate in the anterior–posterior (AP), superior–inferior (SI), left–right (LR) directions, as well as its rotational movement, that is associated with changes in bladder volume was predicted. The numerical results showed that the movement of the prostate in the AP and SI directions (3-4mm and 1..5-4mm) was much greater than that in the LR direction (0.5-1mm). The scale of the movement of the prostate with the increase in bladder volume varied considerably among subjects. The numerical predictions were compared with published clinical data and the significance of the results in medical application is discussed. The work showed that subject specific Finite Element modelling could potentially provide crucial guidance for the medical practice on the treatment planning process of the prostate cancer.

Contents

List of Figures

Chapter 3

Chapter 4

CHAPTER ONE

INTRODUCTION

.

1.1 Introduction

The pelvic region is an important area within the human body. It comprises of several soft organs enclosed in a complex bony structure. The pubic symphysis maintains the structural integrity of the pelvis and provides a protective boundary for the internal organs (Gamble *et al*, 1986). The pelvic region provides the human body with several important functions such as reproduction and digestion. The major internal pelvic organs include the bladder, prostate, rectum and the seminal vesicles. These organs have different shapes and material structures that perform different functions. The bladder is a hollow muscular organ forming the main urinary reservoir. The prostate gland is a cone-shaped gland about the size of a chestnut (Boubaker *et al*, 2009) and is made up of connective tissue and smooth muscle. It lies immediately below the urinary bladder, surrounding the upper part of the urethra. The rectum is the continuation of the sigmoid colon. At the point of their junction; the rectum becomes covered by peritoneum only on its anterior surface, and therefore becomes retroperitoneal. The pelvic area plays many important roles ranging from sexual functions, gait support and the secretion of waste products (e.g. urine and faeces). Many of these functions are directly linked to the mechanical behaviours of the organs. One particular feature is the volume change and position change of the organs. An improved understanding of these processes can make a contribution to many a various field such as biomechanics and cancer treatment etc, which would fundamentally increase a patients quality of life. One important research area is the change of shape of the bladder and its interaction with the surrounding organs.

The urinary bladder routinely collects urine excreted by the kidneys prior to disposal by urination (Korkmaz *et al*, 2007). The detrusor muscle of the urinary bladder wall is made of smooth muscle fibres arranged in spiral, longitudinal, and circular bundles. When the bladder is stretched to a certain extent, signals are sent out to the parasympathetic nervous system to contract the detrusor muscle (Laforet *et al*, 2010). This encourages the bladder to expel urine through the urethra reducing the volume of the bladder; Variation in bladder shape/size directly influences many physiological and medical conditions of the bladder. The variation of the bladder can have

urological affects that can influence sensations such as fullness, incontinence and compactness etc. Compactness is used to describe a cross section of a bladder becoming more circular during filling (Kristiansen *et at,* 2004). Within the pelvis the bladder can be susceptible to cancer, which can sometimes lead to surgery. The variation of the bladder volume also directly affects the surrounding organs. For example, during the diagnosis and treatment of bowel cancer, bladder filling can have a significant effect on the position of the bowel, making the treatment more difficult to perform. Another major problem influenced by bladder filling is the diagnosis and treatment of prostate cancer. The prostate is positioned between the bladder and the rectum, the change of bladder volume directly causes positional change of the prostate (Melian *et al,* 1997). This will cause difficulty in identifying the location of the prostate, which is a challenging task to the planning of the radiotherapy process.

After lung cancer, prostate cancer is the most common cause of cancer death in UK for men. According to statistics published by the Cancer Research UK (2006), each year on average around 10,200 men in the UK die from prostate cancer. Cancer develops when cells in a part of the body begin to grow out of control (Liang *et al,* 1992). Cancer treatment is designed to kill and/or suppress the growth of cancer cells. Many methods have been developed over the past decades (to be detailed in Chapter 2). Typically, the choice of cancer treatment is influenced by many factors for example the specific characteristics of cancer; overall condition of the patients and whether the goal of treatment is to cure the cancer, to keep the cancer from spreading, or to relieve the symptoms caused by cancer. The risk factors for prostate cancer include advancing age, inherited factors, hormonal influences, and such environmental factors as toxins, chemicals, and industrial products (Gronberg *et al,* 2003).

Radiation therapy, which uses high-energy rays to damage or kill cancer cells by preventing them from growing and dividing, is currently the most common method of treatment for prostate cancer. In this process, a beam of radiation is attenuated as it passes through a patient, and energy is deposited at each location along the path of the beam (Shepard *et al,* 1999). High doses of radiation can kill cells or prevent them

from growing and dividing. Radiotherapy has been used to treat a wide range of cancer such as head, breast, etc. (Ragaz *et al,* 1997; Fu *et al,* 2000). It is a local treatment used to eliminate or eradicate visible tumours that affects cancerous cells only in the treated area. One of the greatest challenges of radiation therapy is to minimise damage to normal cells by the delivery of an adequate dose aimed and timed accurately to destroy tumour cells and spare their normal counterparts (Moran *et al,* 2005; Sikora *et al,* 2009). This has to be achieved through a complex pre-treatment imaging and planning process. It is particularly challenging during prostate cancer treatment due to factors such as patient setup, change of prostate size, volume change of the adjacent organs. In particular, the positional change of the prostate due to the bladder filling is causing a major issue to the current clinical practice.

Treatment of prostate cancer involves visits to Oncology centres, where the patients will go through medical examinations with a trained oncologist. CT images of the patients are taken; a treatment plan is followed with dose calculations created. The overall aim during radiotherapy is to cover the full target area (e.g. Prostate), to achieve this, a margin is created which could potential destroy healthy tissue. Currently, hospitals use some empirically developed protocols to eliminate changing variables (bladder/rectum filling) that can reduce the accuracy of treatment. One typical procedure involves regulated fluid intake to reduce the amount of prostate movement during radiotherapy. However, even with these protocols, there is still unquantifiable bladder volume variation which makes the treatment planning stage difficult. This requires systematic research to establish the bladder volume change during this process, and to develop an effective method to establish the relationships between the volume and dimensions of the bladder, this would be achieved through detailed analysis of the subject specific measurement, and simulate the filling process of bladder filling and its interaction with other tissues.

1.2 Aims and Objectives

This work aims to establish the variation of the bladder volume/shape during the prostate radiotherapy treatment process and develop detailed subject specific Finite Element (FE) models to simulate the bladder filling process and its effect on the prostate position.

Main objectives are:

- To systematically measure the bladder volume variation during the course of prostate radiotherapy and correlate the volume variation of the bladder to its key dimensional characteristics and prostate movement based on subject specific data;
- To develop detailed 3-D models of the human pelvic system based on subject specific medical images at different planes and FE models with realistic structure and materials properties;
- To simulate the deformation of the bladder based on subject specific models and establish changes in the shape and size of the bladder;
- To investigate the biomechanical responses of prostate during bladder filling and correlate the numerical results with clinical observations and key clinical procedures.

The bladder filling is a complex process and its mechanical behaviour could be strongly subjected specific. Detailed analysis based on multiple patients' data is essential to establish the general trend of bladder deformation during a course of radiotherapy treatments over a long period of time. The developments of subject specific models with detailed three dimensional geometry and material properties are very important for using the Finite Element method to accurately simulate the bladder filling process. The FE analysis would establish some important biomechanical data such as the volume – pressure relationships as well as aspect ratio data, which are difficult to be experimentally measured *in vivo*. These data are vital to improve the understanding of the mechanics of the bladder and establish the trend of prostate movement due to bladder filling. The simulation results will be correlated to clinical

observed data and used to improve the scientific understanding of several problems in the current clinical practices.

1.3 Outline of the thesis

In chapter two, background information on cancers and treatment, structure and functions of the pelvic system and application of Finite Element methods are reviewed. The overview consists of different types of cancers and the mechanism of different treatment processes with emphasis on the radiotherapy process. A summary of current understandings of the mechanics of the organs within the pelvic area are presented, and its potential influence on the physiological and medical conditions of the subject are critically discussed. The effect of the bladder filling process on the planning of radiotherapy treatment for prostate cancer is presented and the areas to be improved are highlighted. The basic theories of linear and nonlinear mechanics and principles of Finite Element methods are reviewed. The application of the FE modelling approach in medical and biomechanics are reviewed with the potential use for improving the understanding of the mechanics of the bladder filling process and its interaction with the surrounding organs is discussed. Technological development for improved radiotherapy accuracy is discussed, as well as the potential use of Finite Element techniques in this important field and the main technical challenges.

In chapter three, systematic data of the bladder dimensions are presented. These are based on the measurement of Computed Tomography (CT) images of a group of 10 patients with prostate cancer over the course of radiotherapy treatment. The inter and intra patient analysis of the pelvic area is performed. A method of measuring bladder wall distance is implemented, and systematic data obtained from the transaxial, sagittal and coronal planes are analysed showing the reproducibility of organ dimensions. The variation of the bladder volume and dimension were analysed between different arms for the same subject and the upper limit of bladder volume variation were determined. A technique is devised for measuring prostate movement by using the apex of the pubic bone as a point of origin and centre of prostate. Key systematic results of prostatic displacement are recorded, using the measurement technique implemented, and inter subject analysis of prostate displacement during a bladder volume variation change is then analysed/established. Several aspects have been discussed based on the experimental data and published works and importance of development of FE modelling is highlighted.

In chapter four, the methodology of developing and creation of the Finite Element model based on magnetic resonance imaging (MRI) images is presented with the key analysing results. High resolution MRI was performed in the transaxial, coronal, and sagittal planes to provide comprehensive structural details of the bladder and surrounding systems. Detailed Finite Element (FE) models that were specific to each participant were developed by rendering the images, and the process of bladder filling was simulated. The effect of mesh size, boundary conditions and material properties was systematically studied to develop a valid FE model with sufficient accuracy and computational efficiency. The overall model of bladder deformation was compared with repeated images of the filled bladder that were obtained using computed tomography (CT) to validate the FE models. The relationship between the changes in the key dimensions of the bladder and the increase in bladder volume during the filling process was also investigated. The numerical results showed that the bladder dimensions increased linearly, its volume during the filling process volume and the predicted coefficients is comparable to some published clinical results.

The bladder pressure volume relationship is established for all three subjects, with a maximum of 100% bladder volume change, which is within the normal criteria for subject protocol. Deformations of the bladder at the three principal directions (AP, SI and LR) are compared with volume change during filling, as is the bladder aspect ratio effect upon prostatic displacement. The final part of the chapter concentrates on the effect of the biomechanical changes of the bladder with respect to prostate displacement. The relationship between bladder volume increase and prostate movement is evaluated and compared to published research. Main issues discussed includes the interpretation of the data in comparison with published data, the key procedures and limitation of the work, materials sensitivity, the mechanics of the bladder filling process and its effect on the prostate positions. The effect of bladder filling on some clinical practice such as the patient preparation protocols, imaging procedures and maximum margin was discussed. The potential use of subject specific FE in prostate cancer treatment planning is also highlighted.

In Chapter 5, overall conclusions are given and future works are highlighted.

CHAPTER TWO

LITERATURE REVIEW

2.1 Cancer and cancer treatment

2.1.1 Introduction to Cancer

Cancer develops when cells in a part of the body begin to grow out of control. There are many kinds of cancer occurring throughout different organs/tissues with over 60 different organs in the body where a cancer can develop (Cancer Research UK, 2009), all cancers start due to out-of-control growth of abnormal cells (Liang *et al*, 1992). Normal body cells grow, divide, and die in an orderly fashion. During the early years of a person's life, normal cells divide more rapidly until the person becomes an adult, then cells in most parts of the body divide only to replace worn-out or dying cells and to repair injuries (Alberts *et al*, 2004). The cancerous cells are different from normal cells, instead of dying, cancer cells continue to grow and divide forming new abnormal cells and outliving normal cells. The exact reason why a cell becomes cancerous is still subjected to further research. A wide range of evidence indicates that the genesis of a cancer typically requires that several independent, rare accidents occur in the lineage of one cell, which then replicates as a cell and multiplies out of control (Alberts *et al*, 2002). If left untreated, cancer can cause severe illness and death (Beyer *et al*, 2001; Bharatha *et al*, 2001; Hing *et al*, 2006). Cancer forms as a tumour, with few exceptions such as leukaemia, in which case the cancer cells do not form tumours, instead, these cancer cells are situated in the blood and blood-forming organs, that circulate through other tissues where the cells begin to grow and replace normal tissue (Hardman *et al*, 2003).

According to the report by Cancer Research UK (2009), there are around 200 different types of cancer. Some are very common, while others are extremely rare. Cancers of the lung, breast, bowel and prostate account for over half of all new cases, whereas some types of blood cancer make up less than 1 in 100 new cases. **Figure 2.1** is a summary of the various types of cancer (e.g. bladder, breast, kidney, leukemia, lung, skin and prostate cancer) and the annual figures of new cases and mortality rates are based on the 2006 data published by the Cancer Research UK. Prostate cancer forms in tissues of the prostate and is most common in older men (Crawford, 2003). As shown in **Figure 2.1**, Prostate cancer has an increasing amount of new cases and more

significantly, the death rate is very high. In addition, cancer of the prostate seriously affects the day to day life of the patients. As the tumour grows, it may press on and 'irritate' the urethra, or cause a partial blockage to the flow of urine. Symptoms may then develop causing one or more of the following conditions: poor stream, hesitancy, toilet frequency increase, urgency and poor bladder emptying (Beyer *et al,* 2001). If the cancer spreads to other parts of the body, various other symptoms can develop. The most common site for the cancer to spread to is to one or more bones, especially the pelvis, lower spine and hips (Nielsen *et al,* 1991; Saad *et al,* 2006). Affected bones can become painful and tender and surgery may be required. As the prostate is positioned within a complex system (to be detailed in section 2.2) and its position is influenced by the volume change of some surrounding organ (e.g. the bladder), it is a challenging task to select a suitable treatment approach and develop effective protocols to minimise the damage to the surrounding living tissues.

Figure 2.1 Summary of different types of cancer (a) and the mortality figures (b) (Cancer research UK, 2006).

12

2.1.2 Overview of cancer treatment processes

Cancer treatment is designed to kill and/or suppress the growth of cancer cells. Many methods have been developed over the past few decades. Typically, the choice of cancer treatment is influenced by many factors, such as the specific characteristics of cancer; overall condition of the patients and whether the goal of treatment is to cure the cancer, suppress the cancer from spreading, or to relieve the symptoms caused by cancer. The main cancer treatment methods and the key technological requirement was summarised in **Figure 2.2**. Detailed mechanisms, procedures and the suitability of the method for different cancer types were briefly discussed below:

Surgery

Surgery is used to diagnose cancer, determine its stage, and to treat cancer. In addition to the removal of the primary tumour, surgery is often necessary for staging, e.g. determining the extent of the disease and whether it has metastasized to regional lymph nodes. A single cancer cell is invisible to the naked eye but can re-grow into a new tumour, a process called recurrence (Beyer *et al* 2001; Dehnad *et al*, 2003; Al-Azab *et al*, 2007). One common type of surgery that may be used to help with diagnosing cancer is a biopsy. A biopsy involves taking a tissue sample from the suspected cancer for examination by a specialist in a laboratory (Watanabe *et al*, 1997). If cancer cells are present in the biopsy it is termed as a "positive biopsy". If cancer cells are not present in the biopsy it is termed as a "negative biopsy" (Fink *et al*, 2003). When surgery is used for treatment, the cancer and some tissue adjacent to the cancer are removed. Examples of surgical procedures for cancer include mastectomy for breast cancer and prostatectomy for prostate cancer (Applewhite *et al*, 2001; Beyer *et al*, 2001; Lehman *et al*, 2007). The goal of the surgery can be either the removal of only the tumour, or the entire organ. Successful surgery requires the understanding of the structure of the organ concerned and its surrounding systems. In many cases, image guided technology and some mechanical modelling techniques, (such as Finite Element modelling), are increasingly being used (Paulsen *et al*, 1999; Pathmanathan *et al*, 2004).

Chemotherapy

Chemotherapy refers to any treatment involving the use of drugs to kill cancer cells. The process may consist of single drugs or combinations of drugs, and can be administered through a vein, injected into a body cavity, or delivered orally in the form of a pill (Alagna, 2001). Chemotherapy is considered to be a systemic treatment, which makes it different from surgery or radiation therapy, in that the cancer-fighting drugs circulate in the blood to parts of the body where the cancer may have spread, and can kill or eliminate cancers cells at sites that are of great distances from the original cancer. For patients who have cancers that respond well to chemotherapy, this approach helps treat the cancer effectively, enabling the patients to enjoy full productive lives. Furthermore, many side effects once associated with chemotherapy are now controlled, allowing many people to work, travel, and participate in normal activities while receiving chemotherapy (Carelle *et al*, 2002).

Hormonal Therapy

Hormone therapy, similar to chemotherapy, is a systemic treatment in that it may affect cancer cells throughout the body. Hormones are naturally occurring substances in the body that stimulate the growth of hormone sensitive tissues, such as the breast or prostate gland (Grimm *et al*, 2003). When cancer arises in breast or prostate tissue, its growth and spread is thought to be caused by the body's own hormones. Drugs that block hormone production, or alter the way hormones work and/or removal of organs that secrete hormones, such as the ovaries or testicles, could be an effective way of fighting cancer (Horwitz *et al*, 2000). Hormonal therapy may be given to the patients in addition to surgery or radiotherapy - this is known as adjuvant therapy. The aim of this combined treatment is to reduce the chance of the cancer coming back. Hormone therapy is widely used for treating prostate cancer. In order to grow, prostate cancer depends on the hormone testosterone, which is produced within the testicles (Horwitz *et al*, 2000). Hormonal therapy of prostate cancer can be administered as injection or tablet form. Injection of drugs (termed pituitary down-regulators) can 'switch off' the production of male hormones from the testicles by reducing the levels of a hormone produced by the pituitary gland (Hellerstedt *et al*, 2002). Other hormonal therapy drugs (e.g. anti-androgens) work by attaching to proteins on the surface of the cancer

cells, which blocks the testosterone from going into the cancer cells. Hormonal Therapy is less painful approach; however, it may cause many side effects such as loss of sexual desire, hot flushes, sweating, increase of body weight, etc. (Kumar *et al,* 2005).

Radiation therapy

Radiotherapy refers to the use of radiation as a means for treating disease. As shown in **Figure 2.3 (a)**, a beam of radiation is attenuated as it passes through a patient, and energy is deposited at each location along the path of the beam (Gerber and Chan, 2008). High doses of radiation can kill cells or prevent the cells from growing and dividing. A large body of evidence supports double-stranded breaks of nuclear DNA as the most important cellular effect of radiation, which leads to irreversible loss of the reproductive integrity of the cell and eventual cell death. This process could happen to both cancer cells and normal cells, but the cancer cells are more sensitive to ionizing radiation than normal cells and the repair mechanism of cancer cells is less efficient than that of normal cells **(Figure 2.3 (b))**. Thus, normal cells are more likely to recover fully from the effects of radiation. Due to the involvement of the cancer cells and the living tissues, the goal of all radiation therapies is to irradiate tumours with a mortal dose while limiting the radiation received by the normal tissue that surrounds the tumour. This requires an effective planning process so that the radiation damage is concentrated within the cancerous region (Gerber and Chan, 2008).

Radiotherapy has been used to treat a wide range of cancer such as head, breast, prostate cancers, etc. (Ragaz *et al,* 1997; Fu *et al,* 2000). Similar to surgery, radiation therapy is a local treatment that affects cancerous cells only in the treated area used to eliminate or eradicate visible tumours. Radiation therapy may be externally or internally delivered. External radiation delivers high-energy rays directly to the tumour site from a machine outside the body. Internal radiation, or brachytherapy, involves the implantation of a small amount of radioactive material in or near the cancer (Theodorescu, 2004). Treatment-related damage to healthy cells leads to complications of treatment, or side effects. These side effects may be severe, reducing a patient's quality of life, compromising their ability to receive their full prescribed treatment, and sometimes, limiting their chance for an optimal outcome from

treatment. Therefore, the treatment process has to be properly planned to limit the radiation received by the normal tissue that surrounds the tumour. This is particularly important for cancer cells within complex structure/systems such as the prostate, which is positioned within the pelvic area, details of which, and the main challenges during prostate cancer treatment, that are associated with the nature of the pelvis structures are to be presented in the next section.

Figure 2.2 Technology used for different types of cancer treatment (Paulsen *et al*, 1999; Alagna, 2001; Hellerstedt *et al*, 2002; Pathmanathan *et al*, 2004).

17

Figure 2.3 Schematic to show the radiation process (Gerber and Chan, 2008) (a) and different reaction of cancerous and healthy cells on the dose intensity (b) (Seiwert *et al*, 2007).

18

2.2 Structure and function of the human pelvis system

The pelvis is the bony structure located at the base of the spine (anatomically known as the caudal end). It forms the lower limb (or hind-limb) girdle of the skeleton. The pelvis incorporates the socket portion of the hip joint for each leg or hind leg (in quadrupeds) (Cilingir *et al*, 2007). The pelvic cavity is a body cavity that is bounded by the bones of the pelvis that primarily contains reproductive organs, the urinary bladder, and the rectum (Miralbell *et al*, 1998; Lee *et al*, 2008; Misra *et al*, 2009) as shown in **Figure 2.4**. The main structures that the project will be focusing on are the bladder, prostate and the rectum. The interaction between these three organs has fundamental importance to the position of the prostate and the prostate cancer treatment planning process. The structures and functions of the organs and their influence on the radiotherapy prostate cancer treatment process are briefly described below:

Bladder
The bladder is a hollow, muscular balloon shaped organ that lies in the pelvis and is a distensible (or elastic) organ (Korkmaz and Rogg, 2007). The urinary bladder collects urine excreted by the kidneys prior to disposal by urination (Korkmaz and Rogg, 2007). The detrusor muscle of the urinary bladder wall is made of smooth muscle fibres arranged in spiral, longitudinal, and circular bundles. When the bladder is stretched, signals are sent to the parasympathetic nervous system to contract the detrusor muscle and expel urine through the urethra (Laforet *et al*, 2010). The change of shape and volume of the bladder associated with the filling and voiding directly affects the position of the prostate causing difficulty when identifying the location of the prostate (Melian *et al*, 1997). Mechanical behaviour of the bladder during filling or voiding is also associated with other bladder disease such as incontinence, bladder cancer, etc. (Lotz *et al*, 2005).

Prostate

The prostate gland is a cone-shaped gland about the size of a chestnut and is made up of connective tissue and smooth muscle (Boubaker *et al,* 2009). It lies immediately below the urinary bladder, surrounding the upper part of the urethra. The prostate also contains some smooth muscles that helps expel semen during ejaculation. The main function of the prostate gland is to secrete a milky, alkaline fluid (one of the components of semen) into the urethra at the point of ejaculation. Although the prostate appears to be one whole structure it is in fact separate by "zones" or "lobes" including the Peripheral zone (PZ) , Central zone (CZ) and Transition zone (TZ) (Applewhite *et al,* 2001). These zones are all made up of materials of different properties (Kemper *et al,* 2004). The prostate is susceptible to many diseases that can affect people lives. Apart from prostate cancer, other main conditions include prostate enlargement, prostatitis (inflammation of the prostate gland) (Melian *et al,* 1997; Constantinou *et al,* 2002; Pinkawa *et al,* 2007). Prostate enlargement is a common condition that is associated with ageing. When the prostate becomes enlarged, it can place pressure on the bladder and urethra. This can cause symptoms that affect urination which includes difficulties starting urination, a frequent need to urinate, and having difficulty to empty the bladder completely. Prostatitis is a general term used to refer to inflammation or infection of the prostate gland. Symptoms of prostatitis include pelvic pain, pain when urinating and pain when ejaculating semen. A detailed understanding of the pelvis organs interaction action would help with the diagnosis and treatment of these medical conditions as well as helping the radiotherapy treatment process of prostate cancer.

Rectum

The rectum is the continuation of the sigmoid colon and, at the point of their junction; the rectum becomes covered by peritoneum only on its anterior surface, and therefore becomes retroperitoneal. The rectum terminates approximately at the attachment of the levator ani to its borders. The function of the rectum is to store the stool until it is socially convenient to eliminate it. The rectum, therefore, needs to have a capacity (volume), and compliance (easily distendable). The inside of the rectum is thrown into folds called rectal valves. These maintain the faecal material until water is removed and a bowel movement occurs. At that point the rectum elongates and the valves become less prominent. The volume of rectum regularly change and this may cause positional change of the prostate. The rectum varies from 10-15 cm in length, while the circumference varies from 15 cm at the rectosigmoid junction, to 35 cm or more at its widest ampullary portion. There are various illnesses that affect the rectum. For example, Diverticular Disease, Irritable Bowel/Crohn's/Colitis, Polyps, Rectal Prolapse and cancer (O' Connell *et al*, 1994; Stollman and Raskin, 2004). Cancer of the rectum, a common form of cancer, is a disease in which cancerous (malignant) cells are found in the tissues of the rectum.

The pelvic organs play many important roles ranging from sexual functions, gait support and the secretion of waste products (e.g. urine and faeces). As detailed in the section above, each soft organ exhibited different structures and properties, and there are complex interactions between the bladder, prostate and the rectum. An improved understanding of the mechanics of the pelvic system can make a direct contribution to the research and technological development in various fields such as biomechanics and cancer treatment etc. All of these would fundamentally increase a patient's quality of life. One particular area is the mechanics of bladder associated with water intake (this is a process most difficult to control) and its interaction with the prostate gland during the course of radiotherapy treatment of prostate cancer, which is the main focus of this work.

Figure 2.4 (a) Sagittal MR images (this work); (b) a diagram of a sagittal section showing the relative position between the bladder, prostate and the rectum (Reprinted from Netter Anatomy Illustration Collection, 2006, © Elsevier Inc. All Rights Reserved).

2.3 Radiotherapy planning and treatment process

Three of the most common treatment methods for prostate cancer are chemotherapy (Chi *et al*, 2001), prostate surgery (Al-Azab *et al*, 2007) and, the most common treatment method, radiotherapy (Langen *et al*, 2003; Ling *et al*, 2006). One of the major challenges during radiation therapy is to minimise damage to normal cells, by the delivery of an adequate dose aimed, and timed, accurately to destroy tumour cells and spare the surrounding normal counterparts (Muren *et al*, 2003; Sikora *et al*, 2009). This has to be achieved through a complex pre-treatment imaging and planning process. **Figure 2.5** shows the main procedure in a treatment planning process. In general, the process can be divided into six stages including patient preparation, CT scanning, tumour localisation, skin reference markers, treatment planning, and treatment. The initial patient preparation **(a)** is used to control the bladder/rectum volume by asking the patient drink a certain amount of the water or evacuating their rectum. The CT imaging process **(b)** is used to scan the affected cancerous area, and gives an indication of the severity of tumour growth. All of the stages are important to increase the accuracy of radiation target convergence. **Figure 2.5 (c)** shows a typical transaxial slice of the prostate bladder and rectum. The yellow, red and blue outlining indicates the bladder, prostate and the rectum. As soon as the initial CT imaging and outlining have been completed the reference points for radiation are marked on the skin as shown in **Figure 2.5 (d)**. These markers are an indication to the oncologist of the initial origin points and are used as a reference point gauging prostatic movement (Stroom *et al*, 1999). The next stage is to create a radiation field using a planning system. The planning system used at Clatterbridge Centre of Oncology is Phillips Pinnicle Version 6.2. This is used to administer the delivery dose to the geometrical region for each specific patient. The main outcome is to achieve even radiation dose distribution throughout the prostate, whilst minimizing exposure to the surrounding tissues. A three dimensional virtual simulation is run using the software program to give an indication of target convergence, as well as approximating healthy tissue/organ radiation. The last step is the administration of the radiotherapy to the patient on a conformal radiotherapy machine. A linear accelerator (LINAC) delivers the radiotherapy. The LINAC has a device called a multileaf collimator that moves around the patient and shapes the beams of radiotherapy to fit the specific tumour

shape. External radiotherapy is normally given as a series of short, daily treatments in a radiotherapy department.

The current standard for treatment of prostate cancer is Intensity-modulated radiation therapy (IMRT), which is an advanced form of three-dimensional conformal radiotherapy (3DCRT) (Zelefsky *et al,* 2002). IMRT uses up to date computer technology to produce complex, sculpted dose distributions which increase the dose to the tumour and decrease the dose to surrounding healthy organs. **Figure 2.6** illustrates an example of the benefits of IMRT in prostate cancer treatment. Here the critical neighbouring structure is the rectum, which actually lies just behind the prostate. IMRT treatment planning is distinct from 3D-CRT in that it can generate dose distributions that protect critical healthy tissues adjacent to the target region. In comparison, 3D-CRT is limited to handling the geometrical arrangement where the critical structure is near the target without creating a concavity in its surface (Galvin *et al,* 2006). In these works, treatment is carefully planned by using 3-D computed tomography (CT) images of the patient in conjunction with computerised dose calculations to determine the dose intensity pattern that will best conform to the tumour shape. To deliver accurate radiotherapy it is imperative to ensure that the patient's position, and so the location of the tumour and surrounding tissues, is the same each time (Sikora *et al*, 2009).

(a) Protocol of fluid intake and stool release.	
(b) CT imaging of the Pelvic area.	
(c) Tumour localisation: outlining the key structures (Bladder, Prostate and the Rectum).	
(d) Skin Reference Marker: Markers being placed on the bony prominences for consistent future scanning alignment.	
(e) Treatment Planning & Visualisation: Calculation of the dose plan based on the contoured images.	
(f) Radiotherapy treatment is administered on a linear accelerator.	

Figure 2.5 The main procedures of the planning process of a radiotherapy prostate cancer treatment. (Adapted based on CCO protocol and images taken from (http://www.impactscan.org).

Figure 2.6 Schematic to show the use of IMRT/IGRT to increase the accuracy of the targeting area and reduce side effects (Sikora *et al*, 2009).

2.4 Factors affecting the prostate during treatment planning

Despite the technology development in terms of imaging, there are still many factors affecting both the planning and treatment process such as patient setup, drinking protocol, natural volume change of the bladder and the rectum. During the radiation process, Balter *et al* (1995) recognised that proper patient setup remains an important element of the radiotherapy process; unrecognised positioning errors are a clear point of target coverage failure for conformal radiotherapy and excessive margins are used to ensure target coverage, however this can increase the risk for normal tissues damage. In the case of prostate cancer, the target volume (i.e. prostate) is irregularly shaped and in close proximity to critical structures that must be protected throughout the course of radiation (Galvin *et al,* 2006). This makes it a challenging task for planning the dose distribution during prostate treatment.

In clinical practice, protocol set has to be followed to ensure that the treatment planning during prostate radiation is successful. Factors such as patient position are kept the same through a special couch. Initial preparation follows institution protocol. For example, at Clatterbridge Center of Oncology (CCO), the patient is required to take pre-scanning drinking of 500ml of fluid and empty their rectum through an enema, which is a liquid that is introduced into the rectum to encourage the passing of motions. The treatment plan is then created using dose distribution software (e.g. Phillips, Pinnicle 6.2). The process of the treatment plan can be repeated until there is satisfactory dose coverage of the tumour; once the setup is verified treatment is fixed to the specified location or region of interest (ROI) (Balter *et al,* 1995). Despite the development of strict treatment protocols, there are still several factors, the effects of which are difficult to quantify/control. Typically failure will occur due to internal motion caused by bladder filling (O'Doherty *et al,* 2006), rectal filling (Madsen *et al,* 2003), Intra-fraction organ motion (Jiang, 2006), as well fat concentration levels increase and decrease through the course of treatment. All these variables can alter the position of the ROI, resulting in the change of the position of the intended irradiated area. Currently, whilst treating prostate cancer, there is no way to accurately define the tumour position without constantly scanning the patient or using gold seeds.

Constant scanning of the patient is regarded as un-economical and there is also a worry that constant scanning is exposing the patient's healthy tissue to too much radiation (Brenner and Elliston, 2004). Recently, fiducial markers (Gold Seeds) are emerging as a potential tool for image-guided radiotherapy (IGRT) (Enmark *et al*, 2006). The markers are implantable devices designed to act as reliable surrogates for imaging anatomic structures of interest. Fiducial marker techniques were originally developed in the preconformal radiotherapy era for positional verification of tissues that were not easily visualized using portal X-ray film imaging for patient alignment. The gold seeds are actual gold, which are not radioactive. The markers can help radiologists to locate and treat the often hard-to-target prostate. Using X-ray imaging, doctors can easily monitor the location of the seeds. The movement represents the positional change of the prostate, and the radiation area can be altered accordingly. The prostate is known to move around in the pelvic cavity, depending on how much liquid a patient has consumed and other factors, it can be challenging to locate the prostate precisely during radiation therapy, gold seeds simply allow the prostate's location to be tracked on a daily basis using X-ray imaging to ensure treatment accuracy.

Many recent clinical researches showed that gold seed markers could improve the control of some anatomical positioning coordinates (Dehnad *et al*, 2003); however it is difficult to determine the movement of the markers from its original center of origin and to track this gold seed, thus accurate irradiating the target area is a more challenging task. The positioning reliability with the gold seeds requires further improvement. It has been reported that gold seeds may become unstable and move from the implanted position (Poggi *et al*, 2003). As well as the problem with the potential positional instability of the gold seeds, the use of gold seeds may also affect the quality of the images. When the patient has a CT scan, the images may become fragmented due to the effect of the gold seeds. A thorough approach is required to quantify the movement of the gold seeds. One potential solution for this is to make corrections based on the comparison between the daily 3D images and the reference 3D volumetric data which were obtained from the planning CT images. If that could be accomplished based on tumour in real time or near real time, both systematic and

random errors would be corrected on a daily basis (Ling *et al,* 2006). This could be a possibility by combining advanced CT imagery and the use of a Finite Element software to simulate future displacements, thus increasing treatment accuracy. The FE modelling approach has been successfully used in several medical engineering areas, which potentially could be used during radiotherapy treatment. One key technical challenge for this area is the improved understanding of the mechanism of some key biological processes, in particular the bladder filling process, which requires a systematic approach to cover the detailed structures and realistic materials properties and boundary conditions of the system.

2.5 FE modelling technique and its applications in medical engineering

2.5.1 Introduction to the theory and the principles of Finite Element analysis

Finite Element methods are now widely used to solve structural, fluid, and multiphysics problems numerically (Fagan, 1992). **Figure 2.7** is a breakdown of the finite element method. The methods are used extensively by engineers and scientists who can mathematically model and numerically solve very complex problems. The analyses in engineering are performed to assess designs. The analyses in the various scientific fields are carried out largely to obtain insight into (and ideally) predicting natural phenomena. The Finite Element approach involves dividing the continuum into Finite Elements which are small enough for the stress or displacement fields (or other physical parameters) to be approximated with displacements that are continuous and are in equilibrium, thus satisfying the problem's boundary conditions. The approximation comes about when transforming the differential equation approach to an algebraic problem, wherein the building blocks or Finite Elements have all the complex equations solved for a simple shape. Once this is completed the problem is transformed to a linear algebraic relation and not a differential equation and can easily be solved with computers. There are many different commercial packages available such as the ABAQUS, ANSYS etc.
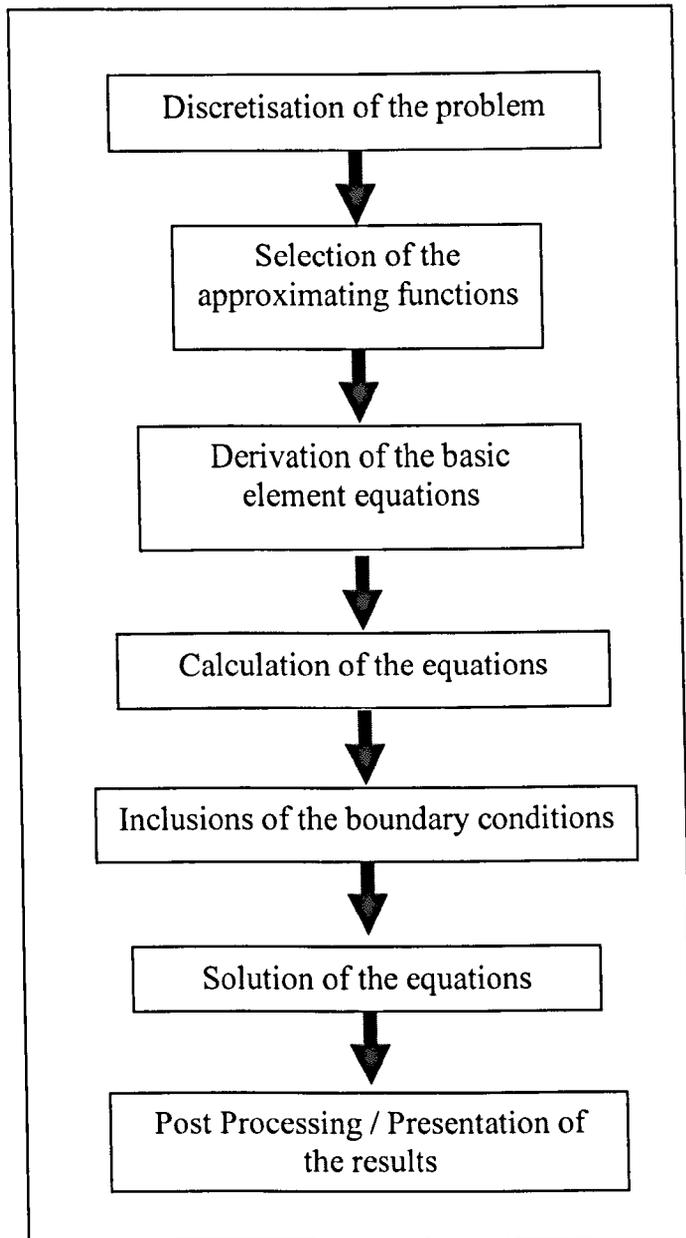
Figure 2.7 The main steps in a Finite Element modelling process.

Structural analysis is based on the discretization method, by which, the mathematical model is discretised in space, i.e., converted to a discrete model of finite number of elements, taking into consideration degrees of freedom, loading, boundary conditions and different material properties.

The displacement is denoted as U. Corresponding forces due to displacements are F. The general relationship between force and displacement is;

$$F = K \bullet U \qquad\qquad (2.5.1)$$

Where F is the force, U is the displacement, and K is the "stiffness" matrix coefficient. The matrix K is called the stiffness matrix. It is the matrix which defines the geometric and material properties of the structure. Stiffness matrices are a fundamental part of FEA. These matrices define inherent properties of the system being studied. Energy derivations are commonly used to form the stiffness for a variety of element types. The elements have restrictions on their behaviour, the result is always a stiffness matrix that can then be treated like any other stiffness matrix and can be rotated and transformed. When combining the elements, the same considerations about boundary conditions and matching degree of freedoms (DOFs) at the nodes must be accounted for. Additional considerations are also generated since the shape function assumption can affect the accuracy of the results. The most common elements are the membrane (planar), plate, shell and solid elements. Each element has a given set of nodes and displacements associated with those nodes. There are many types of elements suitable for different materials or systems. Shell/membrane elements are most widely used to simulating thin sheet structures in engineering or biological materials (Firat, 2007; Elkut et al, 2010). The membrane element is a two dimensional flat extensional element known as triangular and rectangular elements. The membrane element has no rotational stiffness or stiffness normal to the plane of the element. It can be situated arbitrarily in space but the resultant forces must lie in the plane of the element. The flat plate element is a two dimensional element that acts like a flat plate. There are two out of plane rotations and the normal displacement as DOF. These elements model plate-bending behaviour in two dimensions. The solid element is a three dimensional extensional element and has three translations at each nodal DOF. The eight-node element has some linear variation of stress throughout the element. The solid element has no rotational stiffness. Elements found vary from the 4-node tetrahedron to the 27-node brick element. The most common version is the eight-node brick element; also Tetrahedrons

(tet) and hexahedrons (hex) are popular for use in mesh generation and adaptive mesh refinement.

The order of interpolation refers to the degree of the complete polynomial appearing in the element shape functions. Every element has a size "h" and an order "p". h employs elements of variable size, p influences the polynormal degree. There are three basic approaches to FEA: the "h", "p", and the "h-p" methods. In the h method, the element order, p is kept constant, but the mesh is refined by making the size h smaller. The p method, the element size h is kept constant and the element order p is increased. In the h-p method, the h is made smaller as the p is increased to create higher order elements. Either reducing the element size or increasing the element order reduces the error in the FEA approximations, but increases the demand on the computational resource.

Finite Element analysis obtains stresses or other desired unknown parameters in the Finite Element model by minimizing energy functional. Energy functional consists of all the energies associated with the particular Finite Element model. Based on the law of conservation of energy, the Finite Element energy functional must equal zero. The minimum of the functional is found by setting the derivative of the functional with respect to the unknown grid point potential for zero. The basic equation for Finite Element analysis is:

$$\frac{\partial F}{\partial \rho} = 0 \qquad\qquad (2.5.2)$$

Where F is the energy functional and ρ is the unknown grid point displacement to be calculated. This is based on the principle of virtual work, which states that if a particle is under equilibrium, under a set of a system of forces, then for any displacement, the virtual work is zero. Each Finite Element will have its own unique energy functional. In the Finite Element displacement method, the displacement is assumed to have unknown values only at the nodal points, so that the variation within the element is described in terms of the nodal values by means of interpolation functions. Thus,

33

within any one element, $D = N.U$ where N is the matrix of interpolation functions termed shape functions and U is the vector of unknown nodal displacements. (U is equivalent to p in the basic equation for Finite Element analysis.) The strains within the element can be expressed in terms of the element nodal displacements as;

$$\varepsilon \;=\; B \bullet U \tag{2.5.3}$$

Where B is the strain displacement matrix. Finally, the stresses may be related to the strains by use of an elasticity matrix (e.g., Young's modulus) as;

$$\sigma \;=\; E\varepsilon \tag{2.5.4}$$

The most basic approach to post-processing can all be done within the FE package. The types of output data in ABAQUS are field output, history output, data file output and results file output. This includes plotting contours, rotating the object, creating an XY plot using selected data, animating the results, and even performing selected basic calculations using the output data for optimisation.

2.5.2 Application of FEA in biomechanics and medical engineering

During the last two decades, Finite Element based modelling has been extensively used to model biological systems. This in turn has lead to its application in many biomechanical and biomedical fields such as image guided surgery, diagnosis, tissue recovery (Papademetris *et al,* 1999; Carter *et al,* 2005; Hamidian *et al,* 2010).

FE modelling has been used in modelling during surgery of different systems, a typical example of which is the study and surgery upon the human brain (Carter *et al,* 2005). For image guided surgery soft tissue deformation jeopardises the accuracy of image-guided surgery based upon preoperative images, thus restricting its applicability to surgery on or near bony structures. A detailed biomechanical model incorporating the deformation of soft tissues could greatly increase the accuracy of image-guided surgery. **Figure 2.8** shows a typical method to use FE modelling in image guided surgery (Carter *et al*, 2005). It involves first scanning the patients using CT imagery, and then using Finite Element software to aid a surgeon during image guided surgery. The Finite Element model developed based on the preoperative images was utilised as a biomechanical tool to predict tissue displacements, based on boundary conditions determined in the intraoperative measurements, and improvement of the surgical accuracy was achieved by compensating for the non-rigid deformation. **Figure 2.9 (a)** shows a typical method of using FE modelling in real-time deformable modelling for surgery simulation when organs change volume resulting in large deformations (Meier *et al,* 2005). The works involved simulating the deformation of a gall bladder with a spring-mass model from a wire frame view of un-deformed gall bladder and then using Finite Element software to aid a surgeon during image guided surgery.

Figure 2.8 Use of FE modelling in image guided surgery (Carter *et al*, 2005).

Figure 2.9 Typical application of Finite Element modelling simulating the bladder displacement with the use of needle insertion into prostate (Meier *et al*, 2005).

Figure 2.10 Typical application of Finite Element modelling in the simulation of tissue reconstruction (Keeve *et al* 1996).

As well as predicting organ deformation, the Finite Element technique has been used to simulate large tissue movement, such as the human skin (Keeve *et al*, 1996; Tsap *et al*, 2000). A study by Keeve *et al* (1996) showed an anatomy-based 3D Finite Element tissue model could effectively predict tissue changes according to the realignment of the underlying bone structure. In the work, the adapted model was based on CT volume data, laser scans, and a generic facial mesh is used to map general anatomical structures to the individual patient data, from which a 3D Finite Element model is created (as shown in **Figure 2.10**). The 3D Finite Element model was successfully integrated into the computer-aided surgical planning system and used for a few case studies.

Finite Element modelling was also extensively used in studying the biomechanics of human movement and internal tissue deformations. The method has become an important part in diagnosing and/or simulating sports specific injuries and evaluating the effects of plantar fascia stiffness on the biomechanical responses of the ankle–foot complex using the Finite Element method (Cheung *et al*, 2004; Gu *et al*, 2010). Recently, Gu *et al* (2010) developed a detailed three dimensional (3D) Finite Element (FE) foot model to investigate the effect of the mat material and thickness on stress distribution and concentration within the metatarsals during inversion landing position **(Figure 2.11)**. Foam material mat inserts between the foot and ground with different thickness were systematic studied. The predicted plantar pressure distribution showed good agreement with experimental data of controlled biomechanical tests. Material properties of the mat could clearly affect the metatarsals' stress. Meanwhile, the influence of thickness in soft material was more effective than the hard material. **Figure 2.12** shows a typical modelling work considering the self weight effect, as a boundary condition, in the gluteus maximus muscle group (Ganz *et al*, 2006). In this process, pressure soreness in wheelchair users over a prolonged period of time was investigated. In this application, quantification of the stress and strain levels within the fats and tissues could effectively provide important data for the design improvement.

Figure 2.11 FE foot model based on reconstruction of CT scans for simulating the foot deformation during landing at an inversion angle (Gu *et al*, 2010).

Figure 2.12 Typical procedures showing the use of FE modelling in deformable image registration and the deformation of internal tissues during sitting (Ganz *et al*, 2006).

2.5.3 FE modelling of the pelvic system and use of FE modelling in cancer treatment planning

Recently, some works has been conducted on the modelling of the pelvic system for different purposes, for example bladder, bowel cancer etc (Crouch *et al*, 2007). Some of these works were directly linked with cancer diagnosis or treatment process. Marchal *et al*, (2005) researched into the feasibility of a discrete soft tissue model for complex anatomical environment simulations concentrating on the prostate bladder and the pelvic bones **(Figure 2.13 (a))**. The research is able to predict the interaction between organs within the pelvic system with a relatively fast computational time, but with main drawbacks such as instability, non-realistic physical conditions and non-preservation of the volume. This is the common problem with the computational discrete approach. Research by Lee *et al* (2008) **(Figure 2.13b)** proposed using deformable image registration algorithms to map prostate displacement. The boundary condition for the target organ is not given explicitly in the paper. Instead it is driven by inter-organ contact forces generated by boundary conditions on surrounding organs; the main protagonist for the force being generated was the displacement of the rectum and bladder. This simplified approach has also been used by other researchers (Lebesque *et al*, 1995; Malone *et al*, 2000; Fuller *et al*, 2006). The validation method of the results has to rely on analysis of repeated CT images of the male pelvis system. One major limitation of the method is in that the deformation was mapped from one scan to another without modelling the real physical process. This may inevitably bring some error and requires a high level of detailing for the surrounding geometry of the organs which is often difficult to achieve.

Figure 2.13 (a) Finite Element modelling of ultrasound imaging of the prostate based on simplified organ shapes of bladder and prostate (Marchal *et al* 2006); (b) Deformation field of the numerical pelvic model of the pelvic system with an applied boundary condition placed upon bladder and rectum (Lee *et al* 2008).

The use of FE modelling in cancer treatment has become a research field of increasing importance, however, most of the published research works associated with prostate cancer (Lebesque *et al*, 1995; Malone *et al*, 2000; Marchal *et al*, 2005; Fuller *et al*, 2006; Lee *et al*, 2008) has been focused on certain aspects of prostate cancer treatment with simplified boundary or loading conditions, which could not provide the essential tool to conduct a subject specific investigation. This requires an integrated

approach combining model development, validation and realistic materials modelling with sensitivity studies. **Figure 2.14** shows the approach of the potential use of FE modelling in cancer treatment planning process. During interaoperative treatment, radiotherapy is constantly updating the imaging and registration of the affected area using the predictive power of FE, with constant plan update using computer assistance. A post operative analysis can take place where a patient image registration with a computer aided assessment can evaluate the radiation treatment process. In order to produce an accurate Finite Element model, patient data has to be taken using a CT or MR images. From these images volumetric data sets must be created in order to produce patient specific, geometrically accurate conditions. Within these data sets both the rectum and the bladder need to be included with prostate and pelvic bones also modelled. To further progress the research, validation of the boundary conditions and material properties need to be analysed using repeated CT/MR data sets using same patient images with different organ conditions (full/empty bladder and or rectum). Only after the material properties and loading conditions have been validated can there be concentration upon prostate displacement. Two main concerns influencing the modelling results are dimensional accuracy, and the material properties which is particularly challenging for the pelvic system. These are two of the main foci of this work.
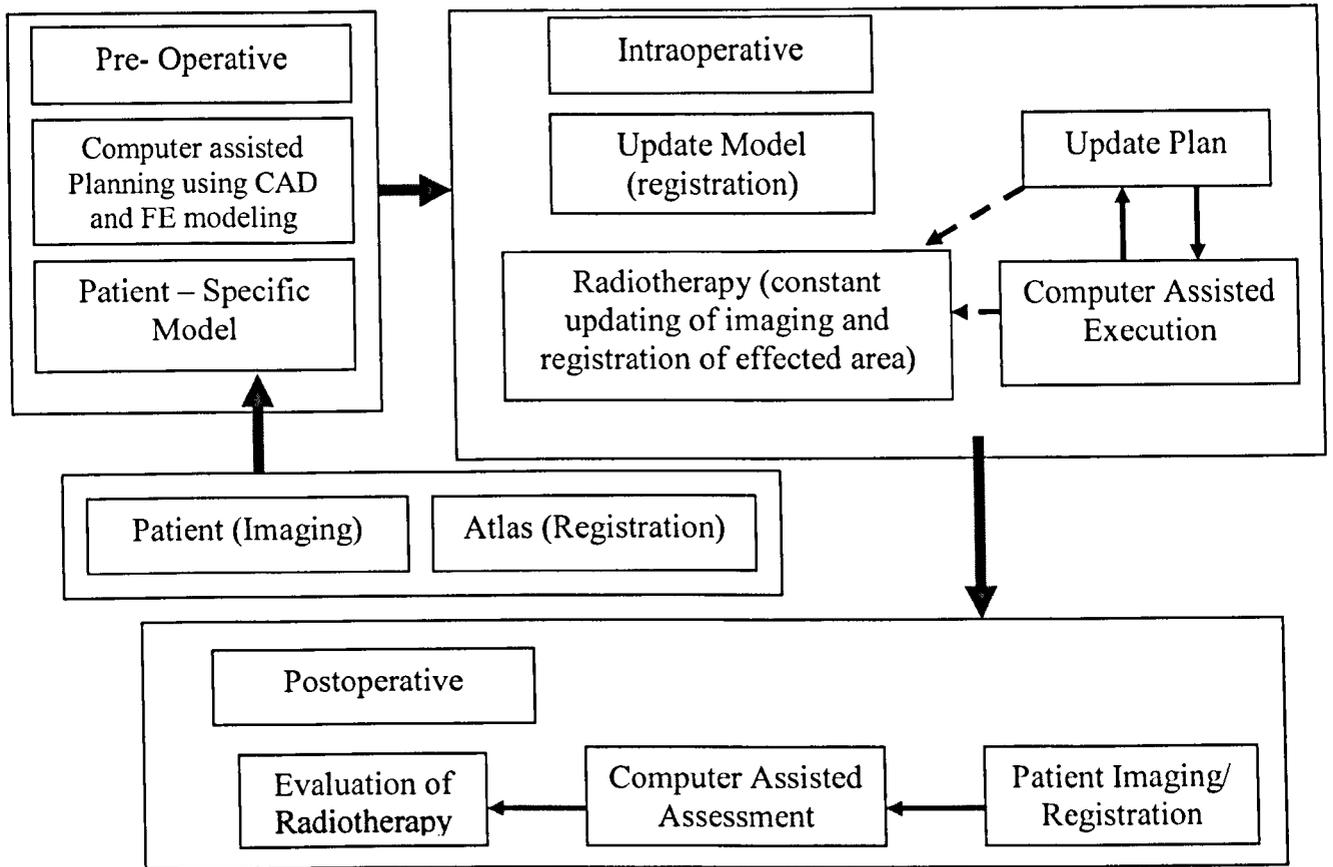
Figure 2.14 Flow chart showing the potential use of FE simulation during radiotherapy of prostate cancer.

2.6 Mechanical behaviours of biological materials

The behaviour of materials subject to tensile/compression forces can be described by a stress-strain graph. **Figure 2.15** shows schematically the three main type of stress strain relationships in soft materials (such as rubber, foams and biological tissues), namely linear elastic (a), elastically non-linear (b) and viscoelastic (c). For an elastic material, the stress is proportional to strain, the strain is recoverable if the stress is removed, i.e. the specimen returns to its original dimensions. This occurs in the initial linear region of the stress-strain curve of rubbers, biological tissues, flexible foams and some rigid foam. A linear elastic relationship between tensile or compressive stress and strain can be described by:

$$\sigma_x = E\varepsilon_x \qquad\qquad (2.6.1)$$

where the constant E is the Young's modulus.

The absolute value of the ratio of the lateral strain (ε_y) to the longitudinal strain (ε_x) is the Poisson's ratio:

$$\nu = -\frac{\varepsilon_y}{\varepsilon_x} \qquad\qquad (2.6.2)$$

At small strain for both compression and tension, the average experimentally observed Poisson's ratio, ν, of foams is about 0.33. For rubbers and most biological materials, the Poisson's ratio (ν) is normally treated as close to 0.5, representing incompressive behaviour. For open celled foams, at larger strains it is commonly observed that Poisson's ratio is effectively zero during compression — the buckling of the cell walls does not result in any significant lateral deformation. However, during tension, the Poisson's ratio is nonzero, which is a result of the alignment and stretching of the cell walls. For an isotropic material, the shear modulus G can be calculated using:

$$G = \frac{E}{2(1+\nu)} \qquad\qquad (2.6.3)$$

As shown in **Figure 2.15 (b)**, non-linear relationships between stress and strain are usually convex upwards in compression (compressive stresses and strains are taken to be positive). While for materials like rubber in tension, the shape of the curve is normally concave. The non-linearity is associated with the internal structure of the material. For foam materials, at small strains the material deforms in a linear, elastic manner as a result of cell wall bending. At large strain, the cell walls rotate and align, resulting in an increased stiffness. For rubber materials, the deformation under tension can be many times its original size, and upon release, it returns to its original shape. In its relaxed state, rubber consists of long, coiled-up polymer chains that are interlinked at a few points. Between a pair of links, each monomer can rotate freely allowing each section of the chain to assume a large number of geometries. At large strain rates when rubber is stretched, elastomers straighten and are taut and are no longer able to oscillate. Once the stress is released, however, the elastomers immediately return to their original shape. When the material is under cyclic loading, it will exhibit a typical viscoelastic material behaviour illustrated in **Figure 2.15 (c)**. This is a type of deformation exhibiting the mechanical characteristics of viscous flow and elastic deformation. Most foam materials and biological material exhibited highly nonlinear and viscoelastic behaviours (Mills *et al*, 2003). Nonlinear materials behaviour is significantly different from linear deformation and it has to be understood based on the nonlinear mechanics. Nonlinear elastic materials (such as rubbers and biological tissues) undergo large deformations. The material can undergo a very large deformation generally known as hyperelastic behaviour. Typical examples include foams, rubber and many biological tissues.

| (a) Linear elastic and isotropic | (b) Non linear | (c) Visco elastic |
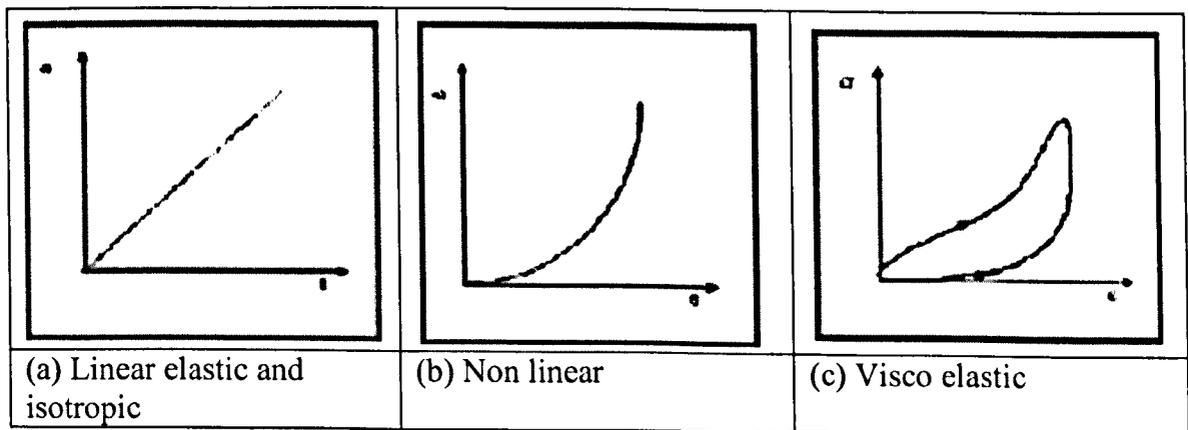
Figure 2.15 Schematics showing linear elastic and non linear elastic material behaviours.

For an elastic material, the stress at any point can be defined solely as a function of the deformation gradient at that point. A change in stress arises only in response to a change in configuration, and the material is indifferent to the manner in which the change in configuration arises in space and time. For a hyperelastic material, the above definition applies, and there is an additional scalar function from which the stress can be derived at each point. The scalar function is the stored energy or strain energy function, W, which can also be defined solely in terms of the deformation gradient (Weiss and Gardiner, 2001). Hyperelasticity provides a convenient framework for the formulation of constitutive equations for materials such as foams or biological soft tissues because it allows for large deformations and anisotropy (Weiss and Gardiner, 2001).

Many strain energy function models have been developed to characterise different material systems which undergo large deformation, typically Mooney-Rivlin model, neo-Hookean form and Ogden model (Ogden, 1972a; Petre et al, 2007). They are generally used to describe incompressible materials (such as rubber and water filled structures). These material models have been employed in several computational software including ABAQUS, which are briefly described:

Mooney derived an expression for the strain energy function for rubber starting from several assumptions: (1) The material is homogeneous and free from hysteresis; (2) The material is isotropic initially and throughout the deformation; (3) The deformations occur without change in volume; (4) The traction in simple shear in any isotropic plane is proportional to the shear (Mooney, 1940).

The linear form of strain energy function Mooney initially proposed is:

$$W = C_1(I_1 - 3) + C_2(I_2 - 3) \qquad (2.6.4)$$

where C_1 and C_2 are constants. It is the most general form admitting a linear relationship between stress and strain in simple shear, and has since been referred to as the Mooney-Rivlin model. With suitable choices of C_1 and C_2, this equation gives a marginally better fit to some of the experimental data of rubber than pure elastic models (Atkin and Fox, 1980).

The strain energy W (Equation 2.6.4) can be split into to two parts, the deviatoric and volumetric terms. Then the form of the Mooney-Rivlin strain energy density becomes (ABAQUS Users Manual 6.4).

$$U = C_{10}(\bar{I}_1 - 3) + C_{01}(\bar{I}_2 - 3) + \frac{1}{D_1}(J^{el} - 1)^2$$

(2.6.5)

where U is the strain energy per unit of reference volume; C_{10}, C_{01}, and D_1 are temperature-dependent material parameters, I_1, I_2 are the first and second deviatoric strain invariants defined as:

$$\bar{I}_1 = \bar{\lambda}_1^2 + \bar{\lambda}_2^2 + \bar{\lambda}_3^2 \quad \text{and} \quad \bar{I}_2 = \bar{\lambda}_1^{(-2)} + \bar{\lambda}_2^{(-2)} + \bar{\lambda}_3^{(-2)}$$

(2.6.6)

Where the deviatoric stretches $\bar{\lambda}_i = J^{-\frac{1}{3}} \lambda_i$; J is total volume ratio; J^{el} is the elastic volume ratio. λ_i are the principal stretches. The initial shear modulus (μ_0) and bulk modulus (K_0) are given by;

$$\mu_0 = 2(C_{10} + C_{01})$$

(2.6.7)

$$K_0 = \frac{2}{D_1}$$

(2.6.8)

Only isotropic thermal expansion is permitted with the hyperelastic material model. The elastic volume ratio, J^{el}, relates the total volume ratio (J) and the thermal volume ratio (J^{th}) following this equation:

$$J^{el} = \frac{J}{J^{th}}$$

(2.6.9)

Jth is given by

$$J^{th} = (1 + \varepsilon^{th})^3$$

(2.6.10)

where ε^{th} is the linear thermal expansion strain that is obtained from the temperature and the isotropic thermal expansion coefficient.

Neo-Hookean form model

The form of the neo-Hookean strain energy potential is given by

$$U = C_{10}(\overline{I}_1 - 3) + \frac{1}{D_1}(J^{el} - 1)^2$$

(2.6.11)

where C_{10}, and D_1 are temperature-dependent material parameters, $\overline{I}_1$ is the first deviatoric strain invariants; J^{el} is the elastic volume ratio.

Ogden form models

Another commonly used model is the Ogden model (Ogden, 1972a). Instead of taking U as a function of I_1 and I_2, the model is based on an assumption that U is a function of the principle values b_1, b_2, b_3 of B.

$$U = \sum_n (\mu_n / \alpha_n)(b_1^{\alpha_n} + b_2^{\alpha_n} + b_3^{\alpha_n} - 3)$$

(2.6.12)

where μ_n are constants, and α_n are not necessarily integers and may be positive or negative. B is left Cauchy-Green strain tensor. b_1, b_2, b_3 are principle values of B. B is left Cauchy-Green strain tensor. The general form of the Ogden strain energy potential is

$$U = \sum_{i=1}^{N} \frac{2\mu_i}{\alpha_i^2}(\overline{\lambda}_1^{\alpha_i} + \overline{\lambda}_2^{\alpha_i} + \overline{\lambda}_3^{\alpha_i} - 3) + \sum_{i=1}^{N} \frac{1}{D_i}(J^{el} - 1)^{2i}$$

(2.6.13)

where $\overline{\lambda}_i$ are the deviatoric principal stretches; λ_i are the principal stretches; N is a material parameter; μ_i, α_i, and D_i are temperature-dependent material parameters (ABAQUS Users Manual 6.4).

48

The initial shear modulus and bulk modulus for the Ogden form are given by

$$\mu_0 = \sum_{i=1}^{N} \mu_i, \qquad K_0 = \frac{2}{D_1}$$

(2.6.14)

Following this form, the Mooney-Rivlin form can also be obtained from the general Ogden strain energy potential for special choices of μ_i and α_i.

2.7 Materials testing and parameters identification

As shown in the previous section, most of these nonlinear strain energy functions include more than one material parameter. It is a challenging task to accurately derive these functions. Conventionally, the determination of material parameters is based on the use of test samples with a standardised geometry and strain state (as shown in **Figure 2.16**). Such that particular conditions on the stress and strain field are satisfied in the sample/or part of the sample. Then the unknown model parameters are obtained *via* curve fitting from experimental data. Soft tissues such as the bladder wall represent a difficult material to test. Conventional methods include uniaxial test tests, biaxial test, etc (Korossis *et al*, 2006; Podder *et al*, 2006; Zhang *et al*, 2007). Dahms *et al*, (1998) aimed to quantify the material properties for the bladder using a tensile testing system. The research compared the mechanical properties of the bladder in comparison to rat and pig bladders. Strips of each of the bladders were tested under tension, and the ultimate tensile strength, maximum strain, and elastic modulus were determined from stress strain curves. The experimental set of the work is shown in **Figure 2.17.** A sandpaper frame was constructed around the specimen to facilitate uniform gripping during tensile testing. The ends of the strips were glued to prevent slippage from the clamps. The experimental data in **Figure 2.17** was shown to have varying Young's modulus between pig, rat and human bladders. Variations of type I and III collagen and elastic fibres, are observed as major anatomical differences of bladder tissue, between three different species. There were more collagen type I fibres in the rat. Human bladder tissue showed higher levels of type III collagen and elastic fibres. These anatomical differences can affect certain mechanical parameters such as ultimate tensile strength, maximum strain and elastic modulus. Validating human tissue via comparing the material characteristic of different species will result in an inaccurate description of human tissue characteristics.

Current standard approaches normally require large numbers of tests and samples with well-defined geometries (Mills and Zhu, 1999; Mills *et al*, 2003; Morcu and Mills, 2004; Petre *et al*, 2007). For example, for rubber materials, a wide range of tests have to be used (e.g. tension test, shear test) in order to predict these parameters. The

method is inconvenient or even impossible where standard specimens are not readily available, or for *in situ* monitoring of the mechanical strength of the materials. Recently, some effort has been made to use non-standard tests under more complex conditions to determine the material parameters. A range of tests have been explored including suction, intension, torsion, bending test or indentation (Vannah and Childress, 1996; Diridollou *et al*, 2000; Knight *et al*, 2001; Elsner, 2002; Vescovo *et al*, 2002; Mattei and Zahouani, 2004). Generally, these tests involve applying a predefined stress/deformation on the sample surface and the monitoring of the load/displacement. Recently, Elkut *et al* (2010) has used a parametric method to inversely predict the properties of thin membrane and then used the properties to predict the water filling process of bladder models made of thin rubber sheet **(Figure 2.18)**. The properties of the rubber sheet were characterised using the indentation bending tests test, in which an indenter is pressed onto the sample surface and the force-indentation depth data is used to represent the resistance of the material. This method is convenient to use and requires smaller testing areas than other testing methods. The nonlinear material properties of the rubber sheet of the phantom were characterised using a novel inverse Finite Element (FE) modelling technique and the results were compared to micro tensile tests. The material properties predicted were then used to model water filling process of balloon mimicking the bladder filling process. The program was then used to simulate the bladder filling process and its effect on the movement and deformation of other organs at different filling levels.

Figure 2.16 Deformation modes of various experimental tests for defining material parameters (ABAQUS User Manual 6.4).

Figure 2.17 (a) Schematic of the tensile testing of bladder strips and typical stress strain curve for (b) Human bladder, (c) Rat bladder and (d) Pig bladder. (Dahams *et al* 1998)

Figure 2.18 (a) Schematic to show indentation bending tests to inversely predict the materials properties; (b) Finite Element model of a balloon deformation field during water filling process (Elkut *et al*, 2009).

2.8 Mechanics of the bladder filling process

The bladder filling cycle represents a complex process. Changes in the shape and size of the bladder occur during the build-up of hydrostatic pressure that results from the accumulation of an increasing volume of urine (Haberstroh *et al*, 1999). These deformations may affect the functions of the urinary and other relevant systems directly. Changes in the shape of the bladder also affect the diagnosis of medical conditions such as bladder cancer, and influence surgical procedures, (Miralbell *et al*, 1998; Meijer *et al*, 2003). In addition, a change in the volume of the bladder causes the movement of other organs such as the prostate and/or rectum, which brings uncertainty with regard to the position of the prostate and adversely affects the planning stage of a radiotherapy procedure (Meijer *et al*, 2003).

The deformation of the bladder caused by filling has been studied during some clinical investigations in which the movement of the bladder wall and the bladder volume were measured using computed tomography (CT) or magnetic resonance imaging (MRI) (Roeske *et al*, 1995; Miralbell *et al*, 1998; Villeirs *et al*, 2004; Pinkawa *et al*, 2007). For example, Roeske *et al*, (1995) recorded the size and location of the prostate, bladder, and rectum throughout the course of external beam radiotherapy. In the work, ten patients with prostate cancer had a weekly CT scan. The location of the prostate, seminal vesicles, bladder, and rectum on subsequent scans were compared according to the CT images. The result showed that the bladder and rectal volumes varied by +30% whilst movement of the prostate was demonstrated in all patients. Location changes of the prostate and normal tissue volumes, during the course of radiation therapy occur and have consequences that may impact tumour control and normal tissue complication. This is particularly important for conformal therapy for prostate cancer, which requires the understanding of biomechanical mechanisms of the anatomic relationships of these structures during filling of bladder and rectum. Research by Miralbell *et al*, (1998) evaluated tumour motion with controlled changes of the bladder volume, and to assess the reproducibility of bladder position using a urinary catheter balloon as an immobilization device. This was used to eliminate the variability/influence of bladder biomechanics on surrounding structures. In the work, three patients with tumour

growths were evaluated. The displacement of the tumours was measured based upon reconstructed CT images when 100 cc were removed from a bladder originally filled with 170 cc of contrast. It was found that changes in bladder volume and shape related to bladder filling can result in clinically significant displacements of the target volume. Although an 80 cc urinary catheter balloon helped to immobilize the bladder, reproducibility was still not consistent.

Another way to evaluate bladder mechanics is to measure prostate motion with magnetic resonance imaging (MRI) during a course of intensity modulated radiotherapy. This process was used by Villeirs et al (2004) and seven patients with prostate cancer were scanned supine using three orthogonal planes of images (transaxial, sagittal and coronal). The bladder, rectal volumes and position of the prostatic margins relative to the bony pelvis were measured. The prostate variability in the anterior-posterior (AP), superior-inferior (SI), and right-left (RL) directions were all found to exhibit displacement. A correlation was found between large rectal volume and anterior prostate displacement. A general correlation was also found between bladder volume and inferior prostate displacement. This variation is provided that a rectal suppository is administered to avoid rectal over distension and that the patient has a comfortably filled bladder. Dependent upon water volume intake, daily bladder volume change can vary by as much as 200ml (Pinkawa et al, 2007). This not only means there is inter-subject variation, but also intra-volume variation. **Figure 2.19** shows typical data of the movement of the bladder wall with its volume changes. It is clearly showed that the displacement of the bladder wall is not uniform which has to be characterized in great detail in order to establish the subject specific effect on the prostate movement. These studies showed that significant changes in the dimensions and shape of the bladder can occur at different degrees of filling. However, because each imaging process takes several minutes, it is not possible to monitor bladder deformation continuously with the conventional techniques that are used in clinical imaging studies. Most published data are qualitative in nature and it has not been possible to quantify the differences between patients. The results are therefore inadequate for the development of guidelines to provide direct assistance in radiotherapy procedures for various conditions. It is necessary to develop an effective method to establish the relationships between the volume and dimensions of the

bladder. However, simulation of the filling of the bladder in the presence of the surrounding organs is a challenging task due to the complex structure of the system, which requires proper imaging plans to provide structural details for FE studies of specific patients, and detailed modelling programs to establish the effective parameters for the boundary, loading and material properties to be able to predict the prostate movement.

Figure 2.19 Bladder wall movement associated with the bladder volume change. (Pinkawa *et al*, 2007).

CHAPTER THREE

VARIATIONS OF THE BLADDER SHAPE/SIZE AND PROSTATE POSITION DURING THE COURSE OF PROSTATE RADIOTHERAPY

3.1 Introduction

Throughout the prostate radiotherapy process, the subjects were scanned using CT imaging. A standardised procedure used at the ClatterBridge Centre of Oncology Protocol is to ask the patient to empty their bladder, drink 500 ml of fluids before treatment and then wait 20 minutes before scanning. This is a procedure widely used in clinical conditions, but the amount of fluid intake may vary slightly between different institutions. Other benefits of having a fully filled bladder include removing any surrounding tissues/organs (e.g. seminal vesicles, bowel loops) from the bladder. Each patient is scanned approximately 20 minutes after fluid intake. Due to the different rate of fluid going into the bladder between subjects, and the different feeling of the subject about fullness of their bladder, there is still a considerable amount of variation of the bladder volume over the course of radiotherapy. A quantitative study of these variations of bladder volume and/or shape and its effect on the prostate position, will improve the radiotherapy treatment planning process. This will also provide quantitative data to guide the development of the FE modelling work to be presented in Chapter 4.

In this chapter, systematic data of the bladder dimension are presented based on measurement of CT images of a group of 10 patients with prostate cancer over the course of radiotherapy treatment. The inter and intra patient difference of the position of key pelvic organs is investigated. A method of measuring bladder wall distance is implemented, and systematic data obtained from the transaxial, sagittal and coronal planes are analysed to study the reproducibility of organ dimensions. The variation of the bladder volume and dimension were analysed between different arms for the same subject and the upper limit of bladder volume variation was determined. A technique is devised for measuring prostate movement by using the apex of the pubic bone as a point of origin and centre of prostate. Key systematic results of prostatic displacement are determined, using the measurement technique implemented, and the relationship between the prostate positional changes with bladder volume variation is analysed.

3.2 Methods, materials and imaging process

3.2.1 Method and procedures

Procedures highlighted in **Figure 3.1** shows the main steps used in this work from imaging to data analysis. In the first stage, the patients were imaged on a CT machine at three different principal planes: sagittal, transaxial and the coronal. For each patient, four sets of images were taken at different weekly intervals during a radiotherapy process representing different bladder conditions. Each interval is clinically described as an arm following standardised convention used in clinical studies. In the second stage, the key dimension of the bladder including wall distance in the AP, L-R and SI directions were measured based on a number of subjects. The accuracy of the measurements made on images from the three different planes was compared to establish a procedure that produces consistent data. In the third stage, measurement of the bladder, were applied to a larger number of subjects together with the volume data for each subject based on the procedure developed in part two. The relationship between the shape and dimensional change of the bladder with the volume change that were specific to each patient were analysed. This dimensional change has a direct relevance to clinical studies in prostate cancer treatment and other medical practice associated with the bladder (e.g. bladder cancer, rectal cancer, surgery, etc,). In the fourth stage, the dimension and volume of the prostate for each subject were measured. The distance of the prostate with respect to the key anatomical land mark (pubic bone) were systematically measured and the positional change of the prostate in the AP and S-I position were determined. The correlation between the bladder volume and the prostate movement were analysed for each subjects and then a systematic evaluation all the subjects as a group.

```
┌─────────────────────────────────────┐
│  CT Scans of subjects at three       │
│  orientations (Transaxial, Sagittal  │
│     and Coronal) using four          │
│  different arms (Time) intervals).   │
└─────────────────────────────────────┘
                  ⬇
┌─────────────────────────────────────┐
│   Measurement of the bladder         │
│  wall distance in the A-P, I-S and   │
│  L-R, direction are recorded for a   │
│   small number (3) of subjects;      │
│   dimensional data obtained from     │
│   CT data taken at different planes  │
│        are cross compared.           │
└─────────────────────────────────────┘
                  ⬇
┌─────────────────────────────────────┐
│   Measurements over a larger         │
│  group of subjects (10) following    │
│  the procedure developed in the      │
│         previous step.               │
└─────────────────────────────────────┘
                  ⬇
┌─────────────────────────────────────┐
│    Analysis of the bladder wall      │
│   distance vs change of bladder      │
│            volume.                   │
└─────────────────────────────────────┘
                  ⬇
┌─────────────────────────────────────┐
│  Measurement of the positional       │
│  change of prostate and the          │
│  correlation between prostate        │
│  movement and the increase in        │
│      the bladder volume.             │
└─────────────────────────────────────┘
```

Figure 3.1 Flow chart showing the procedures in analysing the volume change of bladder during the course of prostate radiotherapy treatment.

3.2.2 Imaging process and pre-scanning subject preparation

Ten patients with localised prostate cancer were prospectively evaluated with multiple CT scans. At each of the points in time they underwent a CT scan with an assumed full bladder and empty rectum. Special protocol was administered, as well as drinking 500ml of fluid before the scan to promote bladder filling, each of the ten subjects was administered a relaxit which empties the rectum. The feeling of the patient to have a full bladder was the relevant criterion before the pelvic scan. Four points in time were chosen for ten consecutive patients scheduled for primary radiotherapy (before, after initial treatment, halfway through treatment, and after four weeks, i.e., in the last week of treatment). A total number of 36 CT scan sessions and over 4000 slices resulted in this analysis. The scans were matched by aligning the bony anatomy of the pelvic ring. During the investigation subjects underwent CT scans in the supine position in a Philips Medical Systems Intera 1.5 T whole-body scanner. Each CT examination, which included T2-weighted turbo spin echo sequences in the sagittal, transaxial, and coronal orientations, lasted for approximately 30 minutes. The acquisition matrices for all orientations had a frequency-encoded dimension of 512 x 512 matrix. Each of the CT scans were performed in the supine position with varying slice thickness of 3 mm (transaxial, coronal) and 5 mm (sagittal) from the anal canal up to the sacral promontory. The patient remained in essentially the same position on the flat scanner table for these scans. The planning scans follow a strict protocol for maintaining positioning than a routine diagnostic scan. The patient's ankle and knee positions are constrained by supports intended to keep his legs in a set position. No bowel or intravenous contrast enhancement was used. The data were transferred to a commercially available stereotactic planning system (Pinnacle, Philips, Germany). The bladder wall (internal and external) and rectum wall (internal and external between the rectosigmoid flexure and the anal canal) were contoured in every CT scan as was the prostate.

3.2.3 Image analysis process

Pinnacle is a commercial machine widely used for the radiation therapy process. Images are taken of patients using CT scans in the supine position (lying down with the face up) using the Philips Medical Systems Intera 1.5 T whole-body scanner. Once the images in all orientations (transaxial, sagittal and coronal planes as shown in **Figure 3.2**) are recorded, the data sets are exported into software imaging program Pinnacle. Philips Pinnacle is used in aiding the planning of the radiation treatment which is a fast, accurate and interactive treatment planning tool. Using the program allows fully integrated photon, electron, stereotaxy, brachytherapy, simulation, image fusion, and IMRT options that allow the performance of treatment planning tasks from a single platform (Ellis *et al,* 2006). The imaging software is multifunctional, for example, region of interest, names, colours and graphics and automatic isocenter placement can be recorded. As well beam sizes and orientations (gantry, couch and collimator) blocks with automatic margins can be accessed. During viewing of the imported images all orientations and arms can be viewed. This enables a cross comparison of each slice at different orientations, and at different time intervals. Functions such as auto contrasting are accessible enabling an increased clarity/resolution of the CT images. Outlining of the organs and the bones can be automatically generated using the Pinnacle system, the program automatically generates contouring by distinguishing between different contrasts of the CT image. For a more accurate detailed outlining, manual contouring of the imaging slice by slice was created using manual outlining function. This enabled a more detailed outlining of organs, eliminating the interference that is generated *via* automatic outlining. This outlining was verified by trained oncologists at Clatterbridge Centre of Oncology. The outlining consisted of the bones, bladder, bladder wall, prostate, seminal vesicles and the rectum. For all 10 patients, each arm, orientation, and slice was manually contoured. The Pinnacle software is capable of generating volumetric data sets calculated from the outlining of the slices. The calculation were cross compared with a given mathematical formula to determine the volume based on the volume equation derived from describing the bladder as a spherical shape (Damser and Lehman, 1995).

3.3 Typical CT images at the transaxial, coronal and sagittal planes and inter/intra subject differences

Figure 3.2 shows a typical example/slice of the CT images at the (a) transaxial, (b) sagittal and (c) coronal planes. The key pelvis area structures have been labelled on each of the slices, including the bladder, prostate, rectum and the pelvic bones. The soft tissues are in grey, the black areas indicate empty space, and the bones are clearly visibly brighter due to the differences in densities (Abbott *et al,* 2009). The contouring demonstrates the outlining of the patient organs using radiotherapy software Pinnacle following the procedure described in section 3.2. As shown in these examples, each slice on different planes has the advantages and drawbacks in terms of the information obtained from the image. The transaxial plane is parallel to the ground, and separates the superior from the inferior regions, or the head from the feet. The advantage of this viewpoint is that it enables greater coverage of the movement of the organs in the anterior-posterior and the left-right directions. The sagittal plane is perpendicular to the ground and separates left from right; it gives a complete view of superior-inferior and anterior-posterior movement of the organs. The coronal plane is perpendicular to the ground, and separates the anterior from the posterior. It can give full coverage of the superior-inferior, and the left-right movements of the organs.
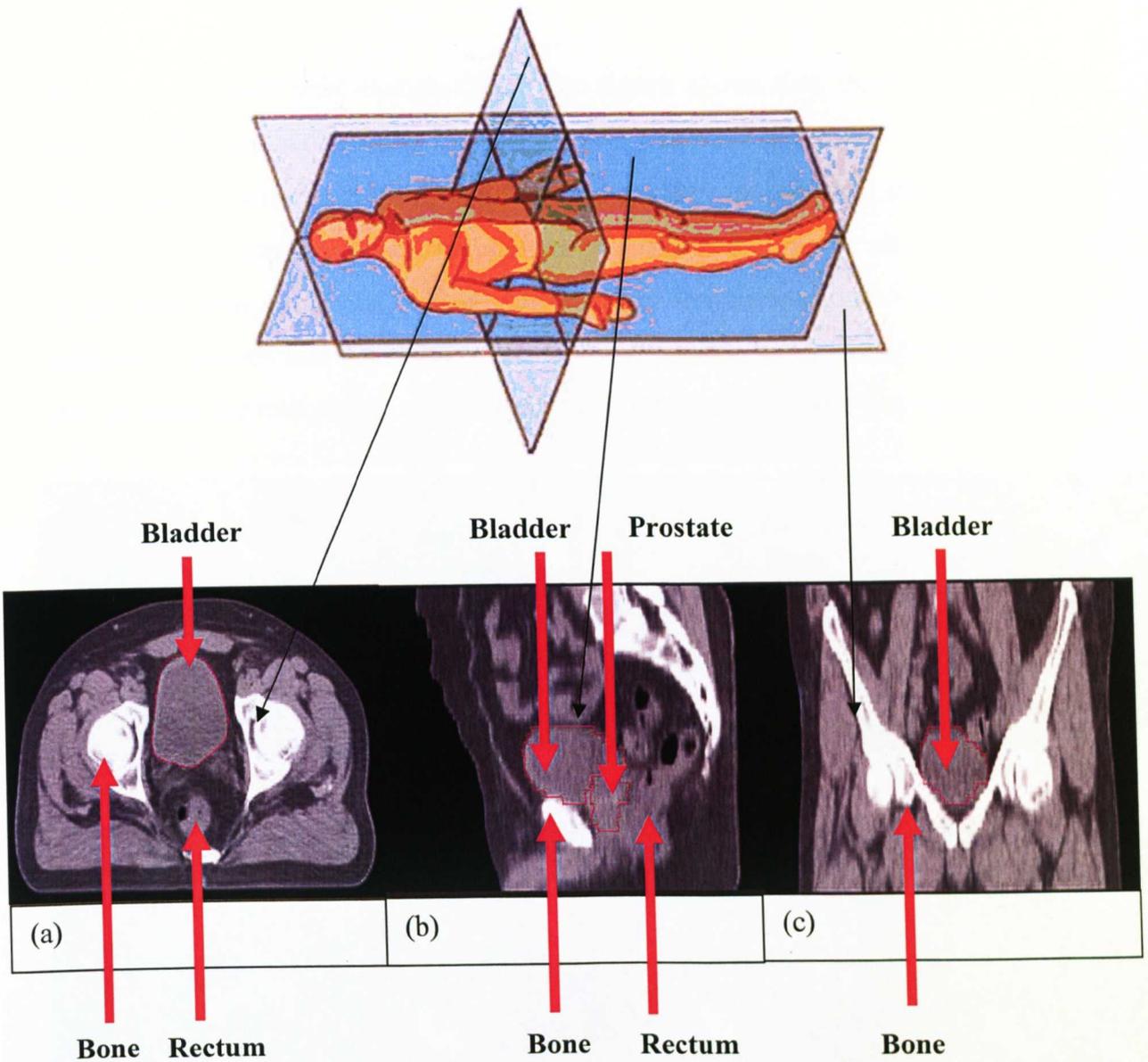
Figure 3.2 Typical CT images taken from (a) Transaxial, (b) Sagittal and (c) Coronal orientations from Subject 1.

Figure 3.3 is a specific representation of three subject data sets taken in the sagittal orientation. For each of the subjects there have been four images taken over varying times scales. In these images, the bladder, prostate and the rectum were fully covered, which is a significant advantage of imaging at the sagittal planes. The subjects were all given the same instructions of drinking fluids, to empty their bladder, drink 500 ml of fluids before treatment and then wait 20 minutes before scanning, and then an enema is administered (full bladder, empty rectum). The images were also chosen at approximately the same slice distance in order to gauge inter patient variability between the images. To compare the change of bladder for the same subject but different time, the images were converted in the same format so that the dimensions of

the bone structure were comparable. The figure shows that there is a clear inter-subject difference between the images. Subject one has a more oval shaped profile of the bladder, while subject 2 shows a flattened bladder, for subject 3 the profile is more oval shape. For each subject, the bladder has followed a similar shape but there are clear dimension variations between some of the conditions/arms. This intra-subject difference despite that the subject has under taken the same drinking protocol; this would cause the uncertainty of location of the prostate during the treatment process.

(a) Subject 1, Arm 1	(b) Subject 1, Arm 2	(c) Subject 1, Arm 3	(d) Subject 1, Arm 4
(e) Subject 2, Arm 1	(f) Subject 2, Arm 2	(g) Subject 2, Arm 3	(h) Subject 2, Arm 4
(i) Subject 3, Arm 1	(j) Subject 3, Arm 2	(k) Subject 3, Arm 3	(l) Subject 3, Arm 4
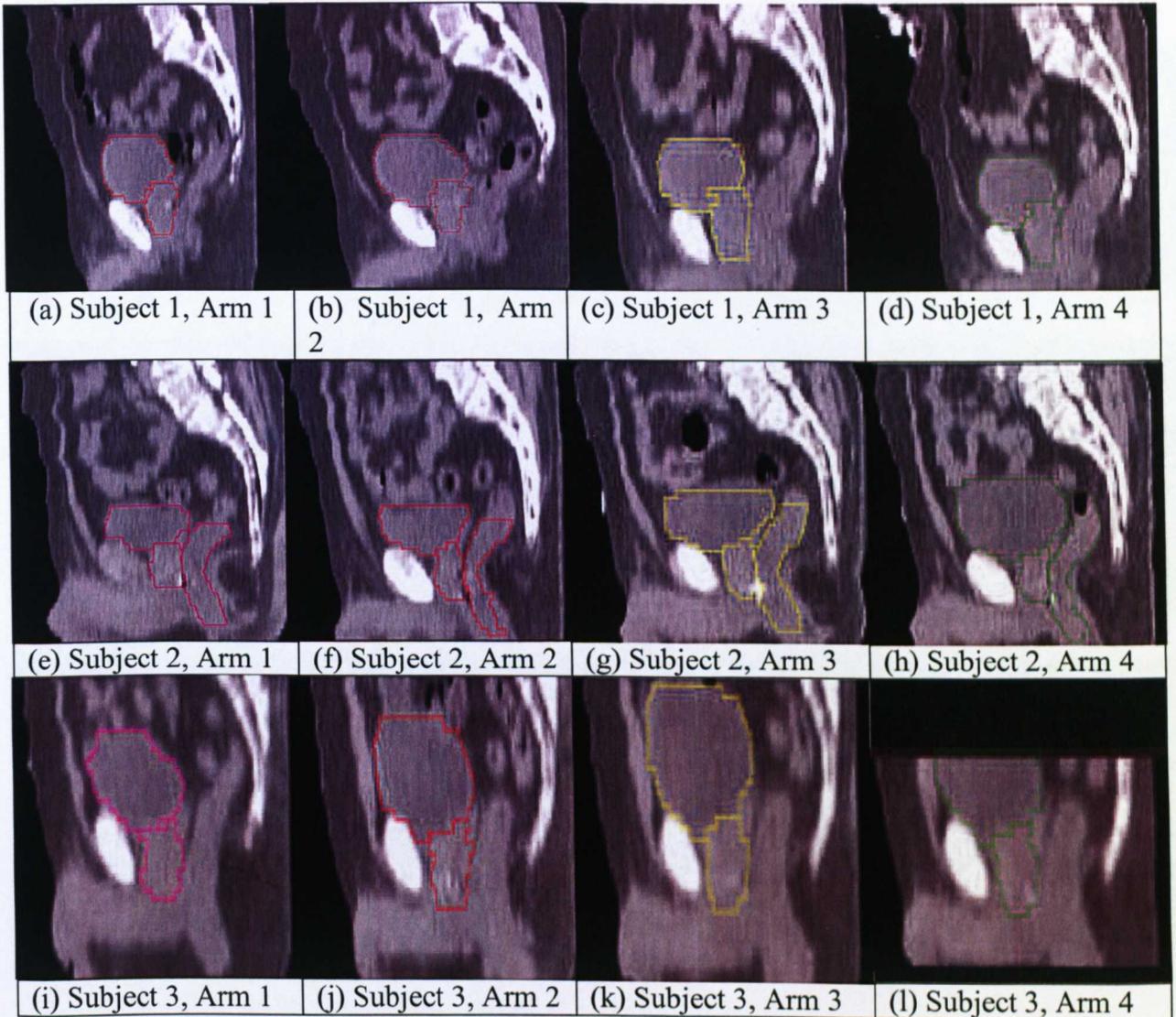
Figure 3.3 Sagittal views showing the variation of bladder shape and the volume of pelvic organs between four arms (i.e. taken at different date during the course of radiotherapy treatment), (a-d) Subject-1, (e-h) Subject-2, (i-l) Subject-3.

The next sets of images **(Figures 3.4)** are taken on the transaxial plane for the same group of selected subjects as in Figure 3.3. The images represent the mid-plane with a maximum bladder dimension in L-R and A-P direction. In all these cases, the bladder was in an oval shape while the rectum is a round structure. As shown in images of individual subject **Figures a-d** for subject one, **Figures e-h** for subject two and **Figure i-l** for subject 3; there is an inter and intra subject difference in the shape and dimension of the bladder between the subjects. The extent of the difference varied between the subjects.

(a) Subject 1, Arm 1	(b) Subject 1, Arm 2	(c) Subject 1, Arm 3	(d) Subject 1, Arm 4
(e) Subject 2, Arm 1	(f) Subject 2, Arm 2	(g) Subject 2, Arm 3	(h) Subject 2, Arm 4
(i) Subject 3, Arm 1	(j) Subject 3, Arm 2	(k) Subject 3, Arm 3	(l) Subject 3, Arm 4
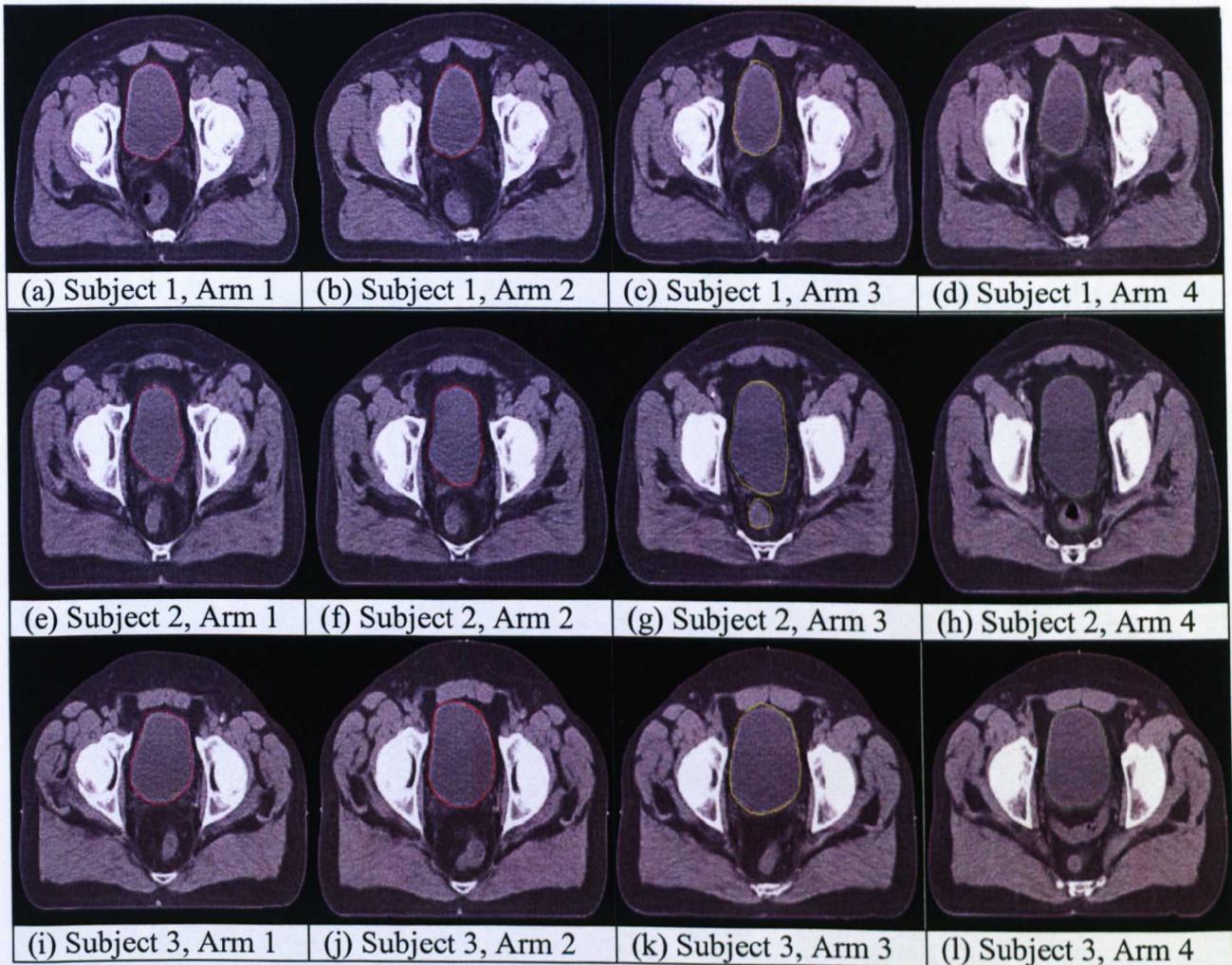
Figure 3.4 Transaxial views showing the variation of shape and volume of the bladder between four arms (i.e. taken at different date during the course of radiotherapy treatment), (a-d) Subject-1, (e-h) Subject-2, (i-l) Subject-3.

The next set of images **(Figure 3.5)** is taken on the coronal plane for the same group of subjects. The slide taken represents the mid plane of the bladder using the coronal orientation, this is commonly used to represent the maximum height and L-R dimensions. As shown in the figures, all the bladders are close to round shape and the difference of the ratio between the L-R wall distance to the S-I wall distances is much less considerable than the images taken in the transaxial plane **(Figure 3.4)**. Clearly there is a significant difference between the subject 1, subject 2 and subject 3. For each subject, there is also a clear difference in the size of the bladder between different conditions.

| (a) Subject 1, Arm 1 | (b) Subject 1, Arm 2 | (c) Subject 1, Arm 3 | (d) Subject 1, Arm 4 |
| (e) Subject 2, Arm 1 | (f) Subject 2, Arm 2 | (g) Subject 2, Arm 3 | (h) Subject 2, Arm 4 |
| (i) Subject 3, Arm 1 | (j) Subject 3, Arm 2 | (k) Subject 3, Arm 3 | (l) Subject 3, Arm 4 |
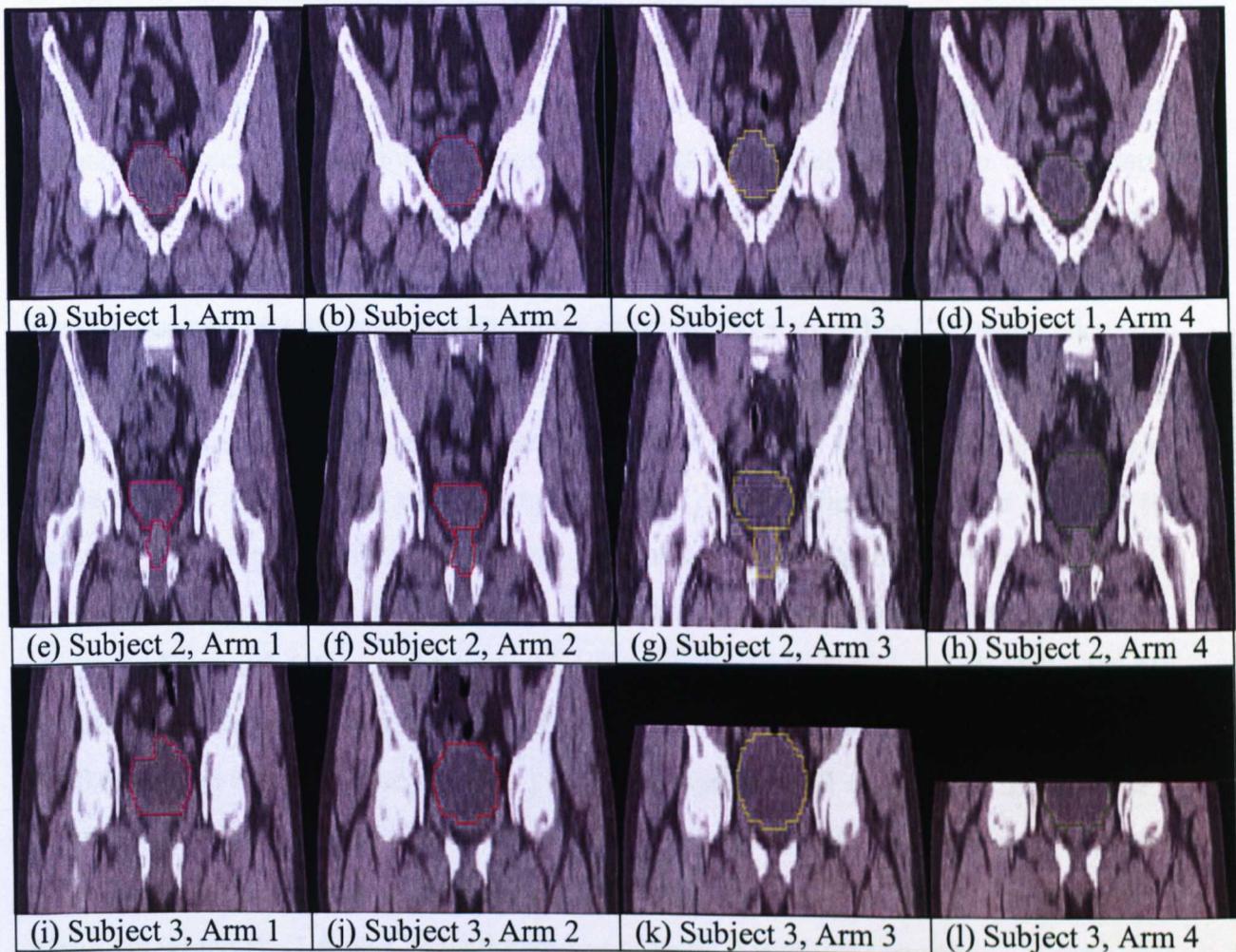
Figure 3.5 Coronal views showing the variation of shape and volume of the bladder between four arms (i.e. taken at different date during the course of radiotherapy treatment), (a-d) Subject-1, (e-h) Subject-2, (i-l) Subject-3.

68

3.4 Measurement of the variation of bladder dimensions/volume and results

3.4.1 Measurement approach and comparison between measurement data made on images taken three scanning planes

As illustrated in section 3.3, there were a clear inter and intra subject difference on the shape and size of the pelvic organ in particular the bladder. A proper approach is required to measure the organ dimension with a reasonable consistence to provide data to establish the trend of bladder dimension and volume changes during the course of radiotherapy treatments. In addition, it is also important to establish the repeatability of the data based on scans taken on different planes as these scan were taken within a total time of 30 - 45 mins. These will provide direct guidance to the clinical practice and data for analysing the effect of bladder filling on the prostate movement. In order to do these measurements of the bladder, key reference points need to be taken for each patient at each orientation. **Figure 3.6** shows the method used to measure key dimensional attributes of the bladder from the CT image taken on the transaxial (a), sagittal (b) and coronal planes (c). The maximum wall distance was used to represent the dimension of the bladder and the ratio between the bladder size at the AP, LR and SI was used to represent the aspect ratio, which can be used to describe the shape change. This is an approach commonly used to represent the dimension of the bladder and it is more relevant to the interaction between organs. As shown in **Figure 3.6 (a)** on the transaxial planes, the wall distance in the LR and AP directions can be measured, designated as "X" and "Y", respectively. **Figure 3.6 (b)** is taken on the sagittal plane. On this plane, the bladder wall distance in the anterior - posterior directions (Y) can be measured as well as the bladder wall distance between the inferior - superior wall, designated as "Z". **Figure 3.6 (c)** is taken on the coronal plane, on which the LR and IS wall distances can be directly measured.

The images of the transaxial, sagittal, and the coronal plane were taken at different times. Transaxial images were obtained 6 minutes after the sagittal, and the coronal images 21 minutes after the sagittal (and hence 15 minutes after the transaxial). The scan order was sagittal, transaxial, and then finally coronal and each imaging can take up a total of 30 - 45 min. It is important to compare the measurements made on these

image orientations, to ensure the results remain consistent. The rationale was to investigate whether or not between the scanning times the bladder would have significantly increased in size.
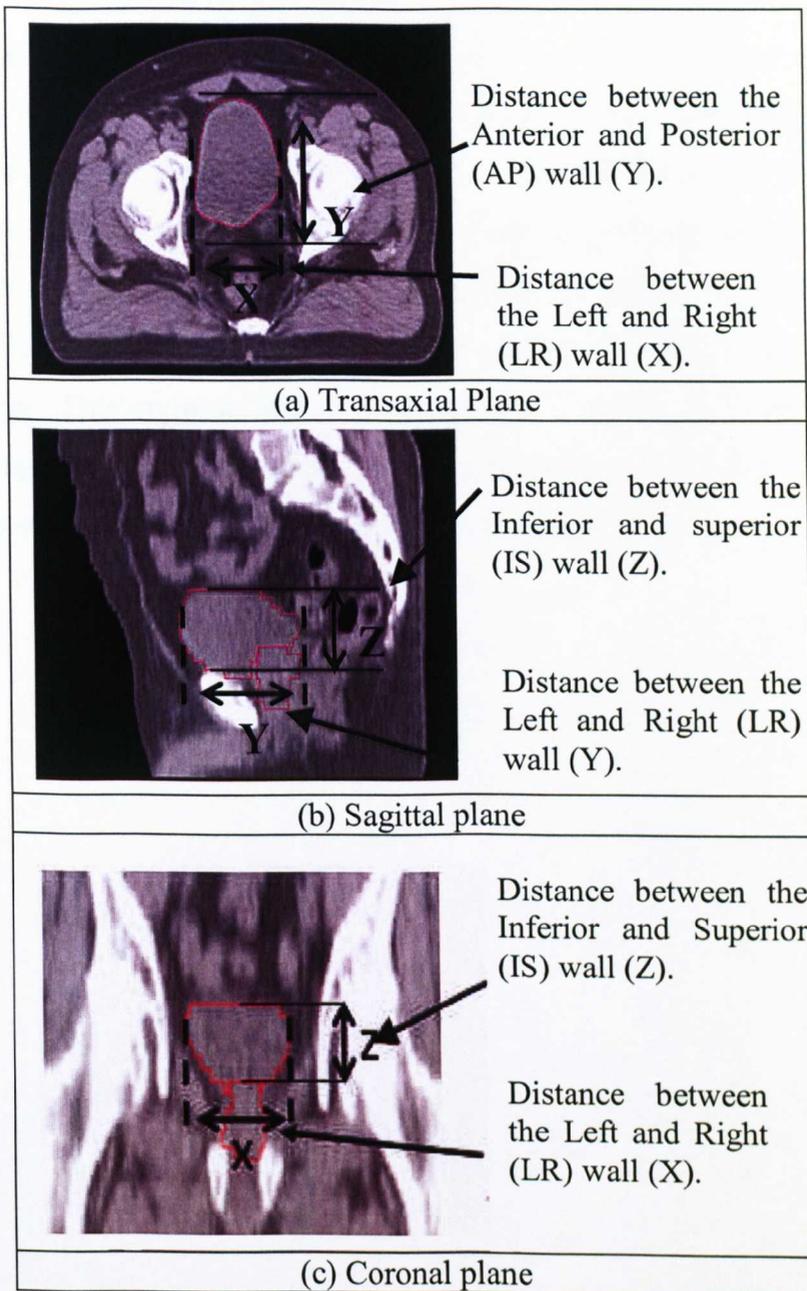
Figure 3.6 Measurement of the bladder dimension based on images taken at the (a) Transaxial, (b) Sagittal and (c) Coronal planes. X, Y and Z represent the maximum bladder wall distance in the LR, AP and IS directions, respectively.

Figure 3.7 demonstrates the comparison of the bladder dimensions measured from the different sets of images taken on the three different planes to evaluate the consistence/repeatability of the scan data. As shown in the figures for all the subjects, the data of bladder wall distances obtained from scans at different planes were in good agreement. **Figure (a)** shows the data from subject 1, in which the X and Z data are near identical with the Y value a 3 mm variation, which is within 5%. This is a reasonable variation for the nature of the work. Similar level of agreement was also observed in the data for the other two subjects selected for this study as demonstrate in **Figures (b & c)**. These data clearly showed that there was little significant variation of the bladder dimension data measured on images taken at different scanning planes. This suggest that it is a reasonable approach to combine the data from these images to provide consistent data of the change of bladder dimensions and use the data to study its deformation with bladder filling.
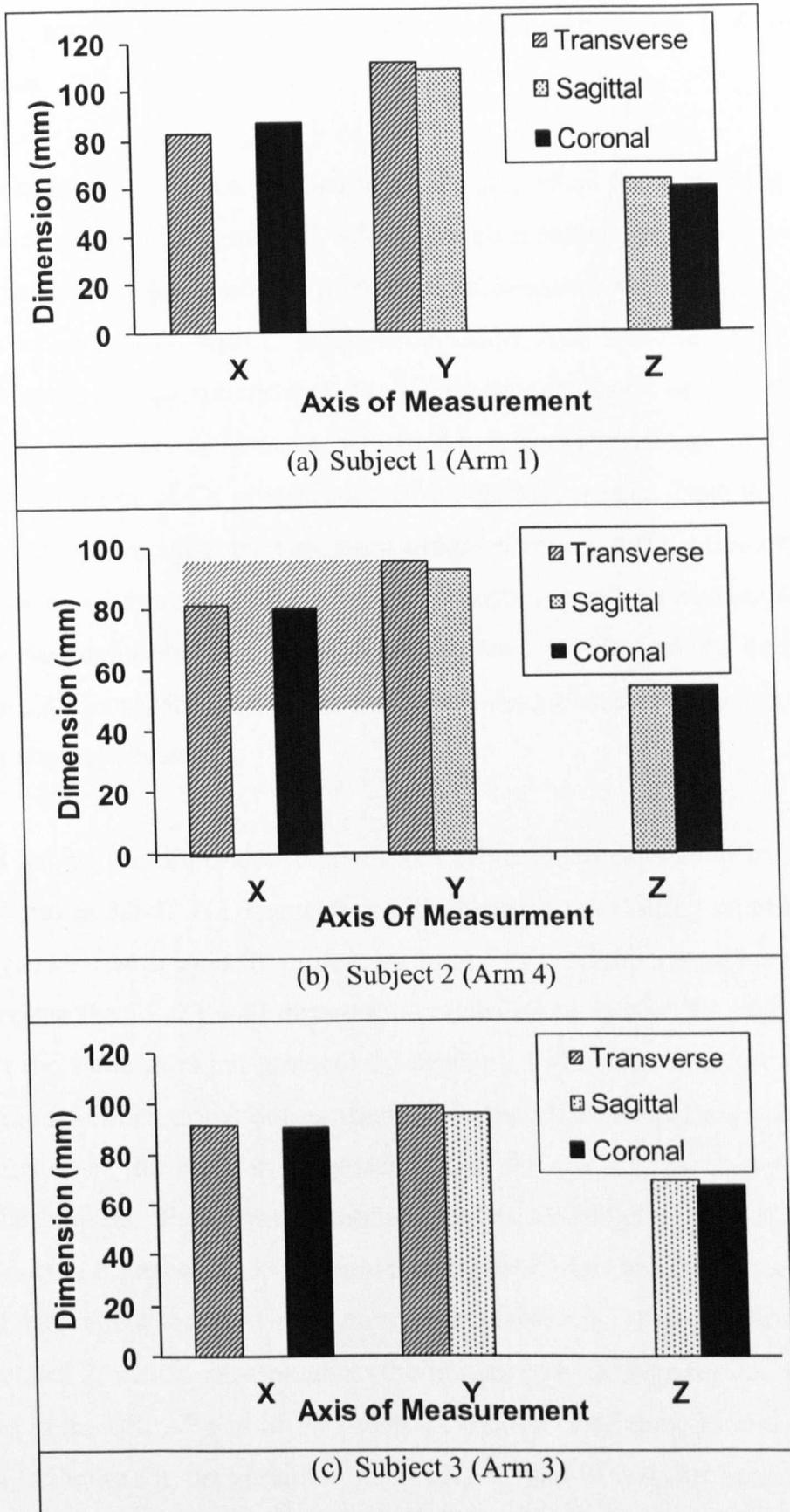
Figure 3.7 Typical data of the bladder wall distances in the LR (X), AP (Y) and IS (Z) axis obtained from the transaxial, sagittal and coronal planes to show the reproducibility of the measurement. (a) Subject 1, (b) Subject 2, and (c) Subject 3.

3.4.2 Subject specific measurement of the bladder dimension and volume at different times

The measurement approach was applied to all the data of all the subjects to establish the variation of the bladder shape and volume for each subject over the 4 scans taken at different times. For each condition more than six measurements has been made and the average value is used with a standard deviation. Inter contour effect was also assess by compare the measurement of three different contours. The error should also cover the wall thickness differences, due to the orientation change and the lower clarity of the resolution of CT images compared with MR images. Then the dimension was determined by averaging the data from images taken on different planes. The AP dimensions were measured by averaging the distance measurement from the sagittal and the transaxial planes. The LR dimensions were determined by averaging the transaxial and the coronal planes while the SI was determined by the averaging of the sagittal and coronal planes.

Figure 3.8 shows the dimension of the three subjects corresponding to the images shown in **Figures 3.3-5**. The legend bar with diagonal strip filling represent the LR (X), the legend bar with solid fill represents the AP (Y) and the legend bar with dotted filling represent the SI (Z) wall distance. As detailed in section 3.1, the subject has undertaken the same drinking protocol by drinking 500ml liquid before scanning at different times (termed arms) during the radiotherapy treatment. However, there is a clear difference of the bladder dimensions. And the scale of the difference varied between the subjects. Figure (a) represents the data for subject 1, which corresponds to image (a-d) in **Figures 3.3-5**. As shown in the data, there are differences in the LR, AP and SI data with a variation of 21 mm, 9 mm and 8 mm. Figure (b) represents the data for subject 2, which corresponds to the images (e-h) in **Figures 3.3-5**. There are differences in the LR, AP and SI data with a variation of 12 mm, 31 mm and 30 mm. As shown in Figure (c), the variation in the LR, AP and SI wall distance for subject 3 is 12 mm, 13 mm and 27 mm, respectively.
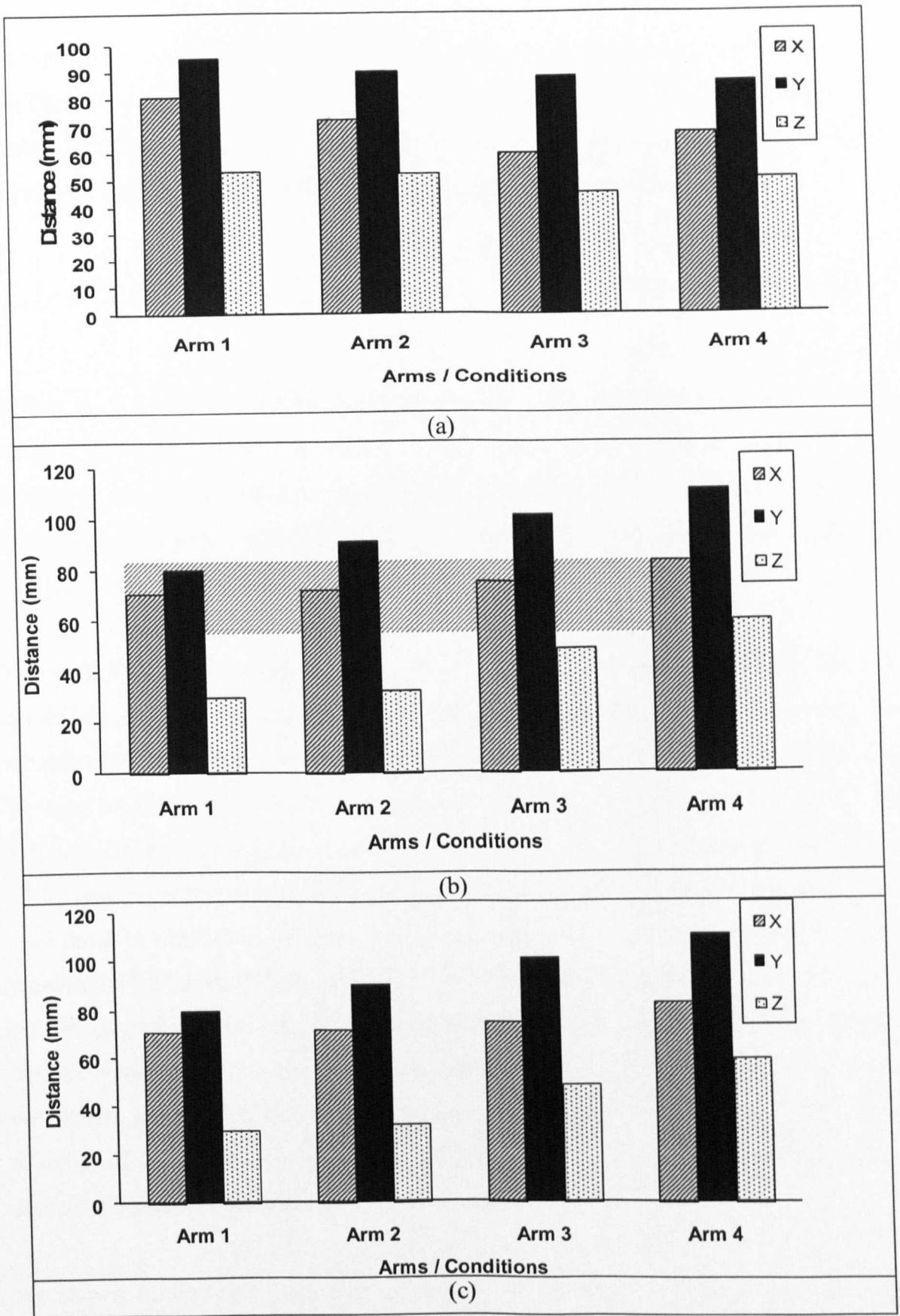
Figure 3.8 Typical measurement results of the bladder wall distance for different arms for the subjects, taken from the transaxial and sagittal planes. (a) Subject-1 (b) Subject -2 and (c) Subject-3.   (X:LR, Y:AP and Z:SI).

The measurement of the bladder dimension could provide important data to determine the bladder volume and its relationship with the bladder wall distances and prostate movement. This is an important variable which can be quantified in a clinical condition (Hedriana et al, 1994). This is calculated following the equation:

$$V = \frac{4\pi}{3} \times \frac{U_1 \times U_2 \times U_3}{8}$$
(3.4.1)

Where U_1, U_2, and U_3 refer to the left-right, the anterior-posterior and the superior-inferior wall distance of the bladder, respectively. The bladder volume was also calculated using radiotherapy programming software Pinnacle. The contouring of the bladder at each slice creates a "stack" of images which the software calculates the surface area and subsequently the volume of each bladder.

Figure 3.9 shows the results of the bladder volume of each subject over the four conditions. Each of the conditions represent a different time of scanning during the radiotherapy treatment. For example **Figure 3.9 (a)** are the results for subject one over the four conditions. The different conditions produced bladder volumes of 187, 156, 119 and 136 ml. The varying volumes of the bladder had a range of 68 ml, which is a 57% variation from the smallest to largest bladder volume. Similarly for subject two over the four conditions **(Figure 3.9 (b))**, the different conditions produced bladder volumes of 108, 116, 193 and 314 ml. The varying volumes of the bladder had a range of 206 ml, which represents a maximum variation of 190% against the smallest bladder volume. As shown in **Figure 3.9 (c)** for subject three, the four different conditions produced bladder volumes of 157, 224, 287 and 176 ml. The varying volumes of the bladder had a range of 130 ml. This accounts for an 82.8% variation against the smallest bladder.

As shown in the data, the bladder volume is automatically calculated using the Pinnacle system and is comparable to the data calculated using (Equation 3.4.1). There are some variations but there is no systematic error between these two sets of data. Pinnacle is an important clinical tool in quantifying 3D volumetric results,

however the use of Pinnacle relies on the system which is not readily available for many conditions. The results suggest that the equation can be used as a simplified mean to calculate the bladder volumes. This is an important consideration as volume data needs to be calculated for the Finite Element models of the bladder filling process.
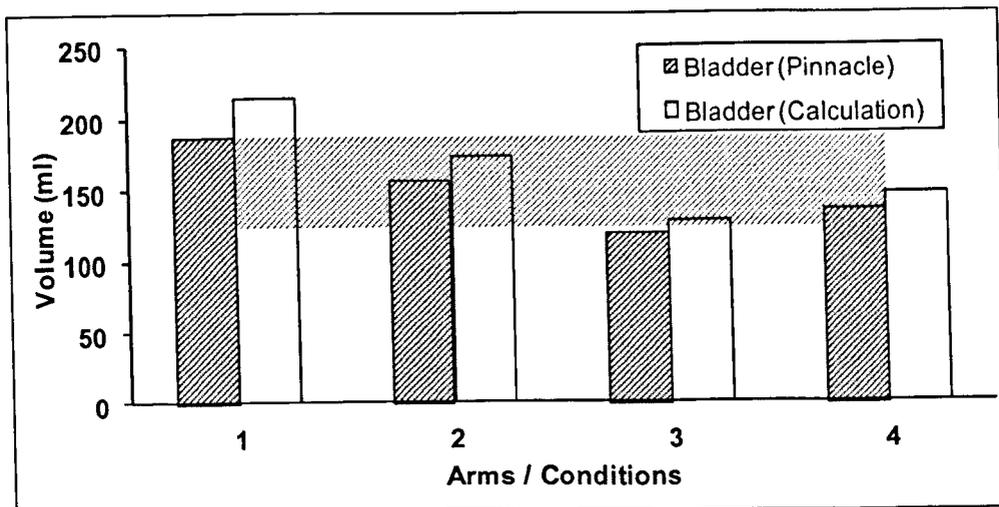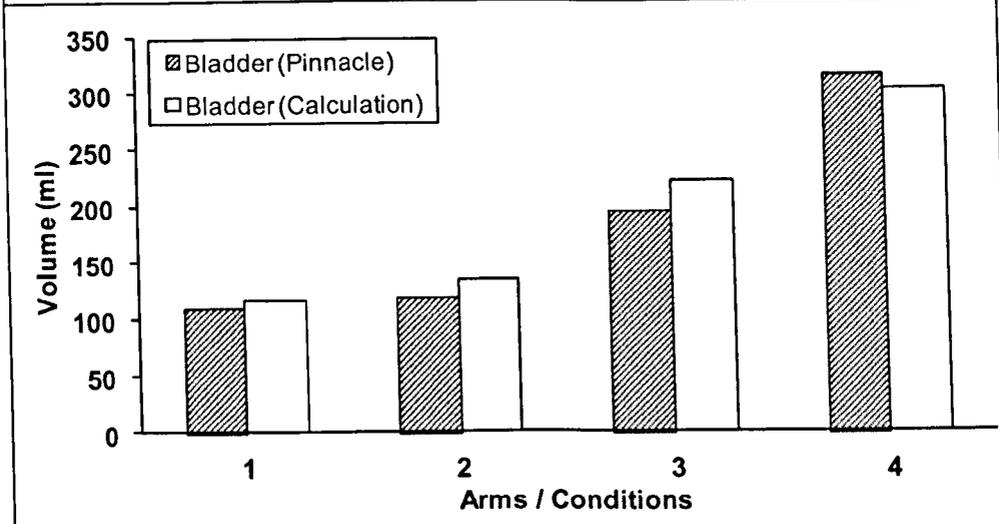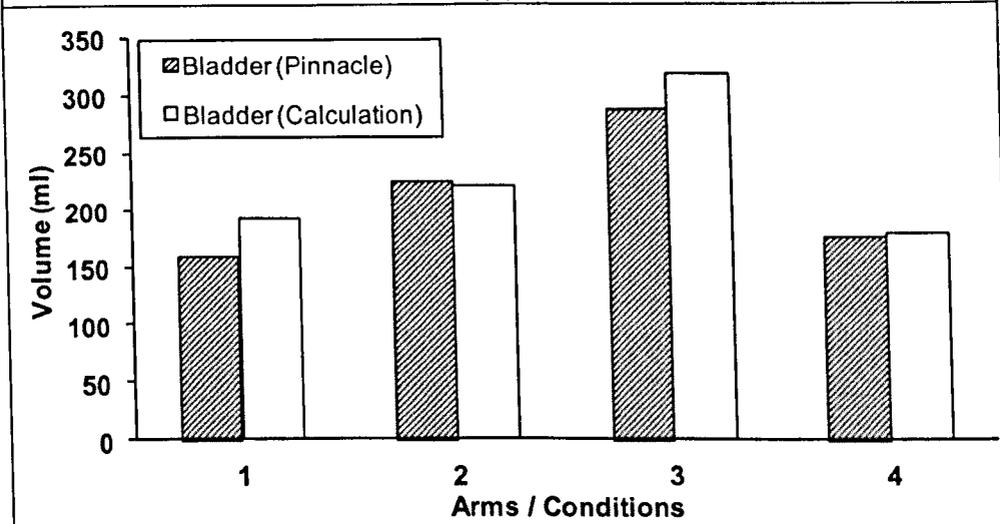
Figure 3.9 Bladder volume of each subject over the four conditions. (a) Subject-1, (b) Subject-2 and (c) Subject -3. Evaluation between Pinnacle volume data, and equation calculation used to estimate volume.

3.4.3 Multiple patients data and analysis

Table 3.1 Bladder dimension data for a larger group of subjects over four different conditions (Arms). N.B All displacements are in millimetres.

		Arm 1	Arm 2	Arm 3	Arm 4
1	Bladder Volume (ml)	187	156	119	136
	X	81	72	60	67
	Y	95	90	88	86
	Z	53	52	45	50
2	Bladder Volume (ml)	108	116	193	314
	X	71	72	75	83
	Y	80	91	101	111
	Z	30	32	49	60
3	Bladder Volume (ml)	157	224	287	176
	X	80	84	92	80
	Y	86	91	99	88
	Z	50	54	67	50
4	Bladder Volume (ml)	48.8	90.3	174.5	102.9
	X	50	63	80	68
	Y	69	80	79	70
	Z	27	36	49	46
5	Bladder Volume (ml)	73.1	97.8	78.2	63.3
	X	65	61	60	58
	Y	72	68	61	60
	Z	30	41	40	41
6	Bladder Volume (ml)	63.4	114.3	63.5	86.7
	X	53	74	53	61
	Y	78	87	78	87
	Z	35	36	35	33
7	Bladder Volume (ml)	180.8	139.4	105.2	229
	X	73	70	60	75
	Y	97	89	88	90
	Z	49	50	40	65
8	Bladder Volume (ml)	127.8	109.2	90.3	96.9
	X	64	62	60	60
	Y	89	80	80	85
	Z	56	42	30	35
9	Bladder Volume (ml)	57.6	109.9	70.7	93.4
	X	67	80	80	80
	Y	81	110	84	92
	Z	26	31	21	30
10	Bladder Volume (ml)	97.8	65.6	59.6	114.6
	X	66	60	55	67
	Y	62	52	52	64
	Z	50	41	40	61

The procedure developed and validated based a selected small group of subjects has been applied to a relatively larger group of subjects based on available data to

establish the trend and investigate the intra and inter patients difference. The data of the bladder dimensions were listed in Table 3.1 and plotted in **Figure 3.10**.
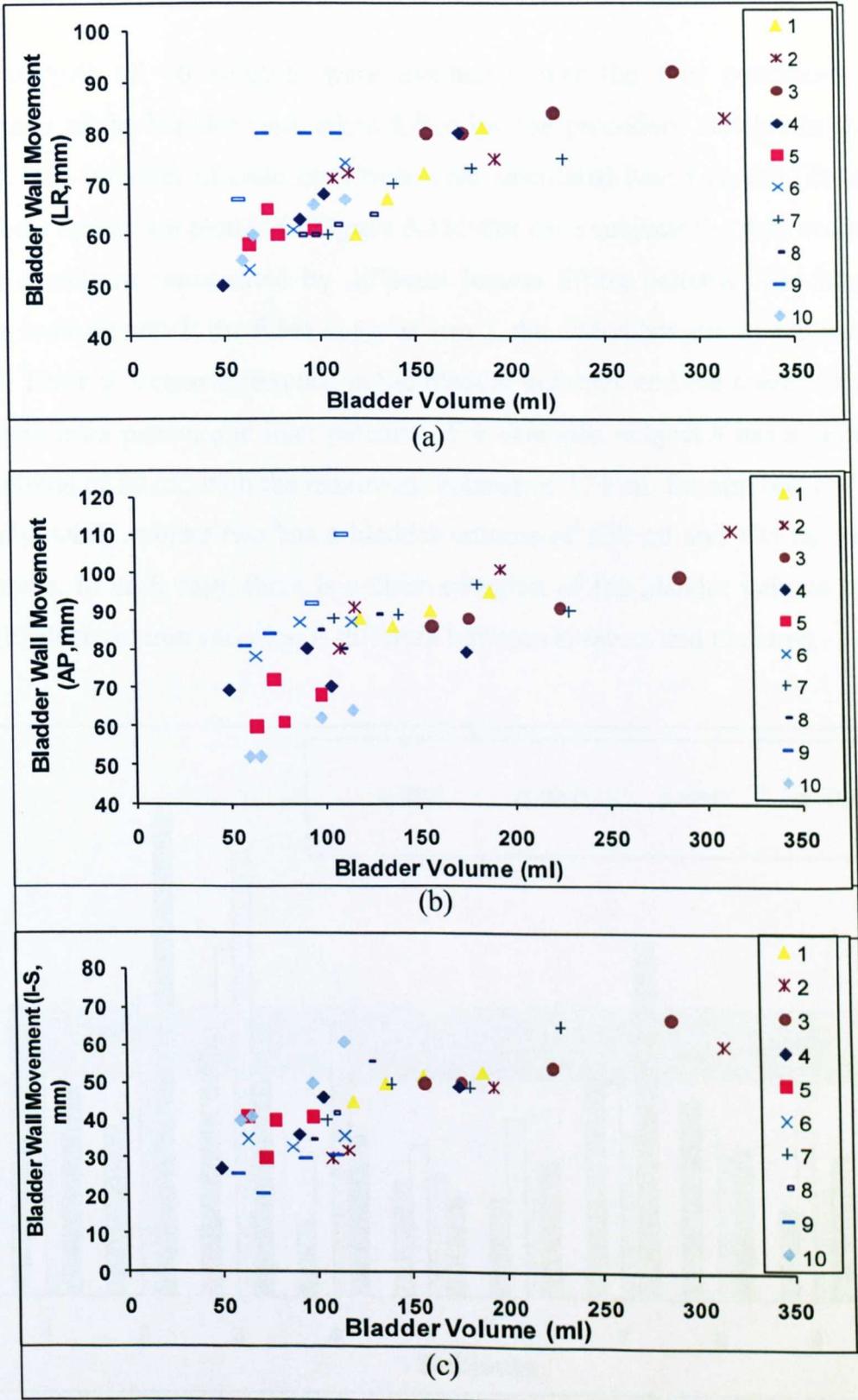
Figure 3.10 Maximum variation of the bladder dimensions with an increase of bladder volume. (a) Subject One, (b) Subject Two and (c) Subject Three. Bladder

wall movement between four arms measuring Left to Right, Anterior- Posterior and Inferior to Superior using CT images imaged using the transaxial plane.

For this analysis all 10 subjects were evaluated over the four conditions. The measurements of the bladder were taken following the procedure detailed in section 3.4.2 & 3. The volumes of each condition were calculated based on the (Equation, 3.4.1) and the results are plotted in **Figure 3.11.** For each subjects the data covers the four arms/conditions represented by different legend filling patterns. The diagonal striped bar indicate arm 1, the filled in bar is arm 2, the dotted bar arm 3, and the open bar arm 4. There is a clear difference in the bladder volumes and the average bladder volume, both intra patient and inter patients. For example, subject 4 has a minimum bladder volume of 50 ml, with the maximum volume of 174 ml, for arm one and three respectively, while subject two has a bladder volume of 108 ml and 193 ml for arm one and three. In each case, there is a clear variation of the bladder volume but the extent of bladder volume variation is different between subjects and the arms.
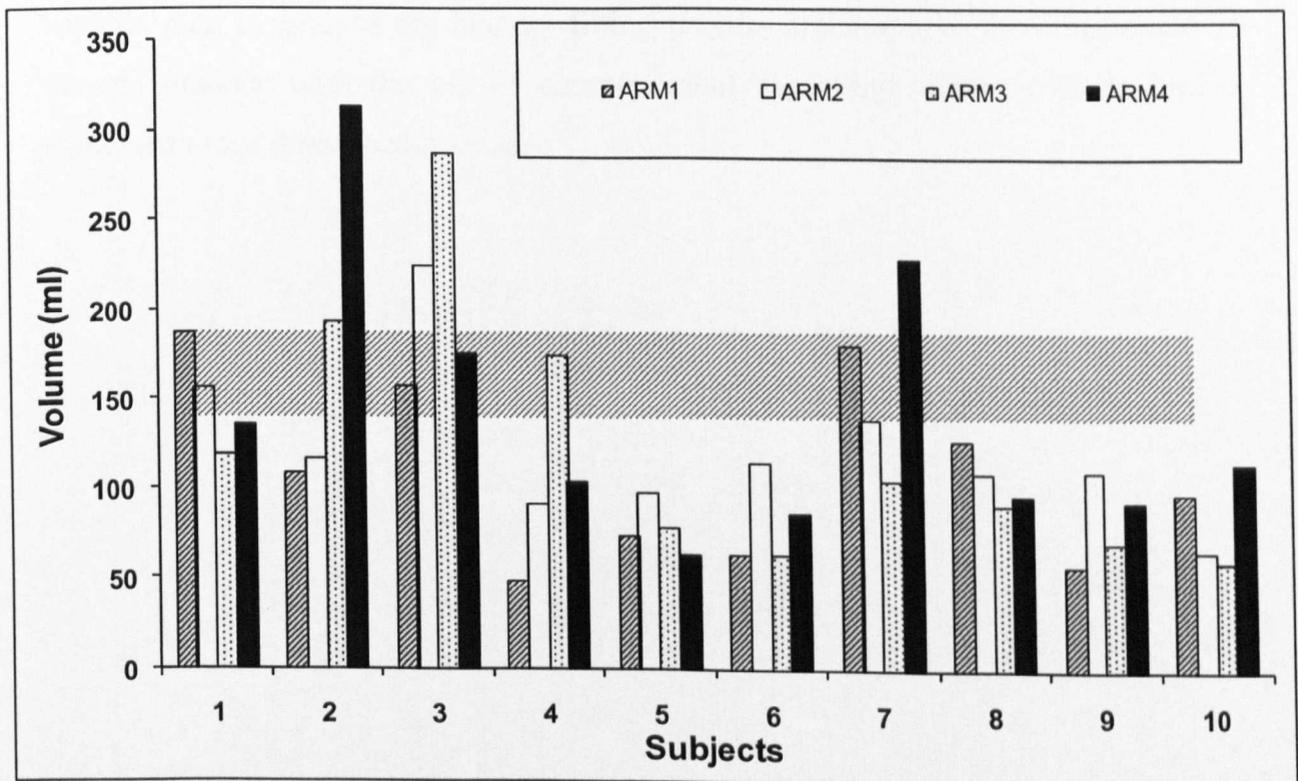
Figure 3.11 Systematic data of the Bladder Volume between arms, of a group of ten subjects.

This conclusion is further represented in **Figure 3.12**. The graph shows the average bladder volume of the subjects and the upper and lower limit was calculated to represent the bladder volume variation. These averaged data showed a clear inter subject differences in the volume data. The average bladder volume was quite similar for six subjects (i.e. subjects 4, 5, 6, 8, 9, 10); however the variation of bladder volume, for each of the subjects, was significantly different. Large variations in bladder volume could be due to various factors, the possibility of the radiation exposure could have promoted urinary hesitancy, this affects people of all ages, but it is most common in older men with enlarged prostate glands, thus promoting increase of bladder volume. The extent of bladder volume variation was further calculated by the percentage as is plotted in **Figure 3.13** as shown in the data, the variation can be as high as to 72%, calculated from the average value of the bladder volume. An important conclusion suggests that even though the bladder is treated as being full, the actual overall volume, for subject bladder, can vary by as much as 206 ml (variation of 109%) over a prolonged length of time. The variation is random with time as the same protocol was administered for each scan. These would provide important subject specific data to analyse the bladder filling process and improve the consistence of clinical practice with the aid of computational modelling. These will be further evaluated in the discussion section.
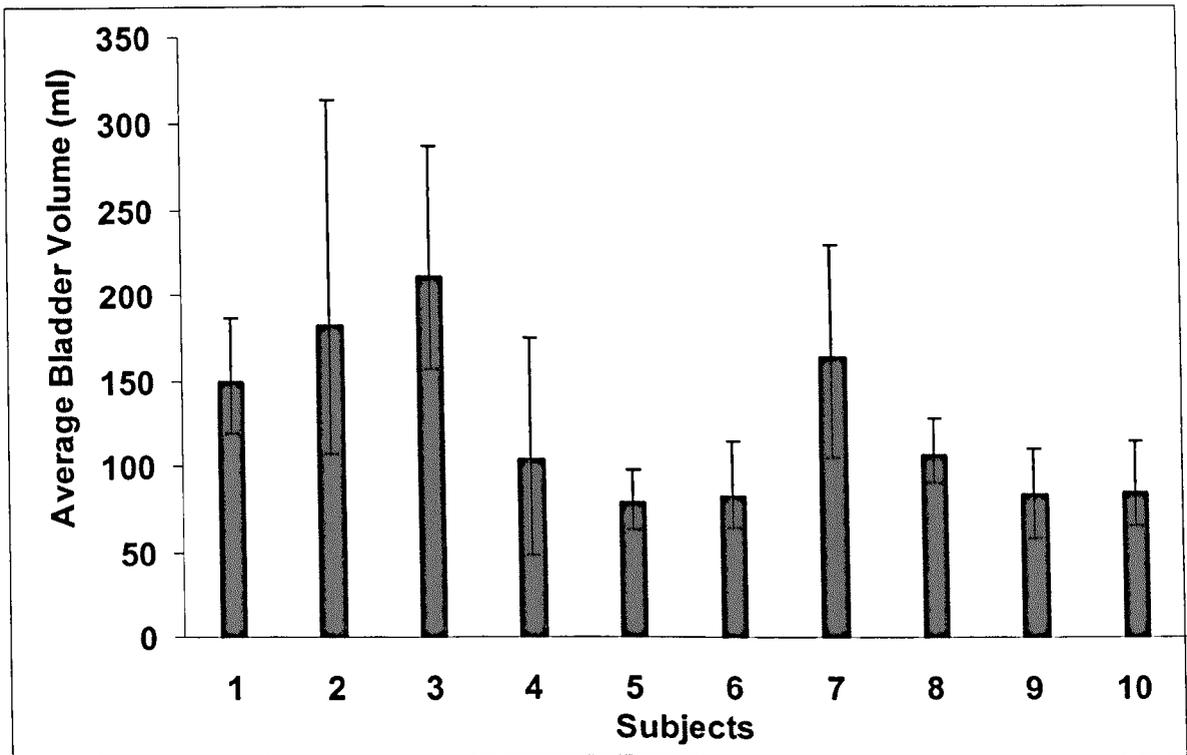
Figure 3.12 Average of the Bladder volume and upper limit and lower limit.
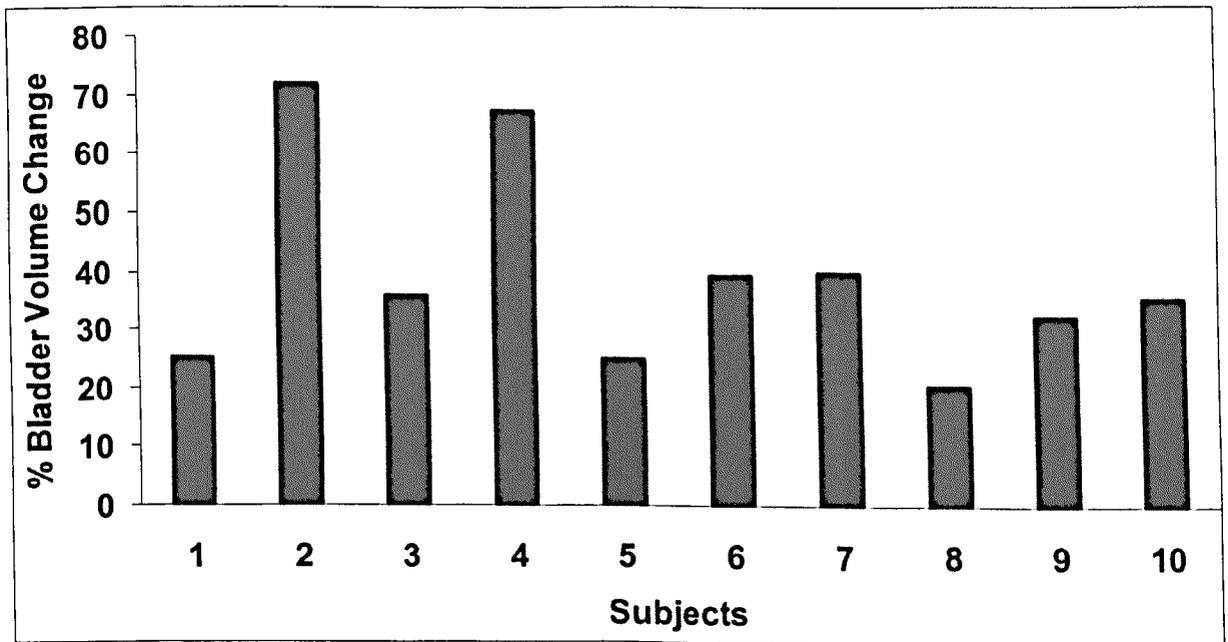
Figure 3.13 Variation of the bladder volume in percentage taken from the average volume showing the inter-subject difference.

3.5 Prostate dimension and its positional change with different bladder volume

3.5.1 Measurement of prostate dimension and results

Figure 3.14 shows the dimensions of the prostate for three selected subjects over four conditions. The legend bar with diagonal strip filling represents the LR (X). The legend bar with solid fill represents the AP (Y). The legend bar with dotted filling represent the SI (Z) wall distance. There is slight variation of the dimension change but not significant differences. **Figure 3.15** shows the volume of the prostate throughout the four conditions over the 10 subjects. Intra subject analysis indicates that there is a minor change to prostatic volume. Inter subject comparisons shows that there is a difference in prostate volume per subject. The maximum discrepancy resulted in an overall volume difference of 30 ml, indicating that the prostate gland is geometrically different between each subject. There is slight variation of the volume change but is not deemed significant. The data suggests that through the treatment prostate volume was not significantly affected from radiotherapy. This agrees with some published work (Deurloo *et al*, 2005). The minor discrepancy can be explained by outlining errors, as the prostate could not be covered fully due to the thickness effect of the scans.
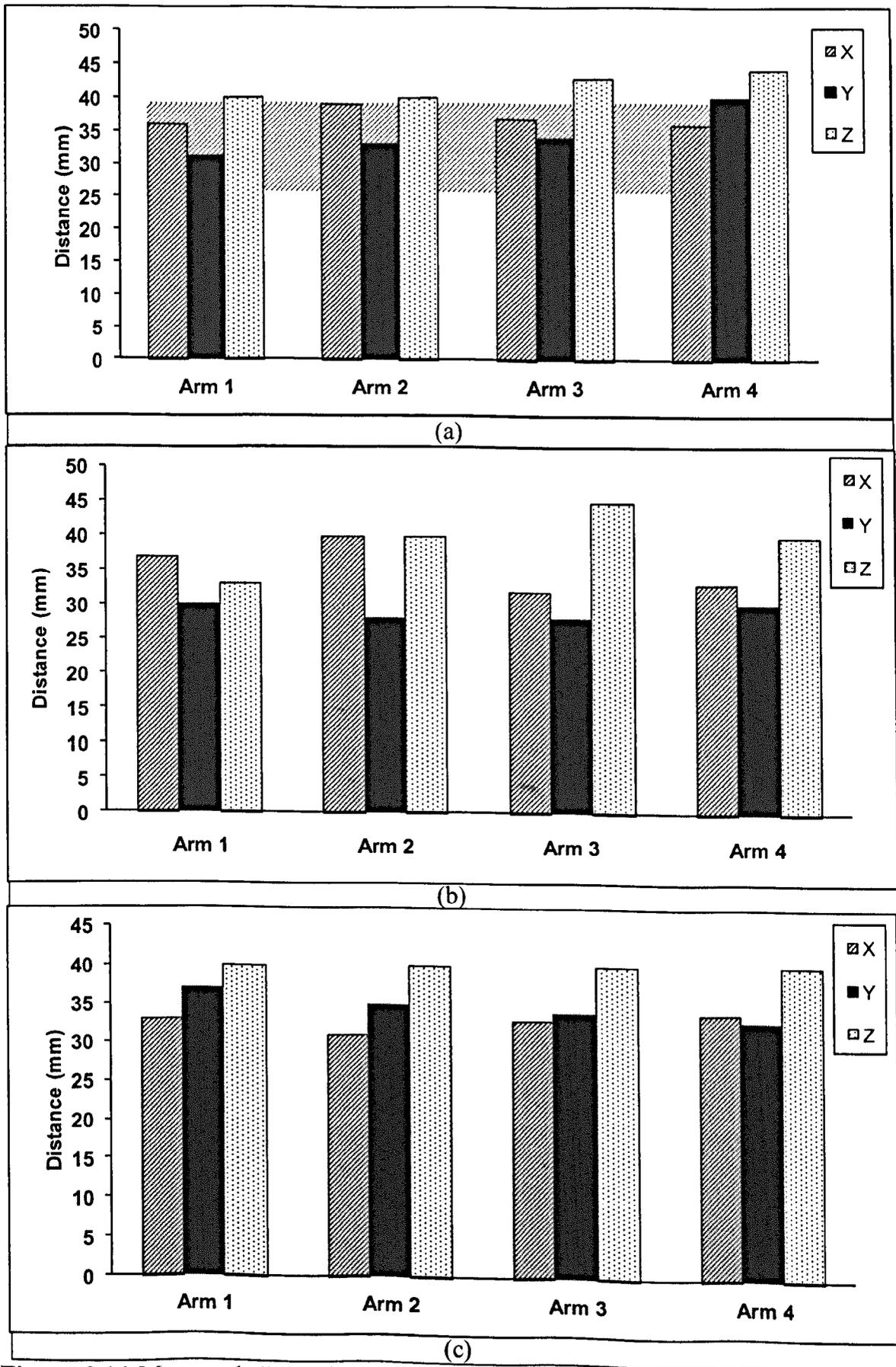
Figure 3.14 Measured dimensions (X,Y,Z axis) of the prostate compared over four arms for (a) Subject-1, (b) Subject-2, and (c) Subject-3.
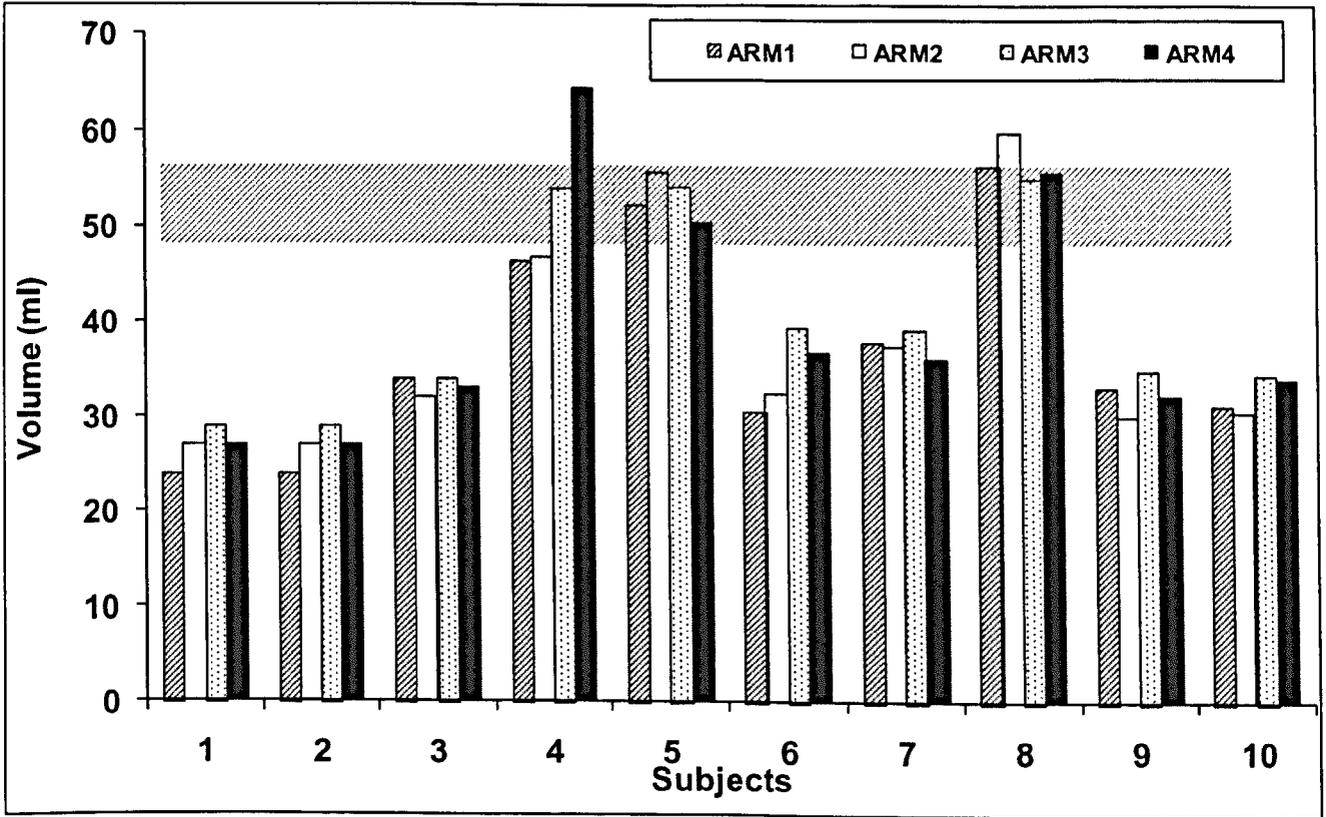
Figure 3.15 Typical prostate volume for ten subjects over the four conditions.

3.5.2 Measurement of the positional change of the prostate and results

An analysis of prostate displacement is done using the bony anatomy as a reference point to track the prostate displacement. As shown in **Figure 3.16,** the prostate distance taken from anterior margin of the pubic symphysis in the mid-sagittal plane to the centre of the prostate. This is adapted from a study by Villeirs *et al* (2004) using a combination of transaxial and sagittal images, bone apex is marked and a reference point is created. Initial trials of measurement were tested. For example the pubic symphysis inferior and mid pubic symphysis were used as a reference point. However the inferior pubic symphysis misses the target area (prostate centre), making measurements difficult to repeat. Mid pubic symphysis could measure prostate displacement; however it is difficult to accurately find the reference point. Based on preliminary trials, among the potential approaches such as apex point, centre of mass etc), this method represents a most consistent measurement as it gives a full coverage of the prostate and the apex point is roughly in line with the prostate, it is a similar height to the bone, and is approximate to prostate gold seed positions. As all subjects have sagittal plane data anterior - posterior ("Y" axis) movement can be tracked. The second point of measurement will be the approximate centre of the prostate, commonly where gold seeds are inserted.
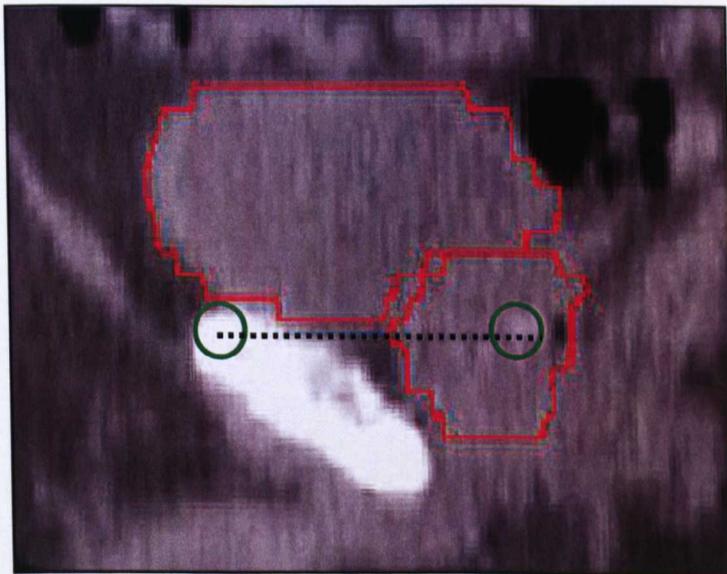
Figure 3.16 The method used for measuring prostate movement using the apex of the pubic bone as a point of origin and centre of prostate. (Both represented by the circles), adapted from Villeirs *et al* (2004).

Figure 3.17 shows some typical data taken from the three selected subjects corresponding to the images shown in **Figure 3.3**. The distance of these values are relative to the pelvic bone apex, in the "Y" axis (AP) for these values was 56 mm, 58 mm, 60 mm and 61 mm. For subject two, the distance was 60 mm, 65 mm, 64 mm and 69 mm. while for subject three, the distance is 60 mm, 62 mm, 63 mm and 63 mm. for all three subjects the resultant bladder volume increase promote anterior posterior movement towards/into the rectum. The prostate position was plotted against the bladder volume and is plotted in **Figure 3.18**. These data clearly showed that there is a link with the change of bladder volume and prostatic displacement. These showed that there is a linear relation at lower volume but the effect becomes less significant at a high volume. There is clear inter patient difference in terms of the trend. For each individual subjects, there is a correlation but the correlation based on the statistic data was rather weak.
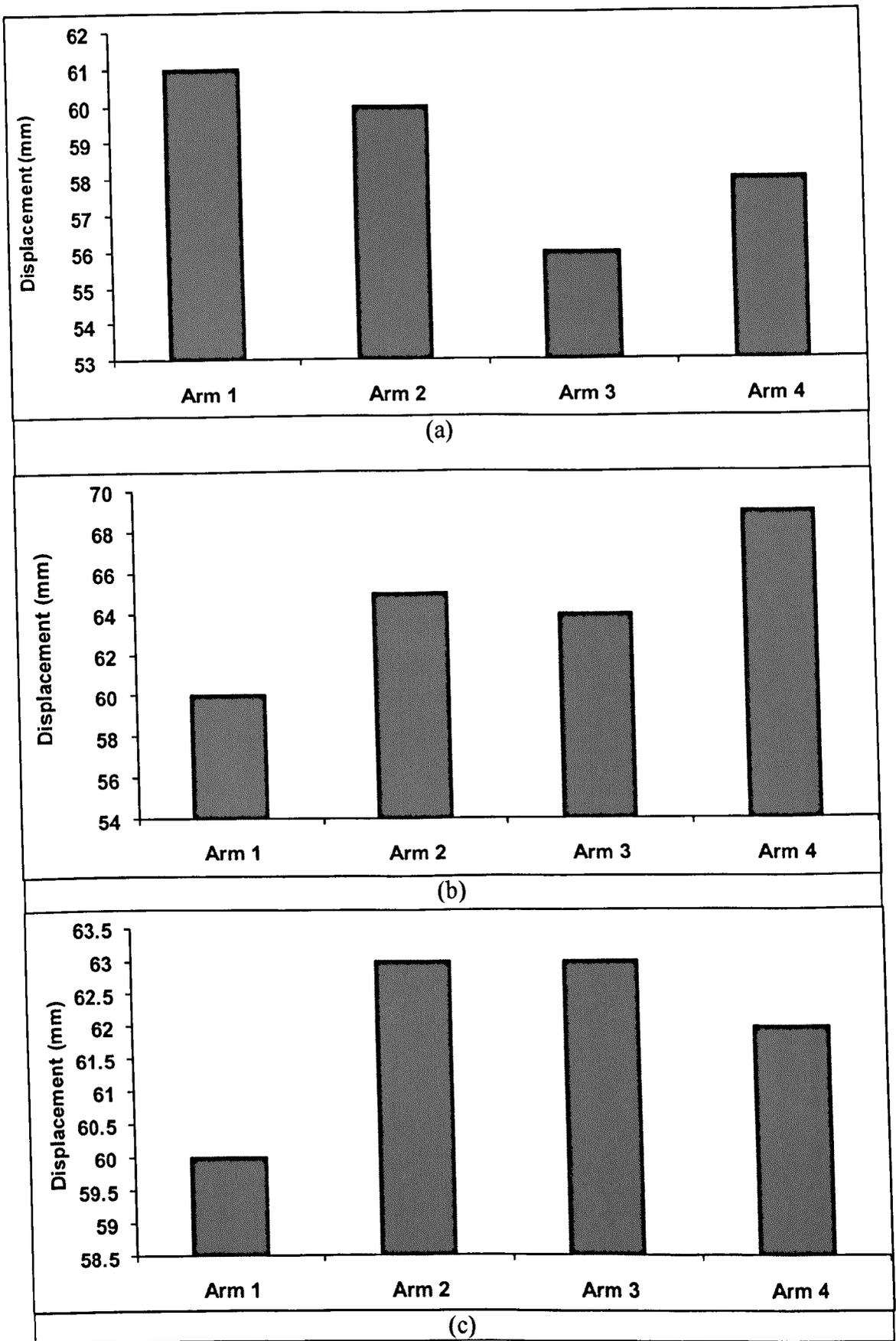
Figure 3.17 Measured distance of prostate A-P compared to changing bladder volume (taken from centre of prostate sagittal plane) using (a) Subject One, (b) Subject Two and (c) Subject Three.
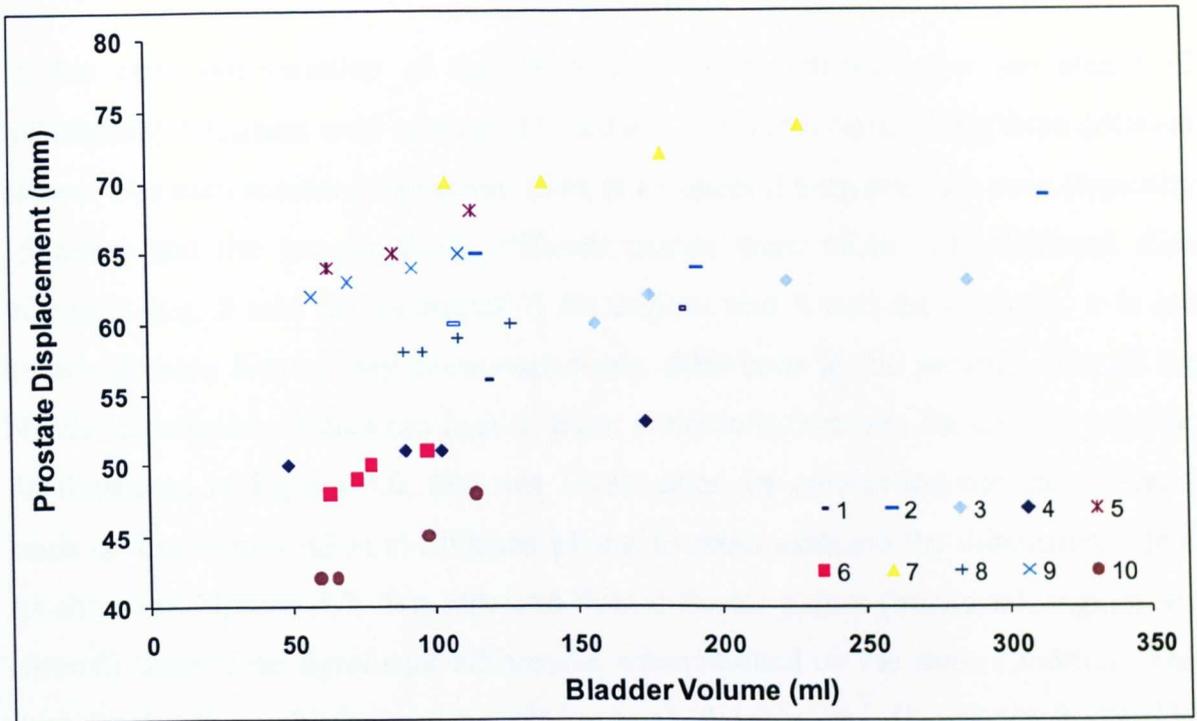
Figure 3.18 A-P prostate distance with the increase in bladder volume, for ten subjects over four arms.

3.6 Discussion

In this work the variation of the dimensions of the bladder over the course of radiotherapy treatment were measured based on CT images taken along three different planes. For each scanning operation, there is an interval between each scan (typically 15 mins) and the images along different planes were taken with different slice thickness (e.g. 3 mm for transaxial; 6 for sagittal and 4 mm for coronal). It is not known if these factors may cause significant difference in the measurement of the bladder dimensions, which has been a major concern/uncertainty for clinical practice. As illustrated in **Figure 3.6**, this was investigated by conducting the measurement made on the images taken at different planes to cross examine the dimensional data. As shown in **Figures 3.7**, data obtained from different planes (transaxial, sagittal and coronal) showed no significant differences when studied on the same condition. This suggests that the multiple scanning approach is a feasible way of studying the bladder volume changes and it would give much more robust data given the nature of CT scanning and many factors may affect the scanning process (such as water intake, patient position, uncertainty of the slice position). This represents a better approach than measurement purely based on transaxial planes

In this work, the analysis was conducted on three selected subjects first to evaluate the methodology then extend to a larger group of 10 subjects whose data is readily available to the project. The results also showed that there is clear inter subject difference in terms of the bladder volume. As shown in **Figure 3.11**, the smallest bladder volume is ~50 ml while the largest bladder is over 300 ml. Due to the highly subject dependent nature of the bladder dimension, directly comparison between data taken at different subject groups are not feasible, however, the overall bladder dimension and volume data **(Table 3.1 and Figures 3.11)** are in a reasonable agreement with some published data.

For example, Pinkawa *et al,* (2007) reported that bladder volume is in the range of 56 ml - 300 ml; Lebesque *et al,* (1995) reported that bladder volume is in the range of 94ml – 317 ml. Empty and full bladder dimensions are also taken for subjects. For example, Tsai *et al,* (2009) reported that on average full bladder wall A-P, S-I and L-R is 67mm, 56mm and 78mm respectively. The bladder volume is associated with many factors such as age, obesity, tumours etc. The fundamental reason of inter subject differences is not the main focus of this work, however, the result highlight the challenging nature of radiotherapy planning and the importance of improved understanding of the mechanics of bladder filling process.

One key focus for this work is to establish the variation of bladder volume and shape during the course of the radiotherapy. The bladder volume data **(Figure 3.11)** clearly showed that, despite the fact that every subject has followed the same protocol of fluid intake, there is still a clear variation of the bladder volume during the course of radiotherapy treatment (scan at different time). As shown in **Figure 3.12 & 3.13**, the bladder volume varied from 20% to 70% depending on the subject. These variations indicates that a subject based approach may potentially be a more effective approach rather than based on average data when studying the bladder filling process and subject specific modelling will provide a better insight into these process. The deformation of bladder is a complex process, which needs to be represented by some practically measurable parameters. In this work, the maximum wall distance has been measured representing the bladder dimensions. This is commonly used in clinical studies as the main focus of the work is the wall movement and its interaction with the surround tissues. Several clinical studies have been performed in order to observe bladder shape and wall movement during the filling process (Roeske *et al,* 1995; Kristiansen *et al,* 2004; Villeirs *et al,* 2004). For example, studies by (Damaser *et al,* 1995; Pinkawa *et al,* 2006) quantify bladder expansion using anterior posterior, superior inferior and left right movement. Due to subject specific nature of the bladder shape and volume, direct comparison between the data in this work with published work is difficult. However, in general, it showed a similar trend to some published data (Lebesque *et al,* 1995; Pinkawa *et al,* 2007). One significant improvement of the work is the quantitative nature of data for the wall movement and the volume rather

than qualitative. For example, in the work by Pinkawa *et al,* (2006), the bladder volume was represented by both full and empty, which is difficult to establish a quantitative relationship.

Another key focus for this work is to establish the variation of bladder volume and the positional change of the prostate, which was measured mainly based on the images taken at the sagittal planes as shown in **Figure 3.3**. The image is able to provide a clearer view of the relative position between bones and pelvis organs. **Figure 3.19** shows the maximum prostate movement with bladder volume change in the A-P and IS directions. The data obtained for the A-P movement is fairly consistent; the maximum AP movement is in the range of 3 – 9 mm. The data for the IS position of the prostate is less consistent; however, the maximum values is within the range of 1 – 3 mm. Preliminary work of the L-R movement showed very limited movement (within 1 mm), this is in agreement with some published work, L-R movement is restricted due to local anatomical features (i.e surrounding tissues, attachment of the Urethra through the prostate, which stabilises the structure in the LR direction). In general, these data showed reasonable agreement with some published shown in the figure, the change of prostate position is consistent with the volume increase. For example, (Roeske *et al,* 1995) used CT images to evaluate the changes in the location of the prostate, bladder, and rectum during a course of external beam radiation therapy. Quantification of the CM motion was found to be less than 1 mm in the LR direction, whereas motion that ranged from 0–5 mm was observed in the AP and SI directions. In another study, Villeirs *et al,* (2004) used MRI to assess the variability in the location of the prostate during intensity-modulated radiotherapy (IMRT) for prostate cancer. They measured the position of the prostatic midpoint (PMP) relative to the bony pelvis and found that the greatest variability occurred in the posterior (2.6 mm), superior (2.4 mm), and inferior (1.0 mm) directions. These experimental data has helped improving the planning of radiotherapy process by giving a more accurate estimation based on statistic data based on a large group. However, most of the current approach was not able to incorporate the subject differences. As shown in

Figure 3.19 (a-b), there is a clear inter-subject difference in terms of the prostate movement with bladder volume. A detailed quantification of this will further improve the accuracy of determining the position of the prostate. A sensible approach is to develop a subject specific model to simulate the filling process thus predict the prostate movement with bladder filling.
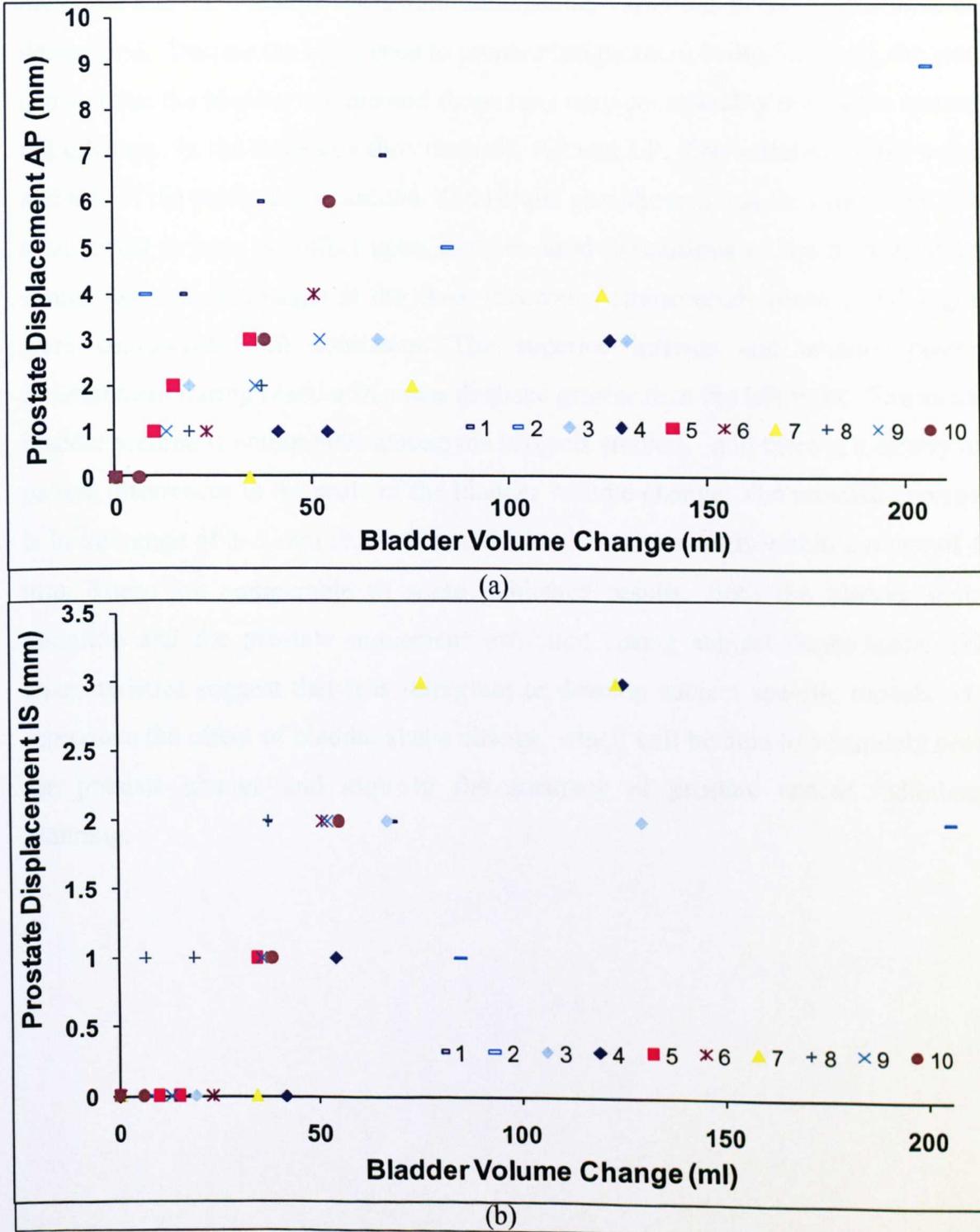
Figure 3.19 A-P prostate movement vs. bladder volume increase (a). I-S prostate movement vs. bladder volume increase (b).

3.7 Summary

In this chapter the variation of the bladder shape/volume and prostate position for ten subjects during the course of radiotherapy has been systematically studied and analysed. The dimensions of the key organs including the bladder, prostate were measured and the potential maximum dimensional variations of the organs have been determined. Despite the adherence to preparation protocol being followed, the results showed that the bladder volume and shape may vary considerably during the course of radiotherapy, in the three key directions SI, AP and LR. The variation of the volume and size of the prostate was limited. The results also showed that the orientation of the scan seems to have no effect upon the measured dimensions of the bladder and the results taken from images at the three directions (transversal, coronal and sagittal) were comparable and consistent. The superior inferior and anterior posterior measurement during bladder increase displace greater than the left right. The variable bladder volume is within 80% among the subjects studied, and there is a clearly inter patient differences in the scale of the bladder volume change. The prostate movement is in the range of 3–9 mm for A-P; and for IS the movement is within a range of 1–3 mm. These are comparable to some published results. Both the bladder volume variation and the prostate movement exhibited strong subject dependence. These characteristics suggest that it is important to develop subject specific models which reproduce the effect of bladder shape change, which will be able to accurately predict the prostate change and improve the accuracy of prostate cancer radiotherapy planning.

CHAPTER FOUR

MR IMAGE BASED FINITE ELEMENT (FE) MODELLING OF BLADDER FILLING AND PROSTATE MOVEMENT

4.1 Introduction

In this work, three dimensional (3D) FE models that are specific to each patient are developed using multiple MR images taken at three scanning planes to simulate the deformation of bladder and investigate the movement of the prostate during the bladder filling process. As shown in **Figure 4.1**, in the first stage, high resolution magnetic resonance imaging (MRI) was performed in the transaxial, coronal, and sagittal planes to provide comprehensive structural details of the bladder and surrounding systems. In the second stage, 3D solid model of key pelvis parts were constructed by contouring the scans with an image processing tool, then, stacking and lofting the slices taken at different planes. The volume of the models build up using images taken at different planes for the same subject were compared to evaluate the advantages and disadvantages of each scanning method and quantify the potential change of bladder volume in between different scans. A complete model was then developed by merging the features from the three models. In the next stage, a 3D assembly of the pelvis system was developed using a slice based positioning process developed. The assembly of the pelvis systems incorporated all the potential structures which may affect the deformation of the bladder and its interaction with the surrounding organs to achieve sufficient accuracy and optimum requirements on the computational resources. The model was validated by comparing the cross-sections of the solid model against MRI slides taken at different planes. Detailed Finite Element (FE) models were then developed incorporating the structural details of key components, and the process of bladder filling was simulated by modelling the physical process of continuous enlargement of the bladder to different volumes, to a level comparable to the bladder volumes change observed during the course of conventional radiotherapy. For validation purpose, the overall bladder deformation was compared with repeated images of a filled bladder that were obtained using computed tomography (CT). The effect of some key Finite Element parameters were systematically examined through ABAQUS parametric studies including: element type, element size and material properties. An optimum meshing scheme was established through detailed mesh sensitivity studies and the materials parameters were identified through ABAQUS parametric studies. The relationship between the changes in the key dimensions of the bladder (wall distances) and the increase in its

volume during the filling process was established. The movement of the prostate in the anterior–posterior (AP), superior–inferior (SI) and left–right (LR) directions, as well rotational movement, was investigated. The relationship between the change in bladder volume and the movement of the prostate and the correlation between the A-P and S-I prostate movements were also established for each patient. Finally, the numerical predictions were compared with published clinical data and the significance of the results for some key clinical practice/procedures is discussed.
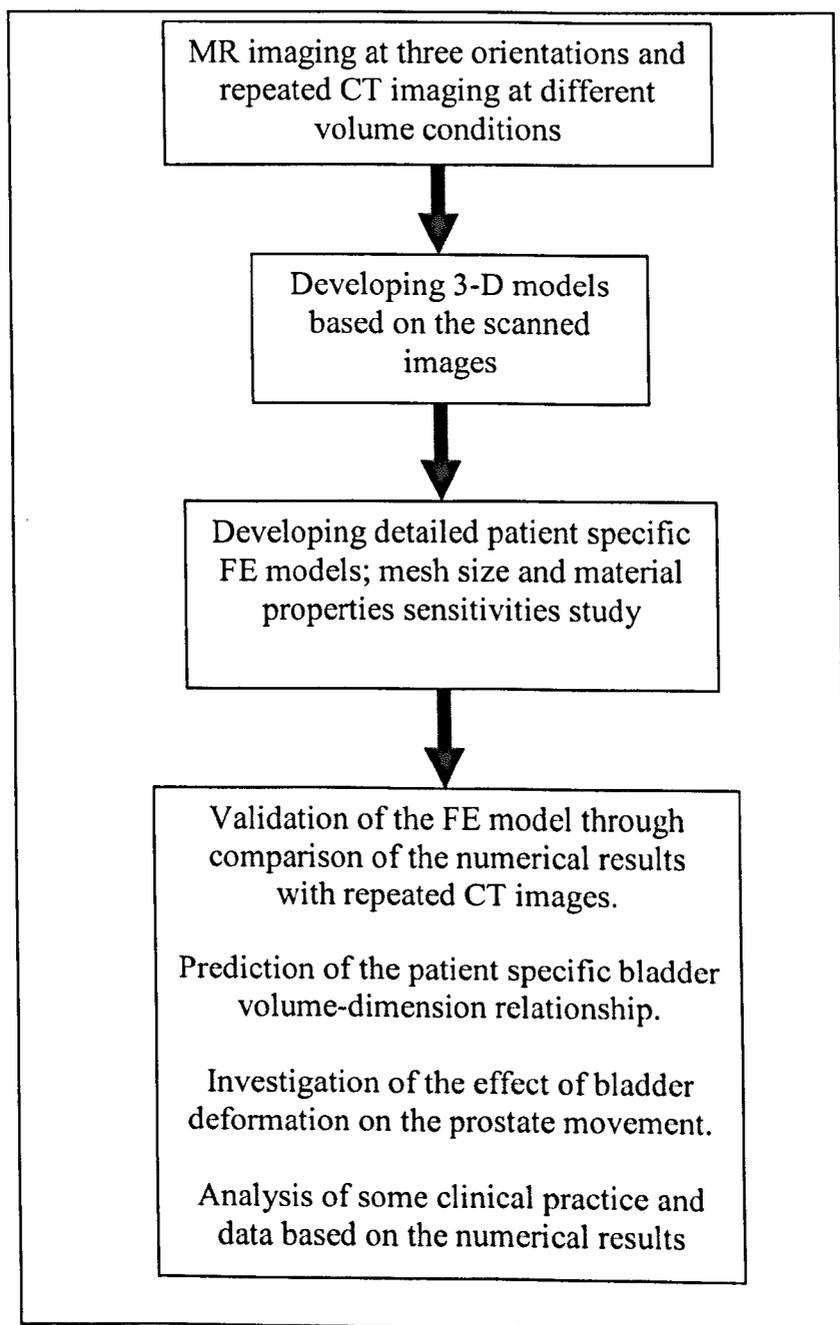

Figure 4.1 Flow chart showing the structure of the imaging and FE modelling work.

4.2 Imaging process and 3-D model development based on scans taken at three principal planes

4.2.1 Imaging procedures and data processing method

The three subjects, who underwent the prostate radiotherapy process, were scanned using MRI and repeated CT imaging. The subjects were asked to empty their bladder, drink 500 ml of fluids before treatment and then wait 20 minutes before scan (CT imaging, full bladder, empty rectum) (ClatterBridge Centre of Oncology Protocol). At each of the points in time they underwent a MR scan with an assumed empty bladder and empty rectum. A special protocol was administered, each of the three subjects was administered a relaxit which empties the rectum before being prospectively evaluated with multiple MRI scans. Each subject was scanned in three different planes (sagittal, transaxial and coronal), as illustrated schematically in **Figure 4.2**. The transaxial plane is parallel to the ground, which separates the superior from the inferior regions, or the head from the feet. The advantage of this viewpoint is that it enables greater coverage of the movement of the organs in the anterior–posterior and the left–right directions. The sagittal plane is perpendicular to the ground and separates left from right; it gives a complete view of superior–inferior and anterior–posterior movement of the organs. The coronal plane is perpendicular to the ground, and separates the anterior from the posterior. It can give full coverage of the superior–inferior, and the left–right movements of the organs.

During the investigation subjects underwent MR and CT scans in the supine position **(as illustrated in Figure 4.2)** on a Philips Medical Systems Intera 1.5 T Whole-Body Scanner. Each MR examination, which included T2-weighted turbo spin echo sequences in the sagittal, transaxial, and coronal orientations, lasted in total for approximately 30–45 minutes (First scan sagittal, transaxial 6min after, coronal 21 min after sagittal). The acquisition matrices for all orientations had a frequency-encoded dimension of 512 x 512 matrix. Each of the scans were performed in supine position with varying slice thickness of 3 mm (transaxial, coronal) and 5 mm (sagittal) from the anal canal up to the sacral promontory. The subjects remained in essentially

the same position on the flat scanner table during the scanning process. The patient's ankle and knee positions are constrained by supports intended to keep their legs in a set position. No bowel or intravenous contrast enhancement was used. The data were transferred to a commercially available stereotactic planning system (Pinnacle, Philips, Germany). The bladder (wall and filling), prostate and rectum wall was contoured in every scan.
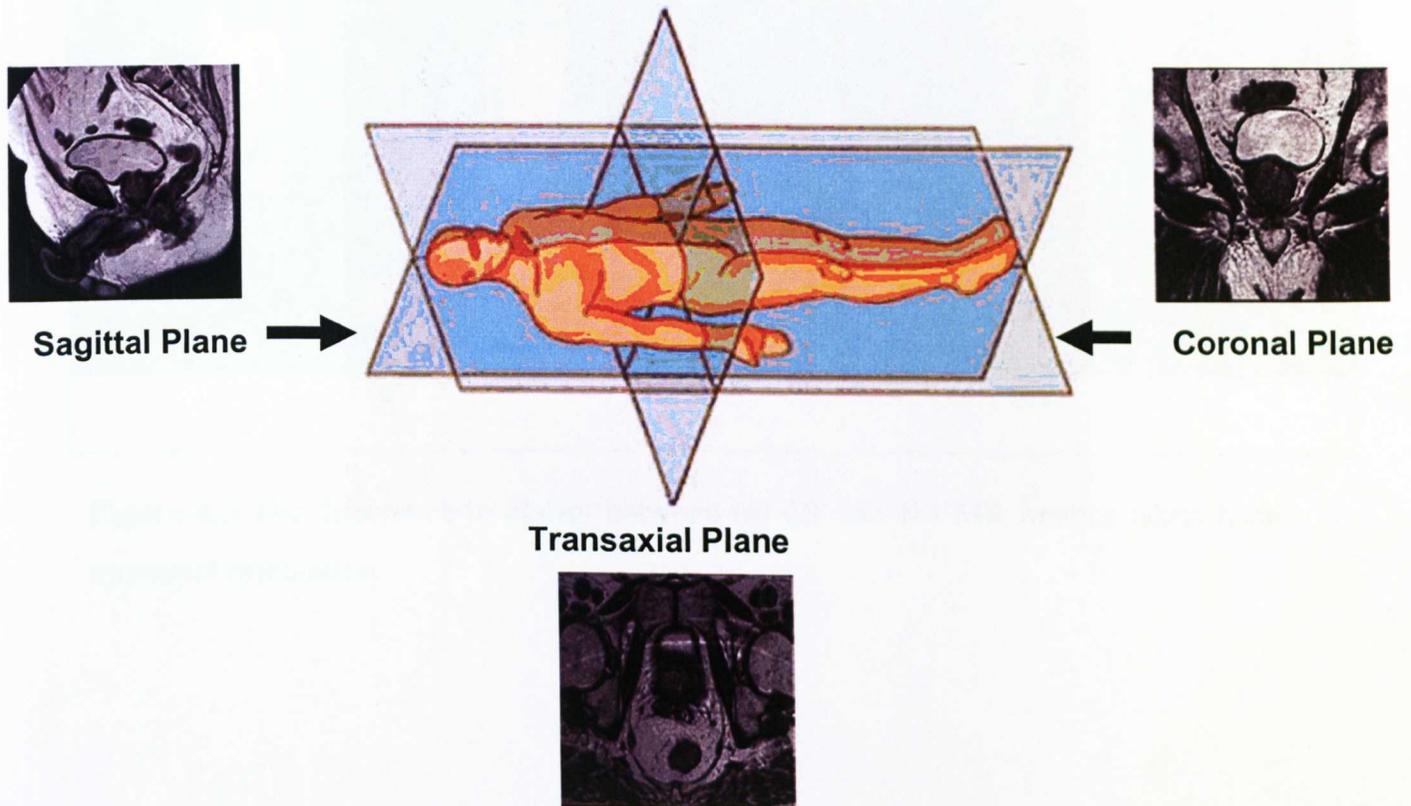
Figure 4.2 Positions of different principal scanning planes used in the imaging process.

The use of MR images could increase the accuracy and resolution for some key components. **Figure 4.3** shows the difference between the CT (a) and MR image (b). The MR image can clearly show the bones, bladder, prostate and the rectum with a much better resolution for the soft tissues than the CT image, which leads to more accurate delineations of both prostate and its boundaries, in relation the bladder and rectum. The CT image could show the bladder, prostate rectum and bones, however

99

the clarity on the tissues is inferior compared to MRI. However, one significant advantage of CT scanning is in the fact that it is much quicker and more economically viable than MRI. An improved understanding of the bladder filling process on the prostate movement could potentially enhance the information obtained from CT images.
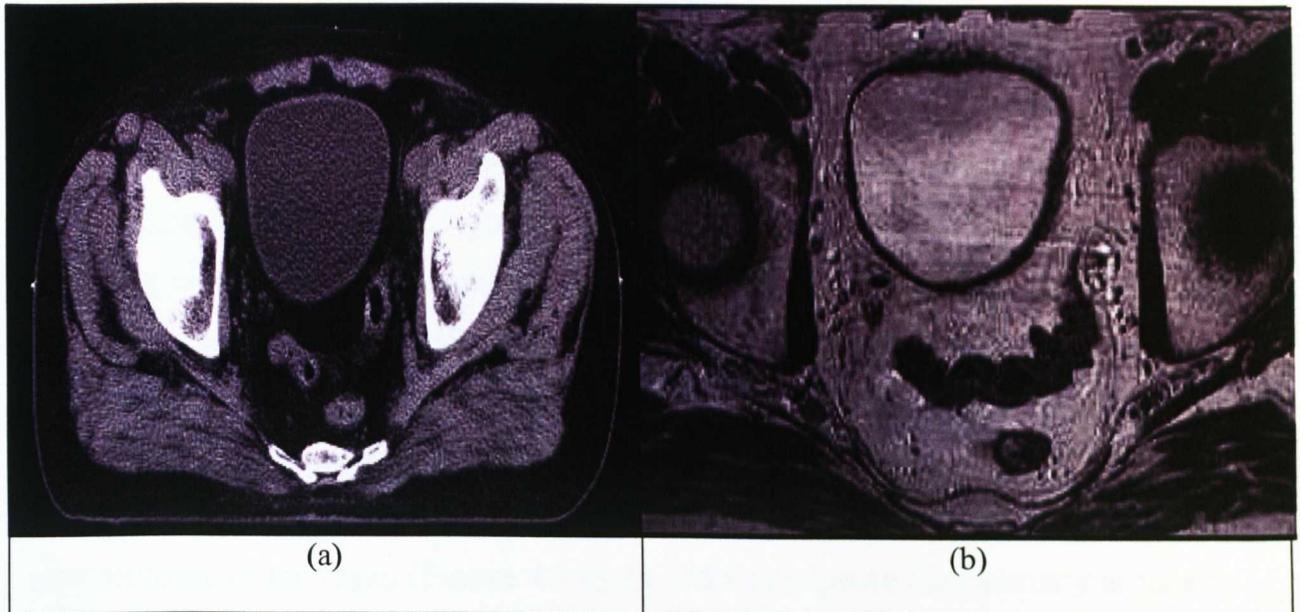
Figure 4.3 The difference in clarity between (a) CT and (b) MR images taken from transaxial orientation.

4.2.2 CAD Model Creation

The MR image slices were exported into an image reading program (DicomWorks, Puech Boussel) where manual outlining of the slice images were created. **Figure 4.4** illustrates the manual outlining process, in which the interface of the intersecting boundary of each organ on the slice was outlined. The accuracy and repeatability of the outlining process has been assessed by comparing the outline taken by the same operator at different times and outlines taken by different operators on the same slice. The results showed good repeatability (results not shown to preserve clarity). Some of the outlining is also verified by a trained oncologist at the collaborating hospital CCO. The point coordinates of the outlining were created for each slice and the 3D model was then created using a 3D modelling software program (Solidworks, 2006), following a similar approach used by (Ganz *et al*, 2006; Boubaker *et al*, 2009). **Figure 4.5** shows the outline contour of each bladder slice for a subject. The loft function was used to link each slice together, eventually creating a 3D image representative of the organ **(Figure 4.5 c)**. In order to improve the geometry accuracy and smoothness of the surface, a fit spline function was used to create curvature between layers at the coordinate points. The process is repeated for other organs and structures such as prostate, rectum and the bones.
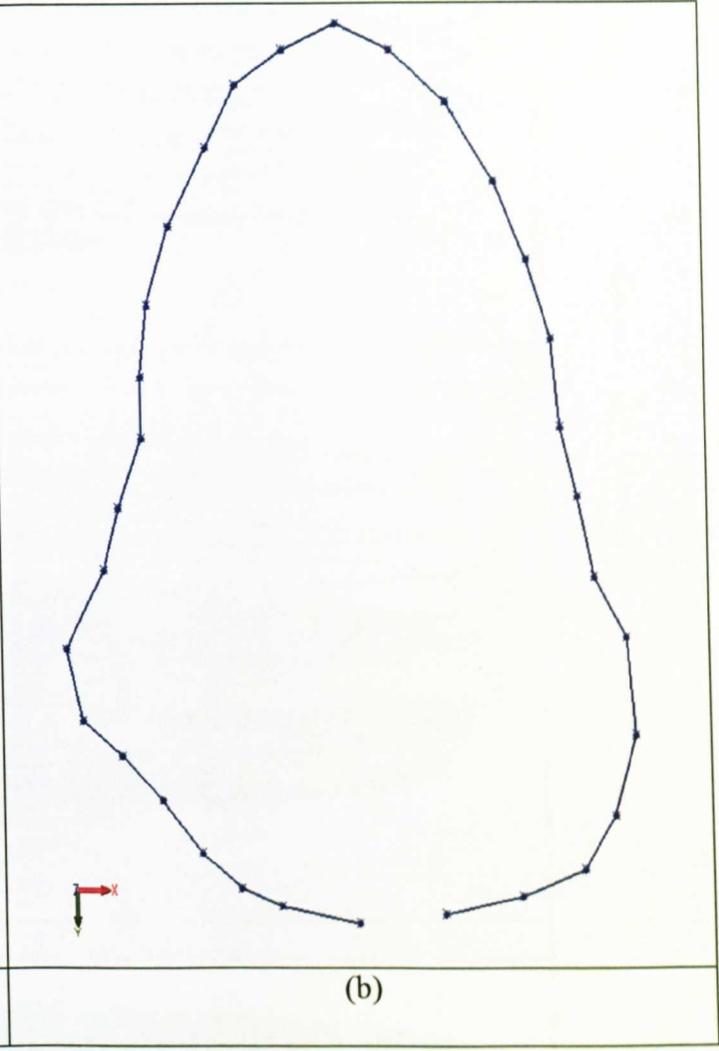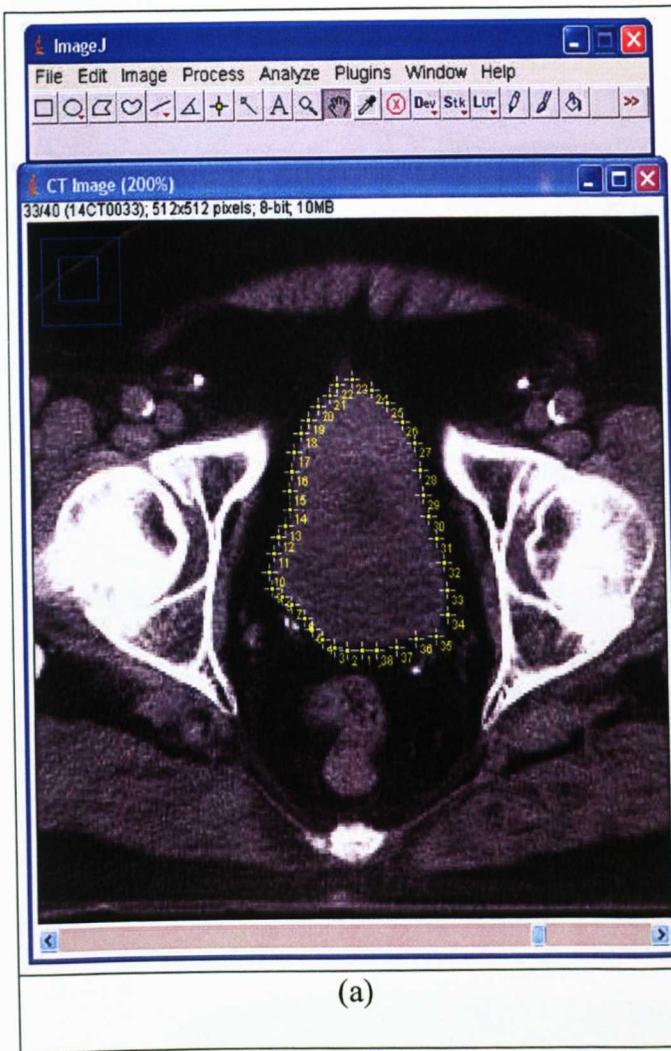
Figure 4.4 (a) Snap shot of image outlining process highlighting the region of interest, in this instance the bladder; (b) Solidworks snap shot of points exported from the outlining program (Image J).

(a)

Profile(Sketch7.)

(b)

(c)
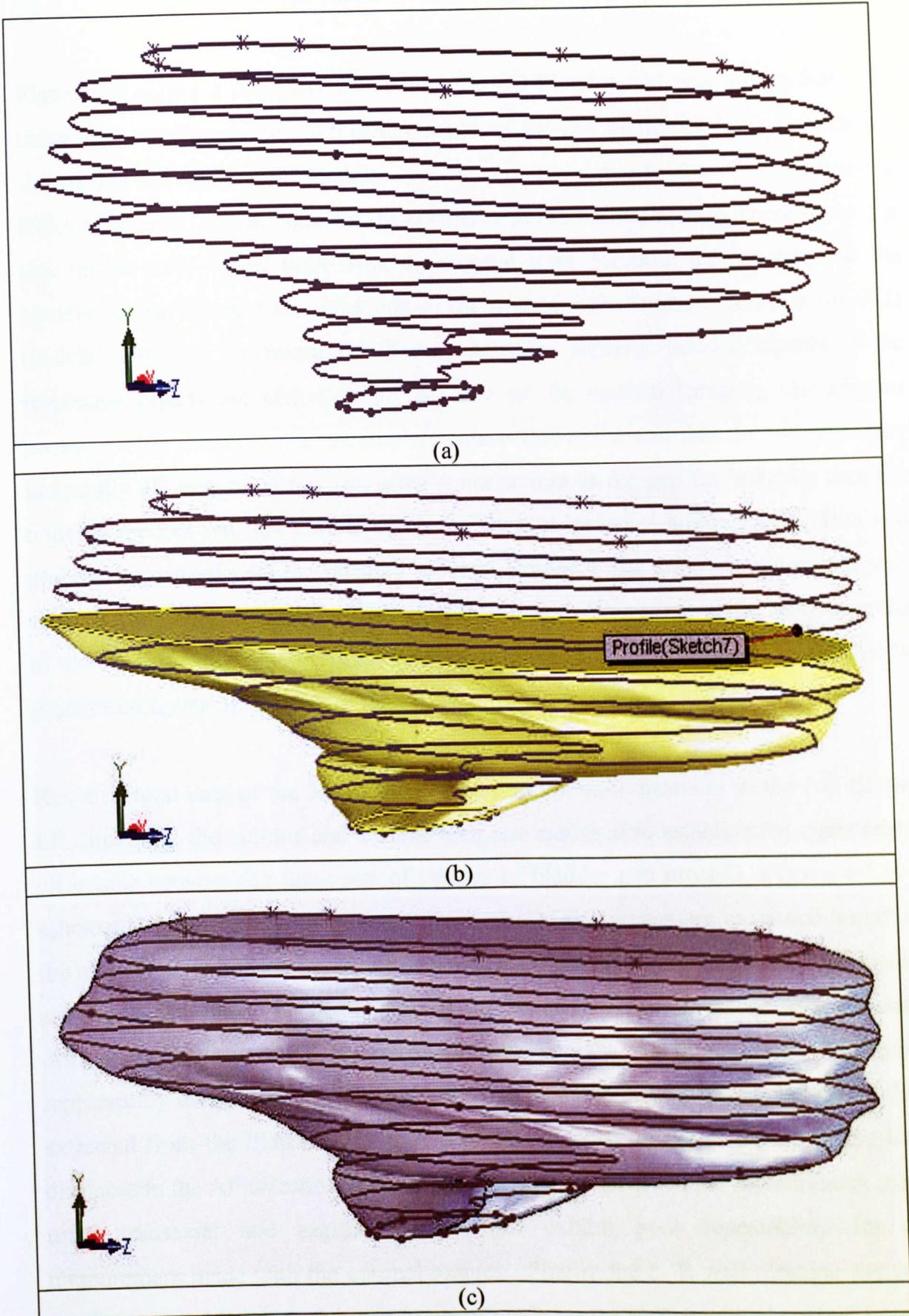
Figure 4.5 (a) Solidworks snap shot showing slices of bladder organ; (b) lofting of the bladder to create 3D model; (c) Full 3D model of bladder.

4.2.3 3D models constructed based on scans taken at different planes

**Figure 4.6** shows a comparison between the 3D bladder and prostate models built using images taken at the three different planes for one of the subjects. It is clearly shown that the some solid models were not complete due to the effect of missing slides by the end, in particular for the coronal and the sagittal model. There was a flat side on the solid model built from the sagittal scan, for both the prostate and the bladder, on the left and the right side of the organs. This is also evident in the 3-D models built with the transaxial slices, where the superior inferior aspects of the respective organs are also flat. In the case of the coronal imaging, the anterior posterior sides are flat. This incomplete data is due to the fact that the MR scans are essentially 2D images. If the final slice is not as thin as the gap for imaging, then the imaging process will not able to catch the slice, therefore a missing slice. This is a problem associated with the imaging process. However, the three set images together would be able to give a full dimension of the organs. This suggests that it is essential to use scans in the three orientations (i.e. coronal, sagittal, transaxial) to be able to produce complete 3D models of the key organs.

Key structural data of the 3D models, including the wall distances in the AP, SI and LR directions, the volume and surface area, are analysed to establish the quantitative difference between the three sets of images of bladder and prostate. **Figure 4.7** is a schematic representation of how the dimension of the organs are measured based on the maximum wall distances of the organ in the three principal directions. The results are shown in **Figure 4.8** demonstrating the accuracy of the measurements for each orientation. For example, the measurements for the SI direction showed good repeatability using the images taken on the coronal and sagittal planes but the SI data extracted from the transaxial images were significantly different. Similarly the wall distances in the AP direction showed good agreement between the measurement made using transaxial and sagittal images, but exhibit poor repeatability for the measurement made with the coronal images. Finally the L–R wall distance was in a good agreement between the measurement made on the transaxial and coronal images but poor repeatability was shown in the data from the sagittal images. These

differences were mainly caused by the slice by slice scanning scheme, but, in general there are no significant systematic differences. In all three cases the measurements taken at various orientations were within a 10% error range. These results suggest that the time interval between the scans has not caused significant structural differences.

A new approach has been developed to produce a complete model of the bladder, and prostate. As illustrated in **Figure 4.9**, the approach is based the transaxial slice with references to the coronal and the sagittal for the SI dimension and shape. The transaxial, sagittal and coronal 3D shapes were merged together using (Solidworks, 2006). The new approach enables an accurate reproduction of an organ using images scanned at the three principal planes instead of the conventional one plane model creation. **Figure 4.9** shows a typical example of the three key organs of interest: the 3D model of the (a) bladder, (b) prostate and the (c) rectum. The bladder and the rectum were created as a hollow structure. This organ thickness was determined by measurements taken from the MR image sets. The thickness measurements values were taken at various organ positions and the average thickness was used. The thickness of the bladder for the three subjects is 3 mm. The thickness of the rectum for the three subjects is 4 mm. The values were comparable to data reported in other published works (Blatt *et al*, 2008). The volume and surface areas of the bladder and prostate were measured and plotted in **Figure 4.10.** The data clearly showed that there is an inter-patient difference of the volumes and surface area of all three organs. The largest variation was with the bladder volume where the prostate volume between subjects was not significantly different. As detailed in section **4.2.1**, clinical procedures have been followed to standardise rectal volume by administering an enema. However, there is still a clear inter subject rectal difference, which is probably attributed to geometrical difference. These differences indicate the importance of using subject specific modelling rather than normalised dimensions, which is the main focus of this work.

(a) Sagittal	(b) Transaxial	(c) Coronal
(d) Sagittal	(e) Transaxial	(f) Coronal
(g) Merged Bladder		(h) Merged Prostate
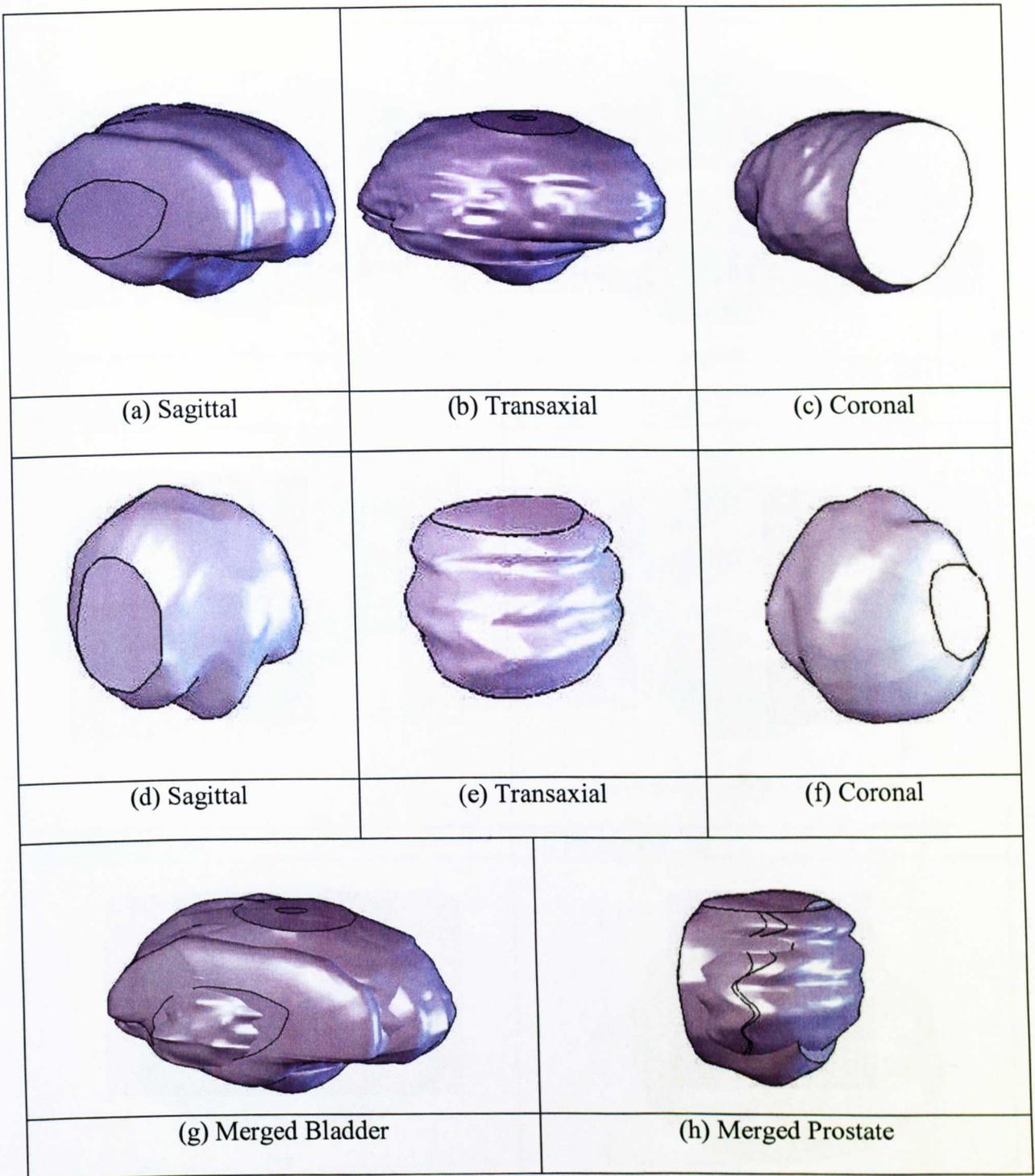
Figure 4.6 Comparison between the 3D bladder (a,b,c) model and prostate (d,e,f) model built using images of a selected subject, taken from three different orientations and the merged models based images from the three orientations of bladder (g) and prostate (h).

(a) Bladder T-AP   (b) Bladder T-LR

(c) Bladder T SI   (d) Prostate T AP

(e) Prostate T LR   (f) Prostate T SI
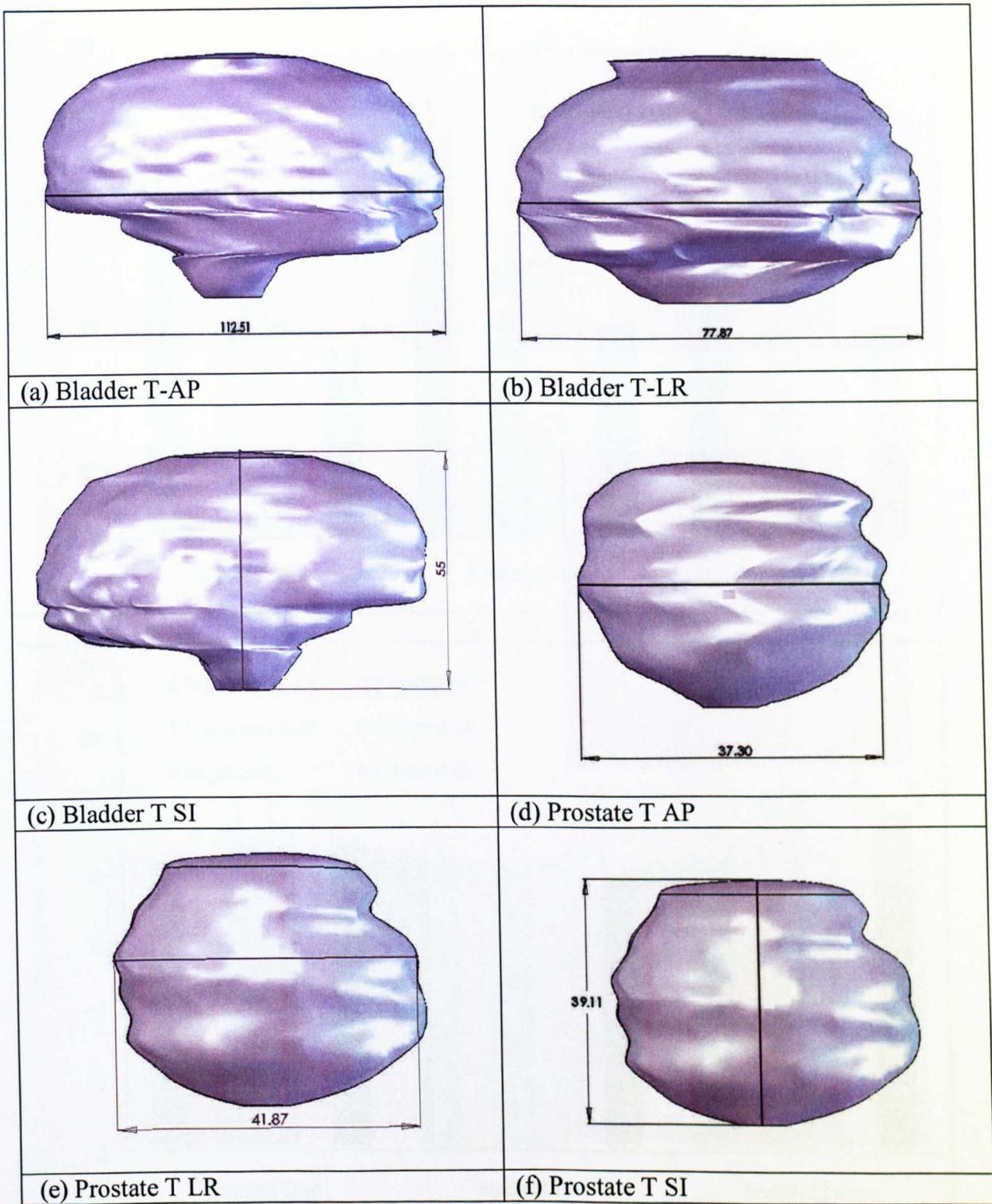
Figure 4.7 Schematic to show the measurements of the 3D bladder and prostate dimension at AP, SI, LR directions.
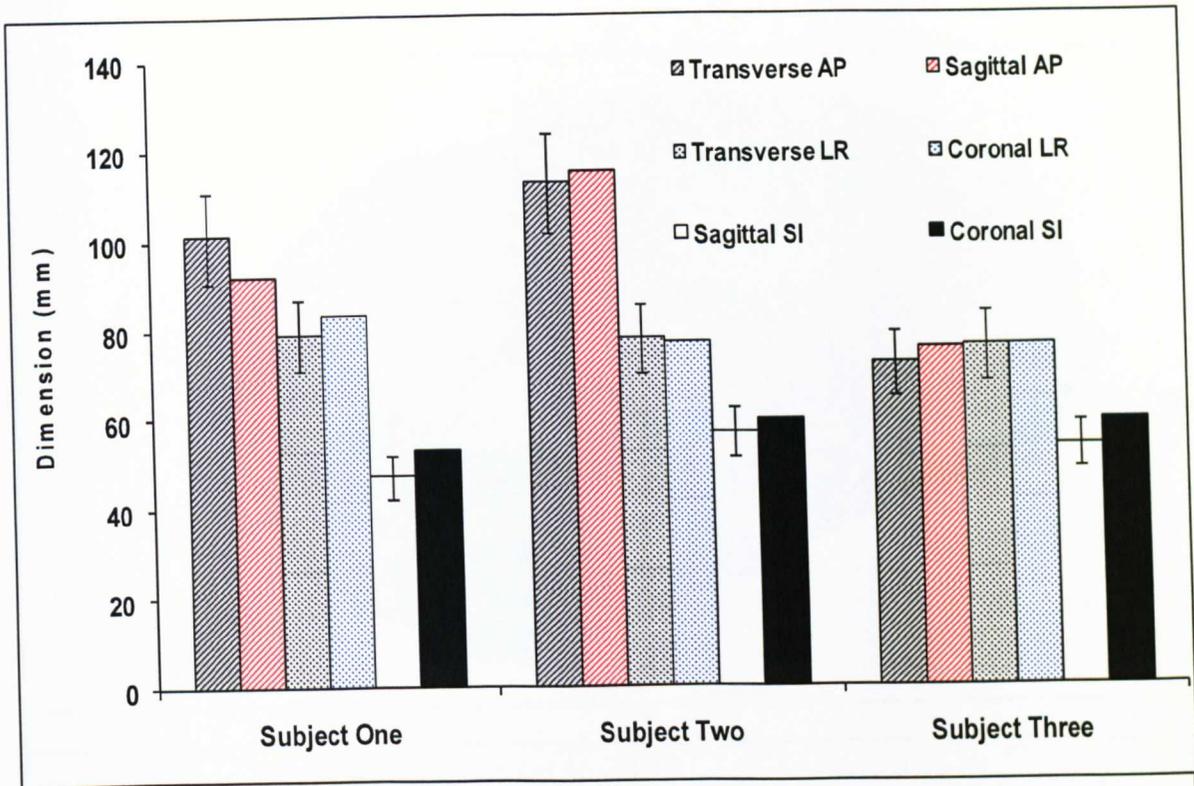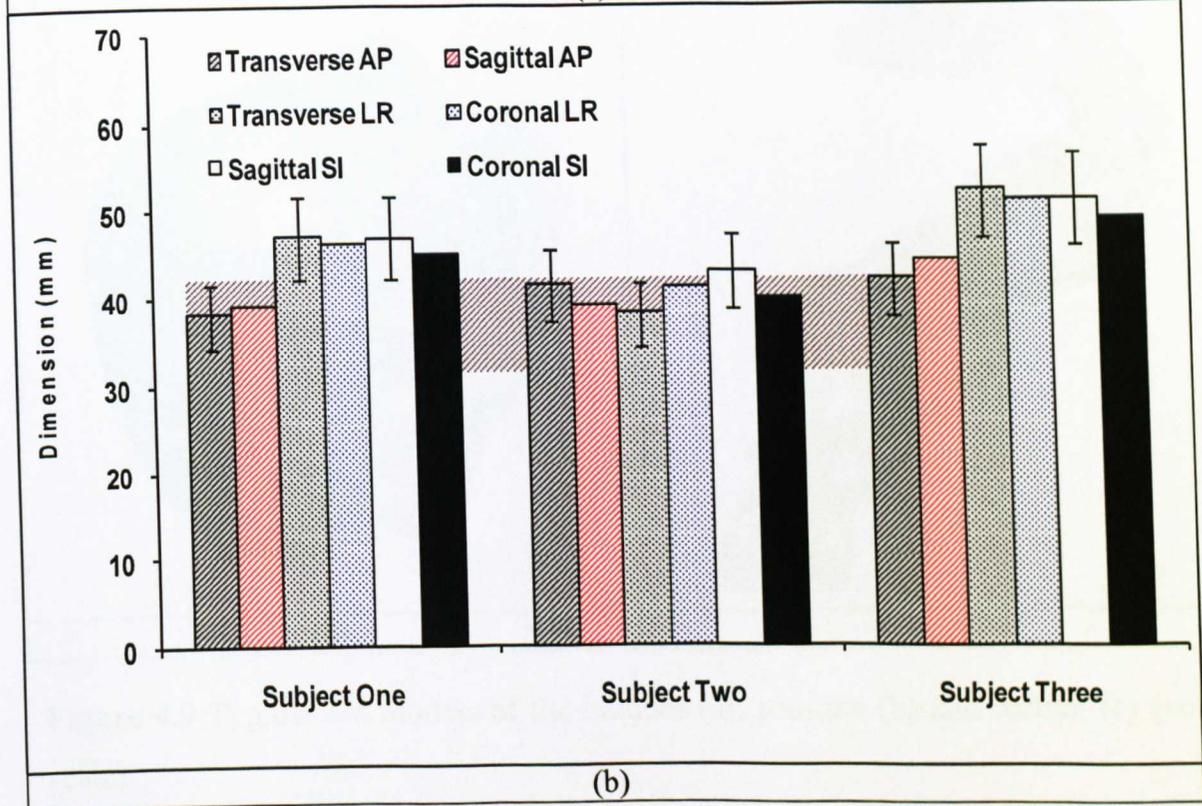
Figure 4.8 Data showing the size of bladder (a) and prostate (b) of the three subjects in AP, LR ad SI directions using transaxial, sagittal and coronal images.

(a)

(b)   (c)
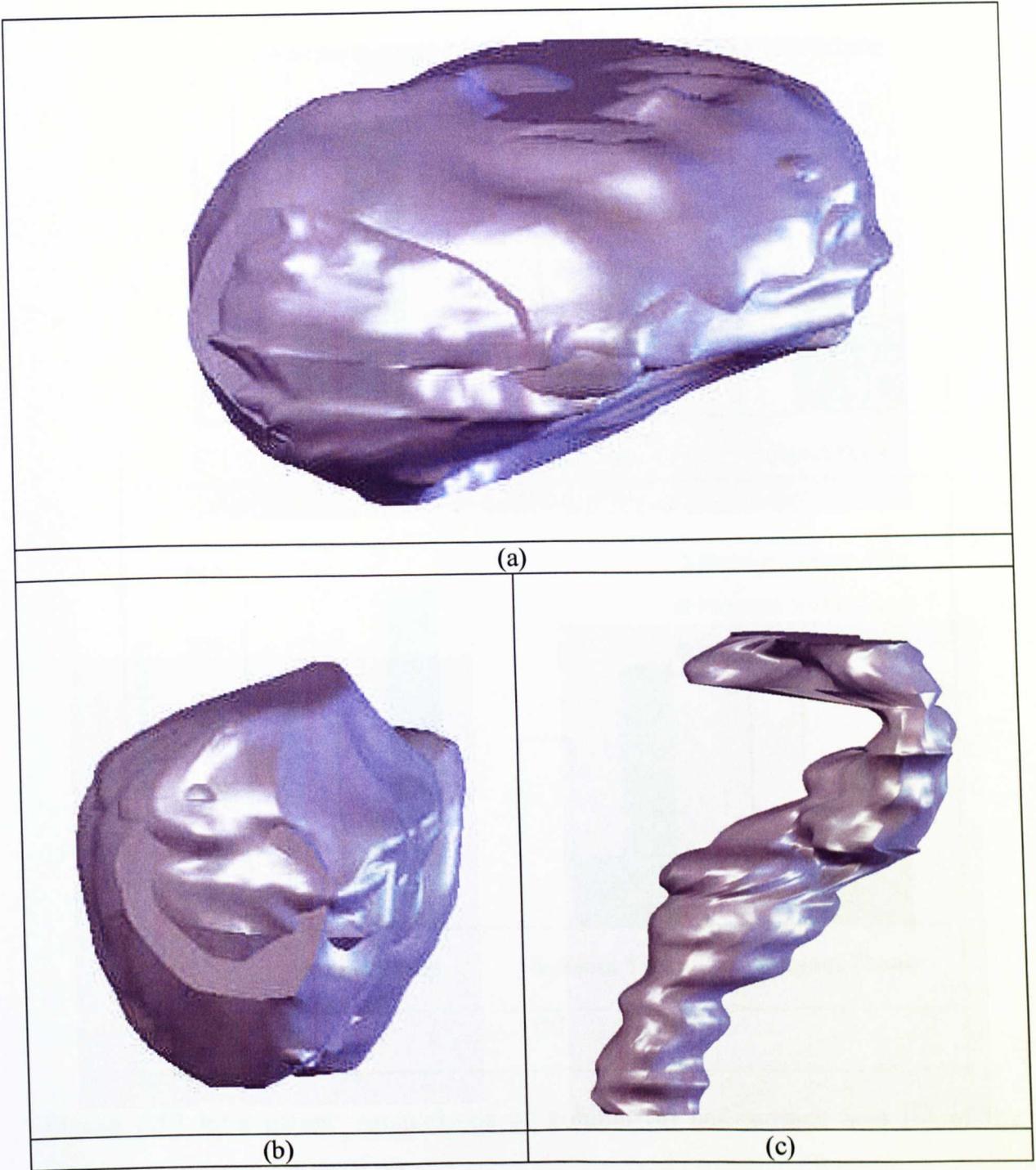
Figure 4.9 Typical 3-d models of the bladder (a), prostate (b) and rectum (c) (not to scale).
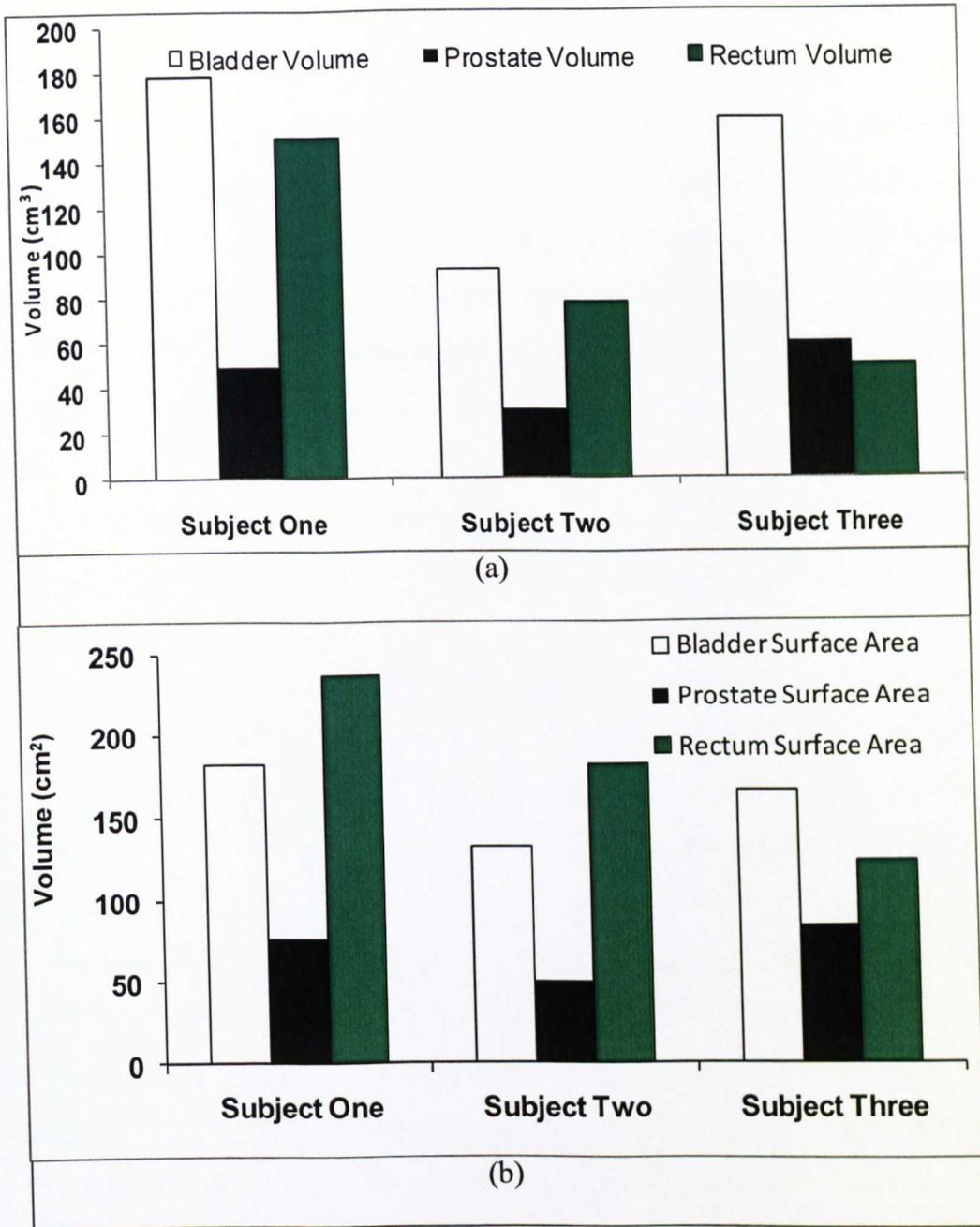
Figure 4.10 Inter patient comparisons of volume (a) and surface area (b) of the bladder, prostate and the rectum.

4.2.4. Assembly of the pelvis system and model validation

Accurate alignment of the 3D organs for setting realistic boundary and loading conditions is a challenging task. These directly influence the validity and accuracy of the simulation results. Many methods have been explored to align the 3 Dimensional structures by different researchers to suit different system being studied (Jaillet *et al*, 2004; Ganz *et al*, 2006; Boubaker *et* al, 2009). One common approach is to use manual measurements, in which measurements were taken from the pelvic bone to the bladder to represent the position of the bladder (Mirabell *et al*, 1998; Kristianen *et al*, 2004; Villeirs *et al* 2004). This manual alignment approach is convenient to use but the final assembly is dependent on the judgement of the operator, and therefore lacks consistency. In this work, a new method using the slice as a bench marking in creating the 3 Dimensional models has been developed/evaluated to determine the accurate position of each organ. In this process, the structure of origin for the alignment is made using surrounding pelvic bones as it was known to be able to maintain its position reliably and can be used as a benchmark for positioning of surrounding structures. The position of the bladder, rectum and prostate can then be accurately located using the bone as a reference. As shown in **Figure 4.11,** a template for organ positioning was created based on a preselected MR image with the bone, bladder, prostate and the rectum (in red). The organs of interest were aligned anatomically to adjacent organs following the template MRI slice. **Figure 4.12** shows a typical example of an anatomically accurate 3-D assembly of the Pelvic area for one of the subjects (Subject No 2). As shown in the figure, the key structures included are the pelvic bone, bladder, prostate, rectum, urogenital diaphragm and the perineal muscle. The same process is repeated for the other two subjects. The accuracy of the modelling and assembling was evaluated by comparing key sections of the CAD model and corresponding MR slices at different planes. **Figure 4.13** shows cross-sections of the model in the transaxial, coronal, and sagittal planes in comparison with the original images from comparable orientations and positions. In all cases, the shape of the key components of the 3-D model resembles that observed in the image at the appropriate orientation. In general, the projected points were aligned along the bony pelvis within the range of expected uncertainty of clinical imaging. This suggests that

the approach was able to create a detailed structural model for FE simulation that was specific to each participant.
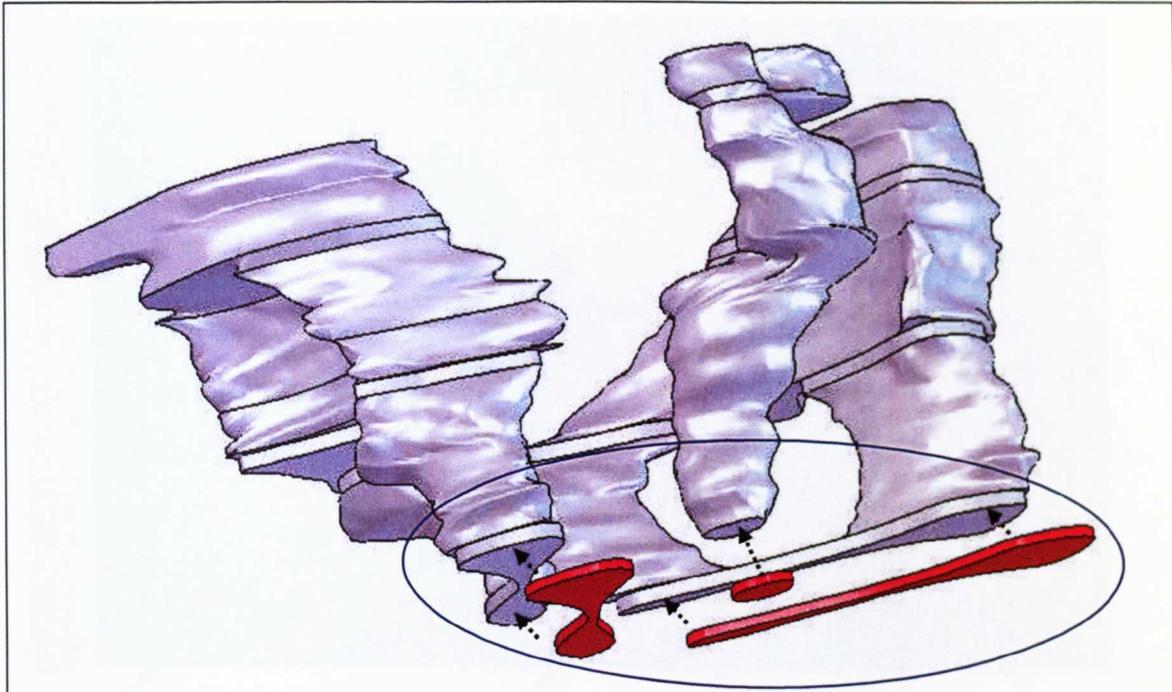
(a) 3D image showing the alignment of the bone and rectum (in red)
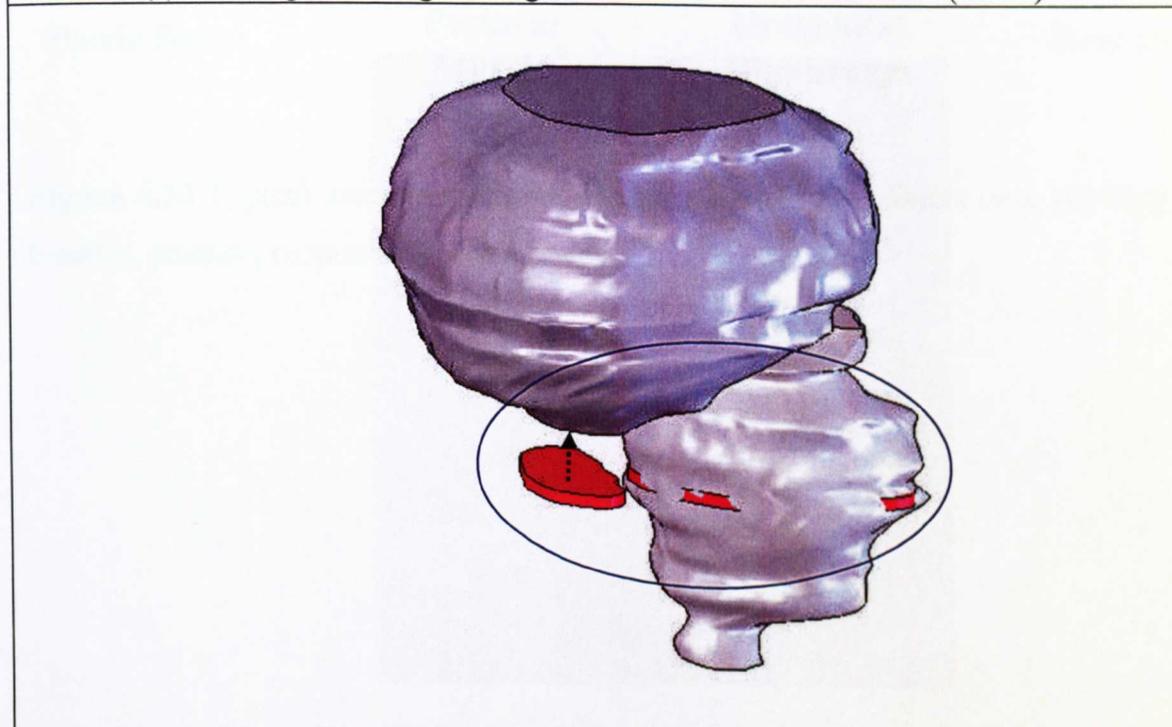
(b) 3D image showing the alignment of the bladder and prostate.

Figure 4.11 Organ alignment based on the bone structure in the Solidwork model.
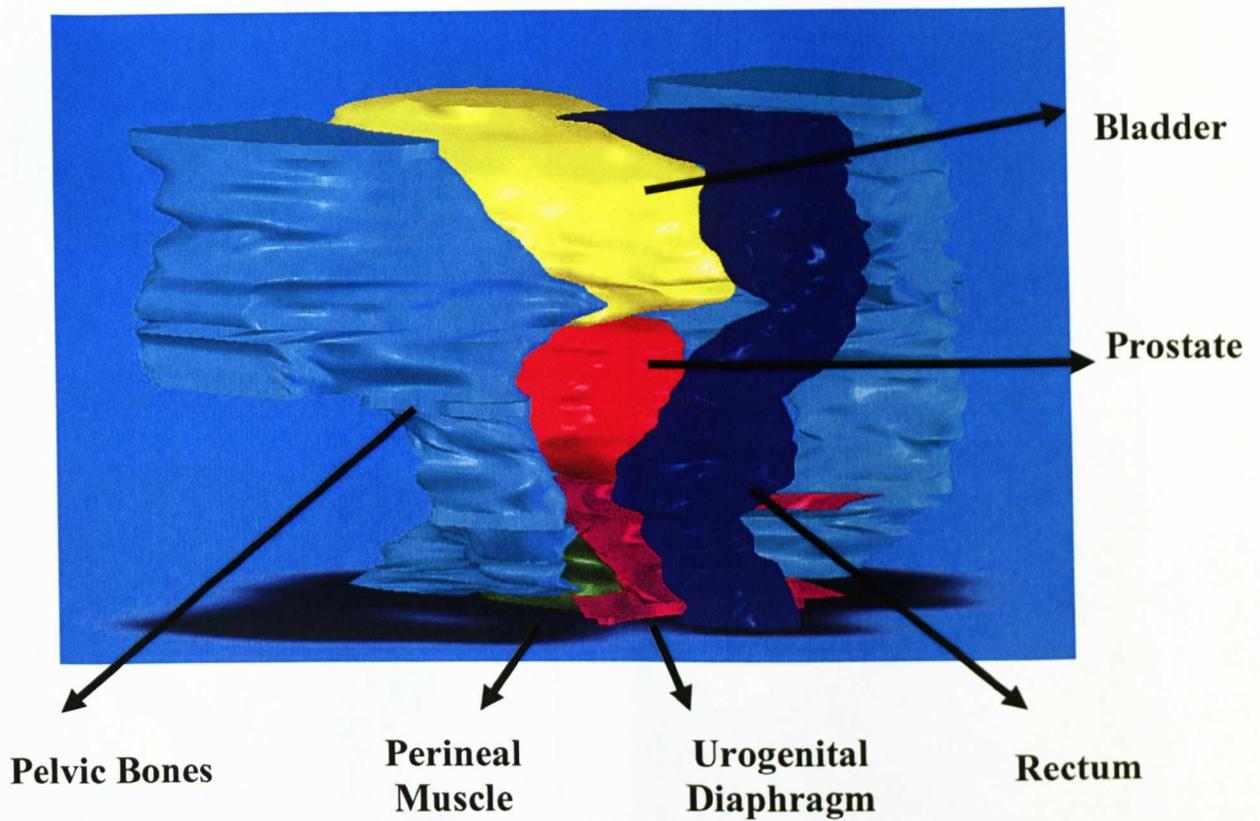
Figure 4.12 Typical assembled model of pelvis system for subject two, showing the bladder, prostate, rectum and pelvis bones.

(a) Transaxial Plane (CAD Model)   (b) Transaxial Plane (MR image)

(c) Sagittal Plane (CAD Model)   (d) Sagittal Plane (MR Image)

(e) Coronal Plane (CAD model)   (f) Coronal image (MR Image)
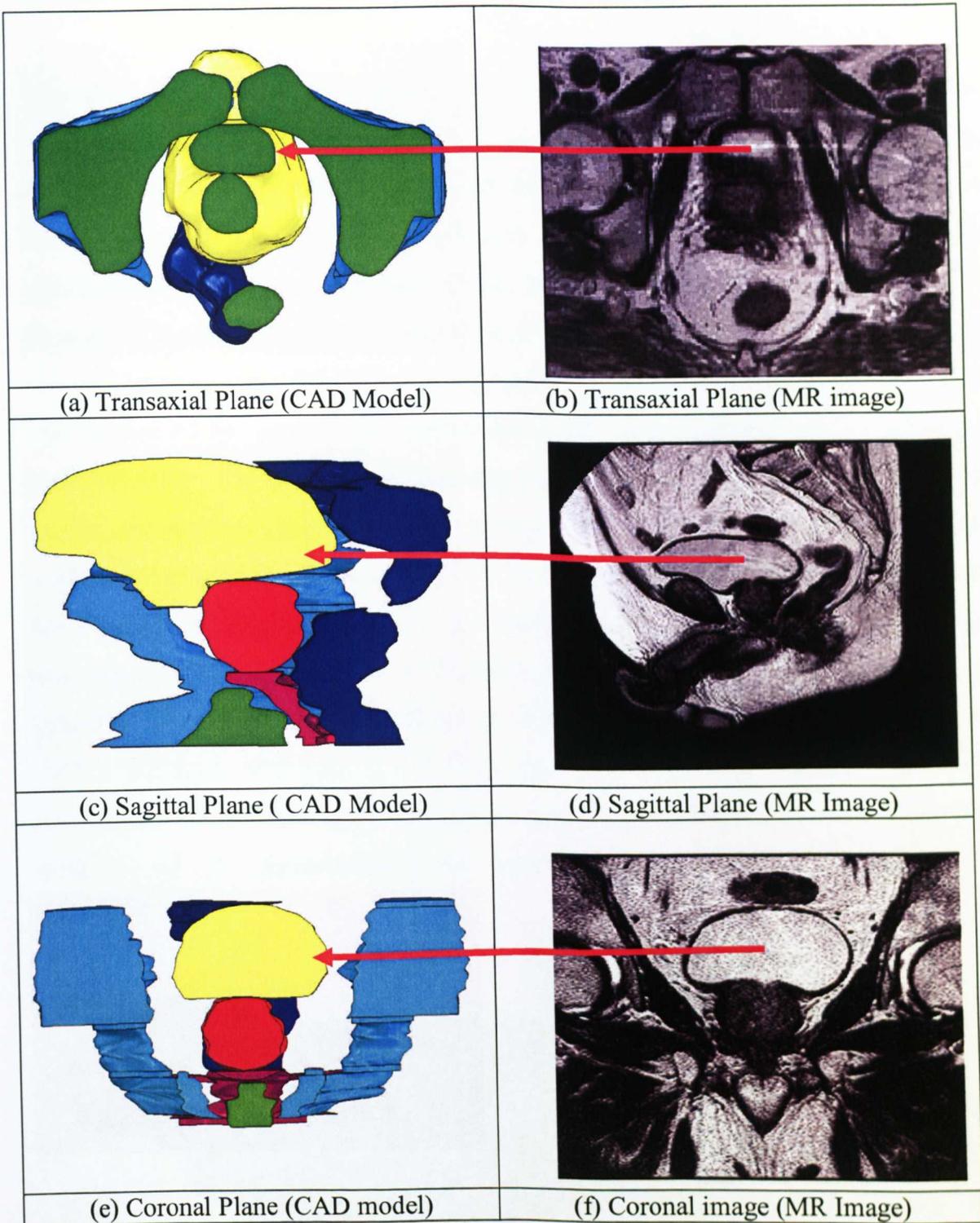
Figure 4.13 Comparison of the cross-sections of the solid model to MRI slides at different orientations/planes for Subject two. (not to scale to preserve full MRI slice, the arrows indicate the position of the bladders).

4.3 Finite Element model of the pelvis system

The 3D assembly model was saved using an IGES (*.igs) file format and exported into a Finite Element program ABAQUS (ABAQUS 6.4). Any geometric errors that occur during the importing of the model were eliminated using a repair function. Once all of the regions of interest had been imported, an assembly was created that incorporated all structures representing the true anatomical position of the organs on the basis of the anatomical landmarks of the pelvic bones. **Figure 4.14** shows a typical assembly and meshing scheme of the bladder, prostate and rectum in the FE model. The meshes of the surrounding tissues (such as the perineum) were not shown to preserve clarity. The type of shell elements used are S3 for the bladder and S4 for the rectum, the element type used for the prostate was C3D10M, while the type of the solid elements used for the bone is R3D4. The shell elements (S3 and S4) account for finite membrane strains and allow the shell thickness to change with the element deformation. The C3D10M is a 10-node quadratic tetrahedron. It is a modified quadratic tetrahedral element, which is robust enough for large-deformation and contact problems and exhibits minimal shear and volumetric locking. The three-dimensional quadrilateral (R3D4) rigid element is used to model the two-dimensional surfaces of a three-dimensional rigid body (ABAQUS Manual 6.4).
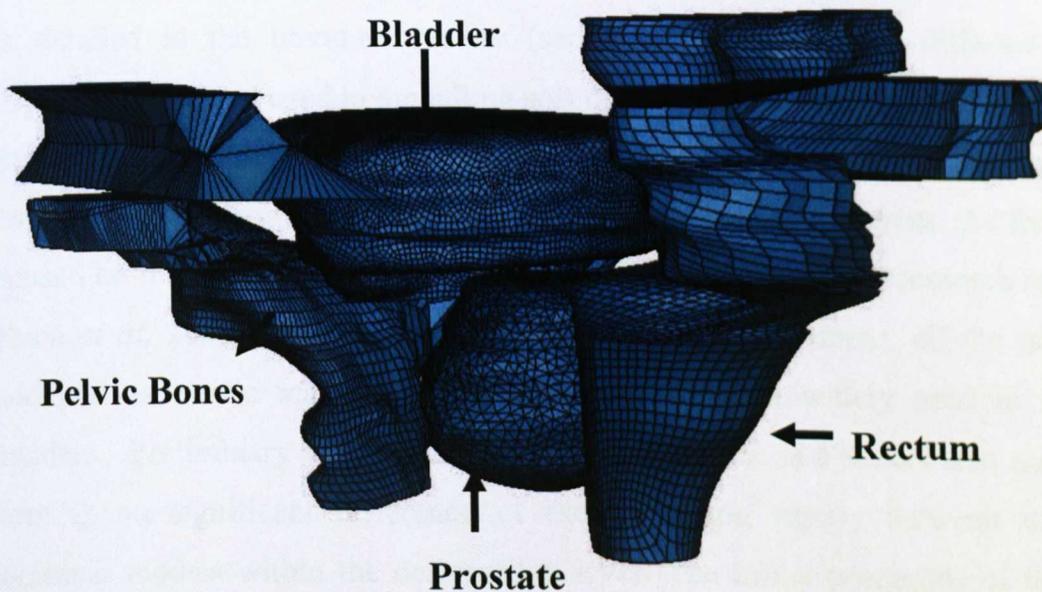
Figure. 4.14 Typical example of the Finite Element meshing scheme for the whole assembly, example shown from Subject two.

The bladder was deformed by applying a gradually increasing pressure on the inner shell, which simulates the filling of the bladder over similar changes in volume (Korkmaz and Rogg, 2007). The maximum volume increase was controlled at about 100% of the original bladder volume capacity. This is a typical limit of volume variation observed in the radiotherapy treatment planning process (as demonstrated in Chapter 3). As shown in **Figure 4.15 (a)**, the inferior section of the bladder is suppressed as is stated in literature based on clinical studies (Pinkawa *et al*, 2007). As shown in **Figure 4.15 (b)** the displacement of the rectum was suppressed inferiorly and superiorly. Preliminary numerical tests showed that this approach will improve the computational efficiency without affecting the accuracy of the modeling results. The surrounding bone was assigned with a zero displacement condition and is classed as rigid bodies within the model. Bones being much stiffer than the soft tissues means the deformation associated with bladder filling can be neglected. The constraint and interaction of the bladder with the surrounding structure was considered in the model using displacement control conditions. Contact definitions were applied throughout the model, including contact between the bladder and the pelvic bones, and mesh ties were introduced at the bladder–prostate interface and at the contact areas between the prostate and the rectum. This allows systematic investigation of the interaction between the bladder, prostate and the rectum.

As detailed in the literature review (section 2.6), a range of different material properties have been used in modelling soft tissues including both linear and nonlinear models. Nonlinear models are more accurate for condition with large deformations, however, it significantly increases the modelling time and resources. As this work is focused on relatively smaller volume change (in comparison with research in urology) (Yuen *et al*, 2002) during the course of radiotherapy treatment, all the tissue were modelled as elastic materials. This approach has been widely used in modelling bladders. Preliminary work in the project using rubber as a model also showed that there is no significant difference of the modelling results between elastic and nonlinear models within the deformation level. The initial properties of the bladder were adapted from published data (Dahms *et al*, 1998), based on the stress–strain curve empirically derived. The material parameters of other tissues were also based on

published results (Bharatha *et al,* 2001; Egorov *et al,* 2006). The bone was described as a solid analytical structure, owing to the high stiffness of its material properties compared with those of the relatively soft surrounding organs and tissues. The effective Young's modulus used for the bladder wall was determined through a systematic sensitivity study by determining a set of material properties which produce comparable results with pressure volume results (to be analyzed in the discussion). The results used were 0.01 Mpa for the bladder, the Young's modulus of prostate tissue was 0.02 MPa, while the properties for the rectum wall was 0.01 MPa. The Poisson's ratio used was 0.49.

The data is in agreement with several published works (Mohamed *et al,* 2002; Hensel *et al,* 2007). The numerical modelling data is shown in the next two sections.

| (a) | (b) |
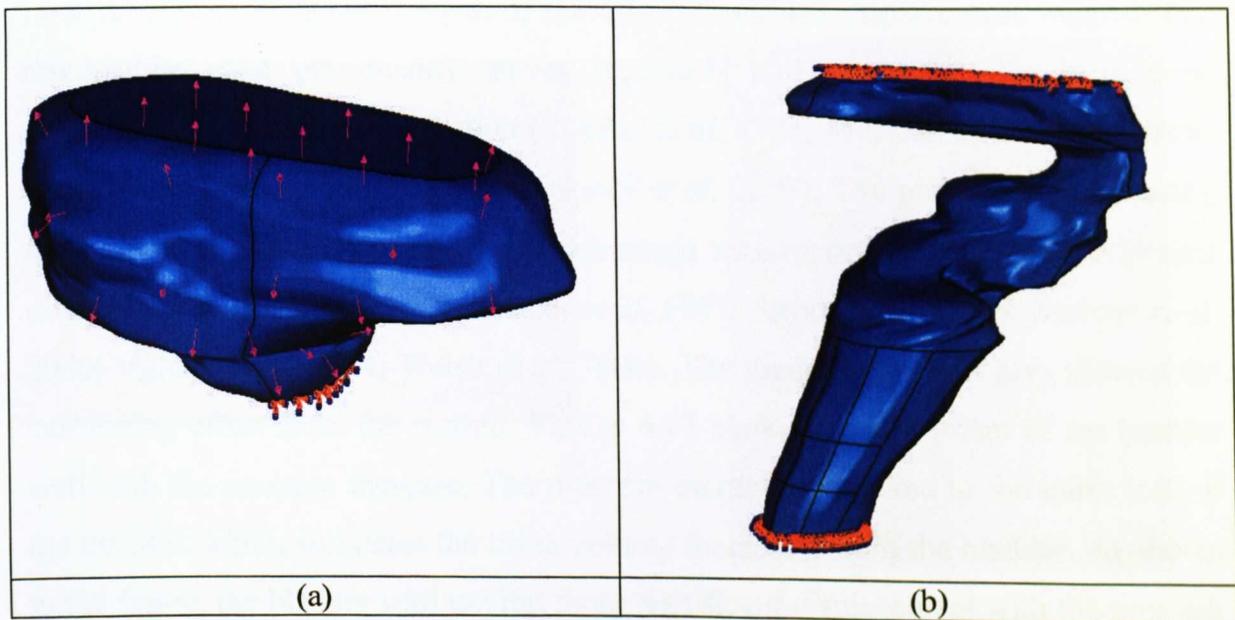
Figure 4.15 Finite Element model showing the loading and boundary conditions on the bladder (a) and rectum (b).

4.4 Finite Elements results and analysis

4.4.1 Typical deformation of the pelvis system during bladder filling

Initial analyses of the Finite Element results are performed to evaluate if the simulation is representative of the biomechanical reaction during bladder filling. A typical example of a simulation during bladder filling is shown in **Figure 4.16**. The conditions shown in the figure represents the overall deformation field (a) and displacement in the, U1 (AP), U2 (LR) and U3 (IS) directions. The blue contours represent zero displacement, the red contours represent maximal displacement. The general deformation filed suggests that the simulation results are in agreement with the clinically observed biomechanical deformation (Damaser *et al*, 1995; Korkmaz *et al*, 2007). With volume increases, the bladder displaces superiorly with limited inferior motion. Detailed analysis of the U1, U2, and U3 displacement suggests that the bladder most prominently moves superiorly and anteriorly, this is in good agreement with clinical observation (Roeske *et al*, 1995; Mirabell *et al*, 1998; Muren *et al*, 2003; Kristianen *et al*, 2004; Pinkawa *et al*, 2007). The prostate predominantly displaces posteriorly which is also in agreement with reported clinical results (Balter *et al*, 1995; Roeske *et al*, 1995; Melian *et al*, 1997; Stroom *et al*, 1999; Malone *et al*, 2000; Villeirs *et al*, 2004; Welsh *et al*, 2004). The modelling results also showed the cushioning effect from the rectum. **Figure 4.17** shows the movement of the bladder wall with the pressure increase. The pressure increase is applied to the inner wall of the bladder, which simulates the urine volume increase within the bladder. As shown in the figure, the bladder wall exhibit more significant displacement with the pressure increase in the initial stage.
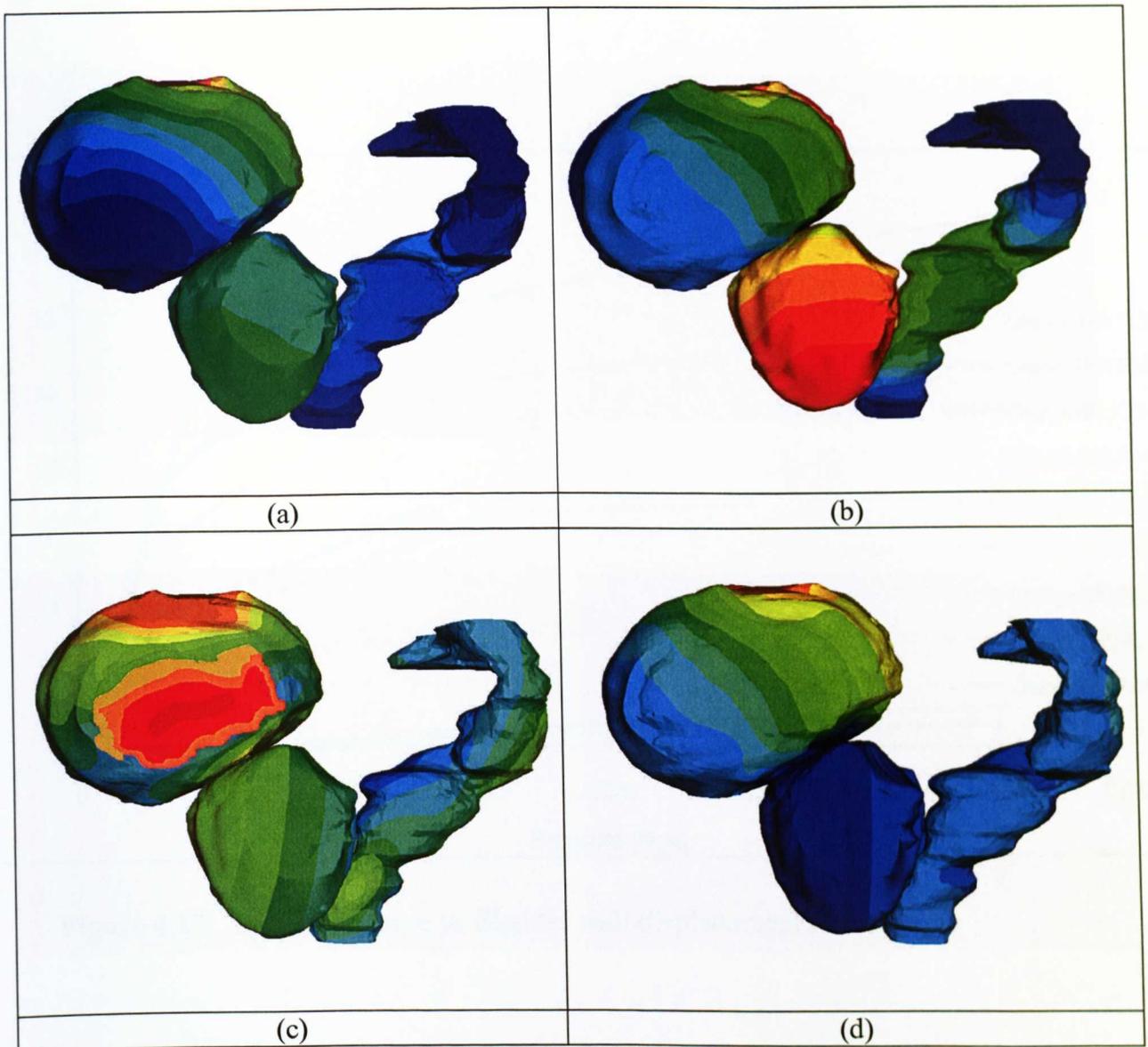
Figure 4.16 Typical deformed field of the bladder, prostate and the rectum for subject 2. (a) Overall, (b) Anterior-Posterior, (c) Left-Right and (d) Inferior-Superior field.
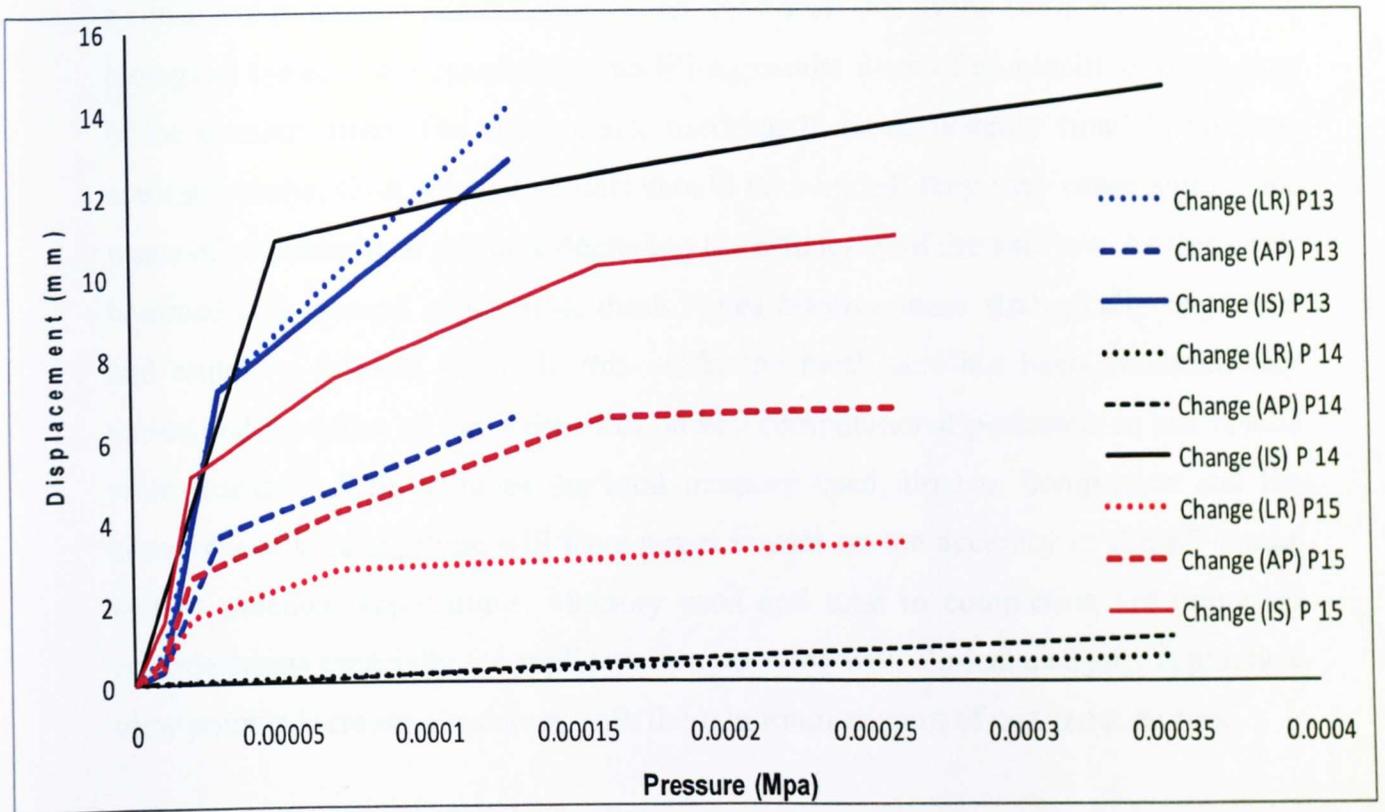
Figure 4.17 Typical pressure *vs* Bladder wall displacement for subjects.

120

4.4.2 Mesh sensitivity study and results

As shown in the section **4.4.1**, the predicted deformation of the pelvic system showed a consistent trend with clinical observation. However, due to the complex structure of biological systems, the quantitative modelling results were often sensitive to the size of the elements used. The element size used has to be sufficiently small to produce accurate results. Over meshed models should be avoided, they may cause significant waste of computational resource degrading the efficiency of the analysis. As this work is aimed at a medical application, these issues become more strategically important and require a detailed study. In this work, the mesh size has been systematically varied and the effect of mesh densities on key computational performance and results were extracted. This includes the total memory used, time to completion and the convergence success, these will have direct impact on the accuracy of the FE model and its potential applications. Memory used and time to completion are important considerations especially for applications associated with clinical analysis. A practical view point is increasing accuracy with the minimum amount of computation time.

Table 4.3 lists some of the results of the mesh sensitivity tests. The first column is the global element size used for the bladder. The criteria for acceptable mesh size was a convergence of displacements of the U1, U2 and U3 (Column 2) fields of bladder filling. The key outcome variable used is the memory used, size of the simulation file, the time to completion and converge rate. As shown in the data, when the element size is too large (e.g. over 5mm), the model becomes too coarse to converge to an acceptable accurate result. Extremely fine meshes (e.g. element size smaller than 1.0) have comparable modelling results, however it increased the time significantly and the result file may exceed the system memory causing failure of the simulation process. The optimum mesh size for the analysis has been found to be a global element mesh size of 2.0. Similar mesh sensitivity tests has been performed on the prostate and rectum to determine the optimum mesh size for the model for each subject.

Table 4.3 The effect of element sizes for the bladder on the modelling results and processing efficiency.

Global Element size for the Bladder (mm)	Maximum Distance (mm)			Memory used (mb)	Size of simulation file (mb)	Time	Convergence
	U1	U2	U3				
5	77	73	57	300	534	1hr	No
2	90.3	88.8	76.1	909	779	3hr 17min	Yes
1	90.4	88.9	76.2	1090	983	10hr 38min	Yes
0.5	90.5	89.4	76.2	1200	1200	19hr 5min	Yes
0.1	------	------	------	1600	---------	--------	No

4.4.3 Comparison of the numerical results with repeated CT images

Figure 4.18 shows a comparison between the original model for each subject and the overall displacement field of the bladder, prostate and rectum with an increase in the bladder volume. The original undeformed models developed for the subjects are shown in **Figure 4.18 (a, c, e)**, whereas the deformed models are shown in **Figure 4.18 (b, d, f)**. As shown in the original models, the shape of the bladder differed significantly among the subjects. The contour plots represent displacement distribution in the AP (U2) direction showing the prostate pushing towards the rectum, while the rectum acting as a barrier cushioning the prostate movement. Data for all of the subjects show posterior movement of the bladder at the prostate attachment zone, as well as anterior posterior displacement of the bladder above the prostate. There is little indication of rectum displacement above and below the interaction of the prostate, this to a certain extent proved the boundary condition used is accurate. The biomechanical movement of the bladder and prostate displacements are consistent with published research, i.e. bladder filling increases the displacement of the prostate posterior which is agreeable to published research (Balter *et al*, 1995; Roeske *et al*, 1995; Stroom *et al*, 1999; Malone *et al*, 2000; Dehnad *et al*, 2003; Villeirs *et al*, 2004; Welsh *et al*, 2004; Hoogeman *et al*, 2005).

Figure 4.19 shows the comparison of the numerically deformed bladder with repeated images of comparable volume. For subject 1, the CT volume was 313000mm^3, the FE

model volume was 327000 mm^3; for subject 2, the CT volume was 192000 mm^3, the FE model volume was 189000 mm^3. For subject 3, the CT volume was 302000 mm^3, the FE model volume was 315000 mm^3. **Figures 4.19 (a, d, g), (b, e, h) and (c, f, i)** represents the initial FE model, the numerical filled model and the CAD models based on repeated imaging of the bladder for the three participants, respectively. As shown, the original bladder model for each subject was significantly different. In each case, the bladder expanded in the anterior–posterior (A-P), superior–inferior (S-I) and left-right (L-R) directions during the process of bladder filling. The bladder became more oval in shape, which agreed with reported clinical observations of filled bladders (Damaser and Lehman 1995). **Figure 4.19 (c, f, i)** represents the 3-D models that were based on repeated CT images of the same patient at a comparable volume to the numerically deformed models shown in **(b, e, h)**. All three simulation results have a similar representative displacement to the actual CT imagery. In all of the three cases, the numerical simulation showed that shape of the bladder geometry becomes more spherical when the bladder volume increases. This is in agreement with clinical observations (Damser and Lehman, 1995) and some phantom study results (Elkut, PhD thesis, in process). For subject 1, the volume changed from 178000 to 327000 mm^3; for subject 2, the volume changed from 92000 to 189000 mm^3. For subject 3, the volume changed from 159000 to 315000 mm^3. In all cases, the overall shape of the simulated deformed bladder showed reasonable agreement with the repeated CT images of the filled bladder for the same participant. Generally, during clinical practice, the deformation of the bladder is normally quantified by its dimensions in the A-P, S-I and L-R dimensions. Measurement are taken of the numerical simulation in the A-P, L-R and S-I directions. The average values for both the simulated deformed bladder and the repeated CT images were measured and are plotted in **Figure 4.20**. The error bar represents the standard error associated with repeated CT imaging. As shown in the figure, the two sets of data were in good agreement (within a 5% error margin as indicated on the graphs). This clearly showed that FE results are comparable to those of the repeated CT images within the standard level of variation of the imaging procedure. This indicates that the FE models are accurate within an acceptable range of uncertainty and are capable of predicting the changes in the volume of the bladder and the key dimensions that are of clinical significance.

(a) Original Model subject One	(f) Deformed model with a filled bladder, subject One
(c) Original Model subject Two	(d) Deformed model with a filled bladder, subject Two
(e) Original Model subject Three	(f) Deformed model with a filled bladder, subject Three
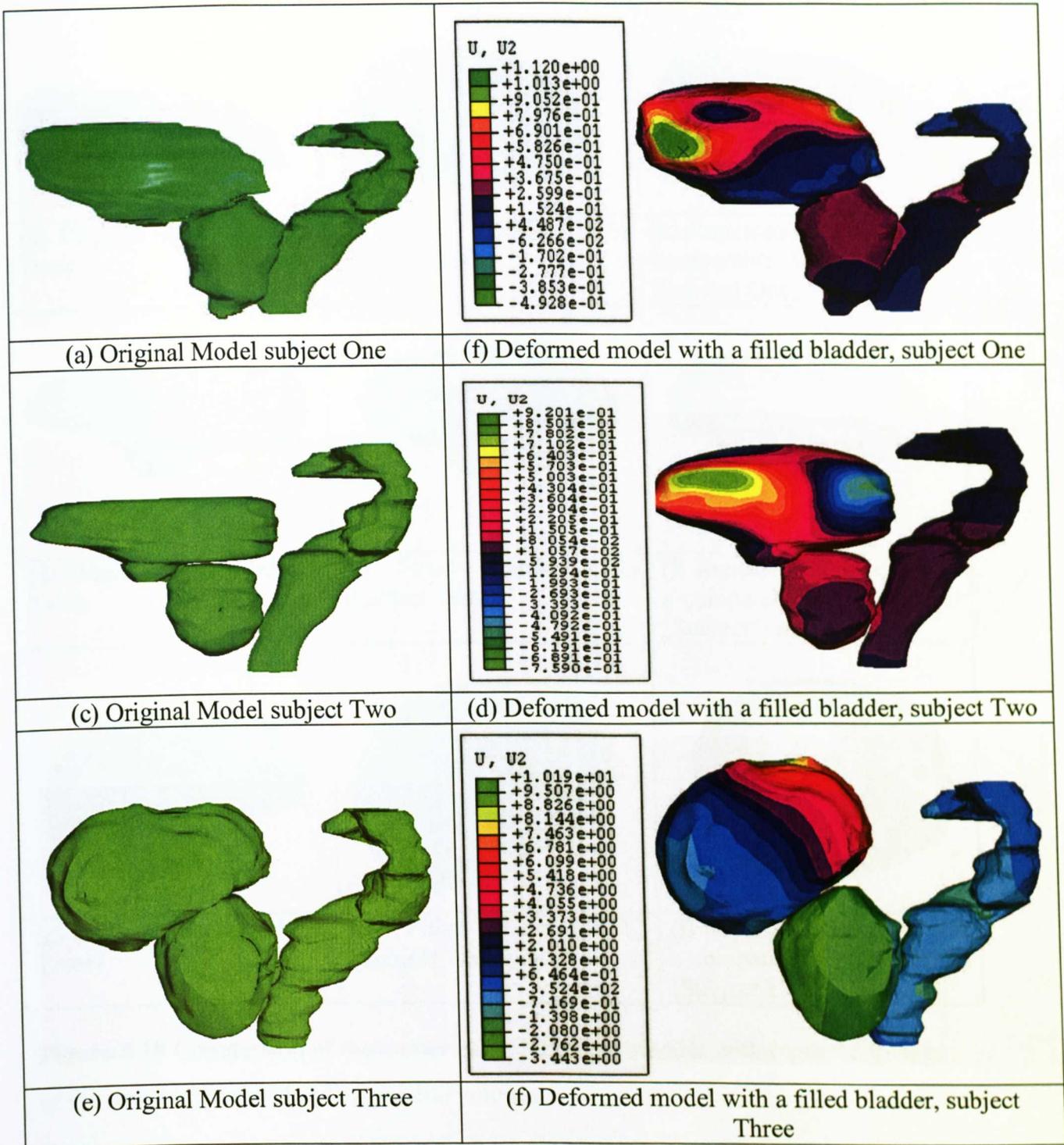
Figure 4.18 Comparison of the original model and deformed model with a filled bladder (The contour plots represent displacement distribution in the AP (U2) direction in order to show the prostate displacement.
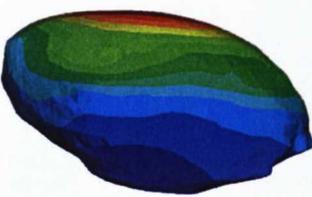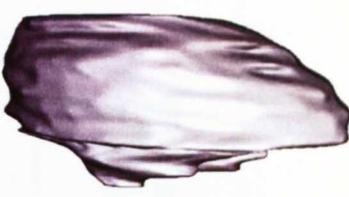
(a) Original Shape (Subject One).	(b) Filled Bladder (FE) (Subject One).	(c) Repeated CT image with comparable volume to (b) (Subject One).
(d) Original Shape (Subject Two).	(e) Filled Bladder (FE) (Subject Two).	(f) Repeated CT Image with a comparable volume to (e) (Subject Two).
(g) Original Shape (Subject Three)	(h) Filled Bladder (FE) (Subject Three)	(i) Repeated CT Image with a comparable volume to (h) (Subject Three)
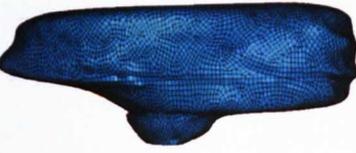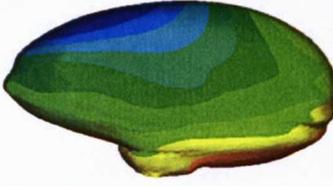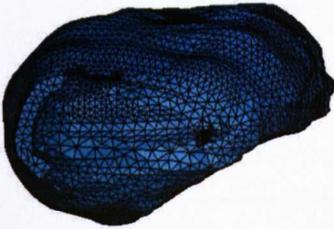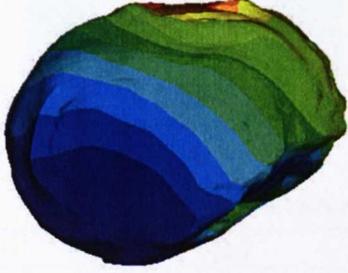
Figure 4.19 Comparison of the numerically deformed bladder with repeated images of the same subject with a comparable volume.
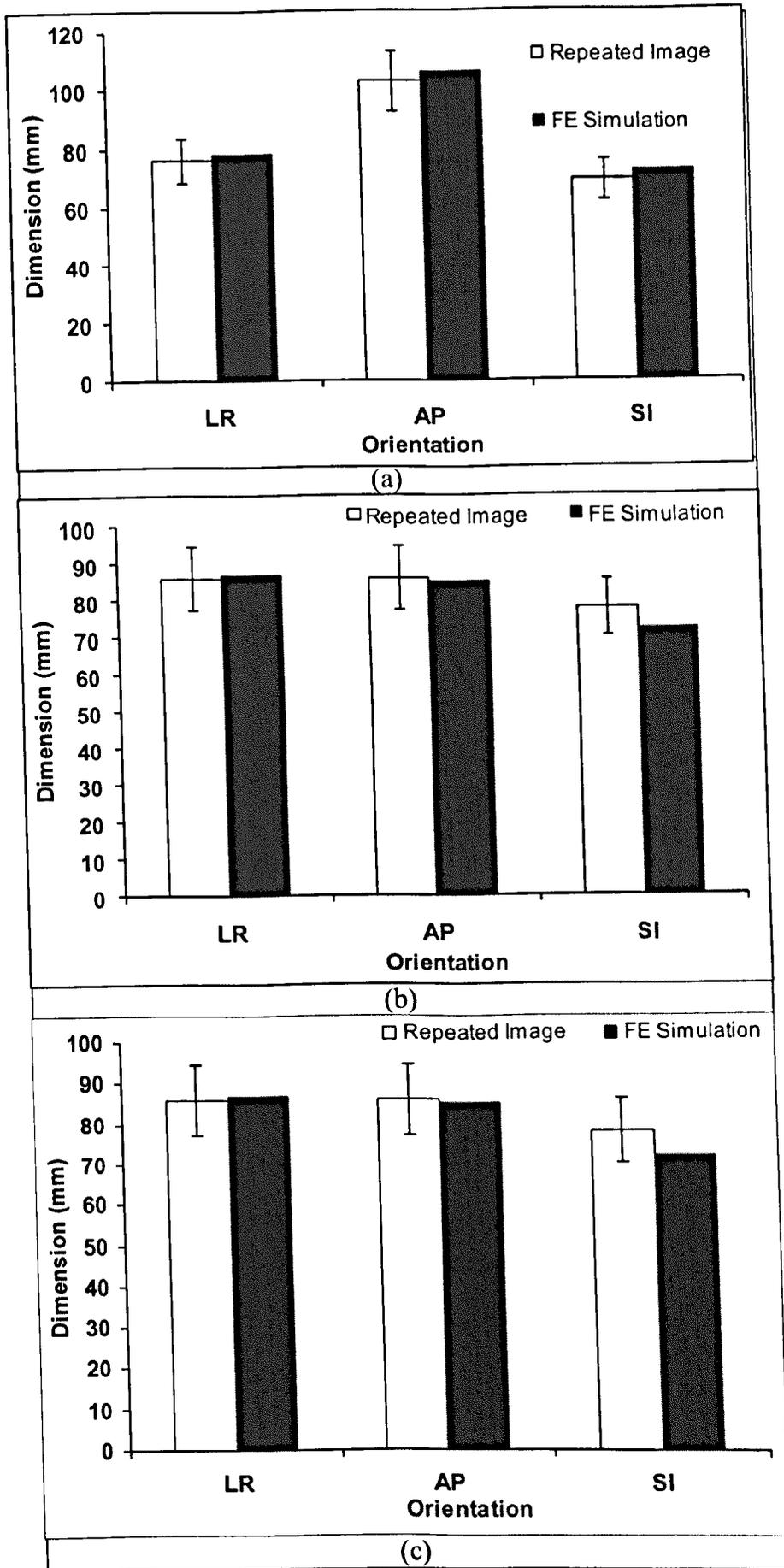
Figure 4.20 Comparison of the main dimension of the numerically deformed bladder and repeated CT images. (a) Subject One, (b) Subject two and (c) Subject three.

4.4.4 Deformation (volume and shape) of the bladder during filling process

As shown in section **4.4.2–3**, the main characteristic of the structural change of the bladder during filling are the volume change and the shape change. The shape change followed a general trend form spherical to oval shape, which can be represented by the aspect ratio (i.e. the ratio between the bladder wall distances at the SI, AP and LR directions). With the numeric model developed, these can be quantitatively investigated offering an improved understanding of the bladder filling process, which is better than pure clinical observations. In addition, quantification of these characteristics will also provide a means to assess the prostate movement in the next stage. During clinical procedures, the measurable controlling parameters are the volume of the bladder, which is directly related to the intake of water during the filling process. Manual extraction of the volumetric data is often required by estimating the bladder volume based on the maximum bladder wall distances following an empherical equation (Hedriana *et al*, 1994).

$$V = \frac{4\pi}{3} \times \frac{U_1 \times U_2 \times U_3}{8}$$

(4.1)

Where U_1, U_2, and U_3 refer to the left-right, the anterior-posterior and the superior-inferior wall distance of the bladder, respectively. **Figure 4.21** shows a plot of the dimensions of the bladder in the three main orientations against increasing volume (filling) for the three subjects. This relationship is important because it could provide an estimate of the change in bladder shape when continuously imaging is not feasible (Miralbell *et al*, 1998). In all three of the subjects, the wall distances increased gradually as the volume was increased; however, the data demonstrated a clear difference in the rate of change between the subjects. Linear regression showed that the trend can be treated as a linear relationship with a correlation coefficient greater than 97%. For all participants, the slope of the regression lines for S-I and L-R was greater than that for the A-P orientation, which implied that, with increasing bladder

volume, displacements in the former two directions are greater. This agreed with reports based on clinical observations (Roeske *et al*, 1995, Miralbell *et al*, 1998). The results also highlighted a slight inter-subject difference between these three subjects with different initial bladder shape and volume. Due to the uncertainty in the measurements, and the nature of the medical imaging techniques used, it is difficult to make conclusions on the basis of results obtained with only three participants. However, the slope of the data presented here is comparable to that of the clinical data reported by Miralbell *et al* (1998). In their work based on the data obtained from a large group of patients, the slopes obtained from the S-I, A-P, and L-R data were 0.016, 0.01 and 0.009, respectively, (to be detailed in the discussion section). This suggests that the FE modelling method described herein could potentially be used to predict the patient specific relationship between bladder dimensions and volume.

As shown in the deformation of the bladder example, there are differences between the wall movement at the anterior posterior and inferior superior directions at different stage. This change of shape will affect the compactness of the bladder (Kristiansen *et al*, 2004). One approach has been developed using the aspect ratio representing the change of wall distance at three orientations (LR (U1), AP (U2), and SI (U3)). The aspect ratios were defined by:

$$A_{\frac{AP}{SI}} = \frac{U_2}{U_3} \tag{4.2}$$

$$A_{\frac{LR}{SI}} = \frac{U_1}{U_3} \tag{4.3}$$

$$A_{\frac{AP}{LR}} = \frac{U_2}{U_1} \tag{4.4}$$
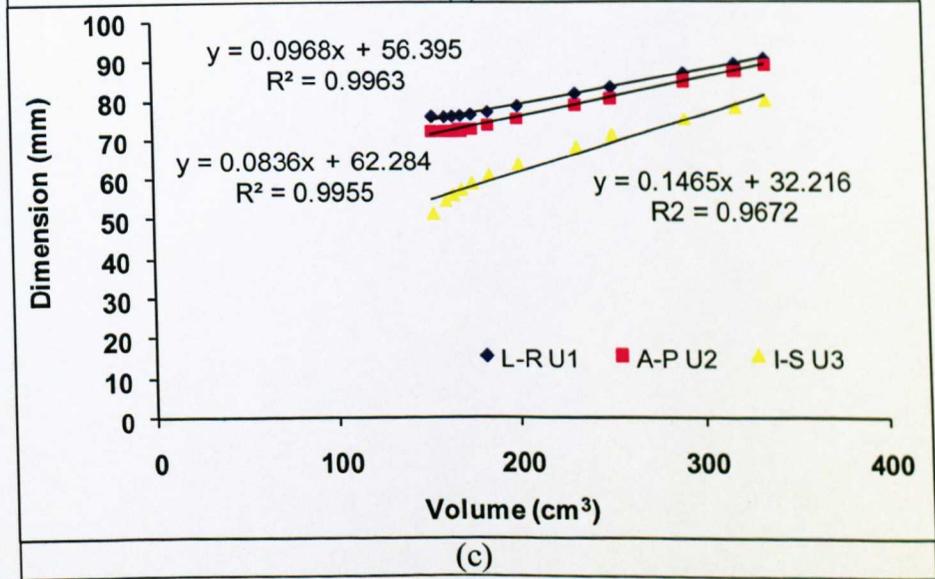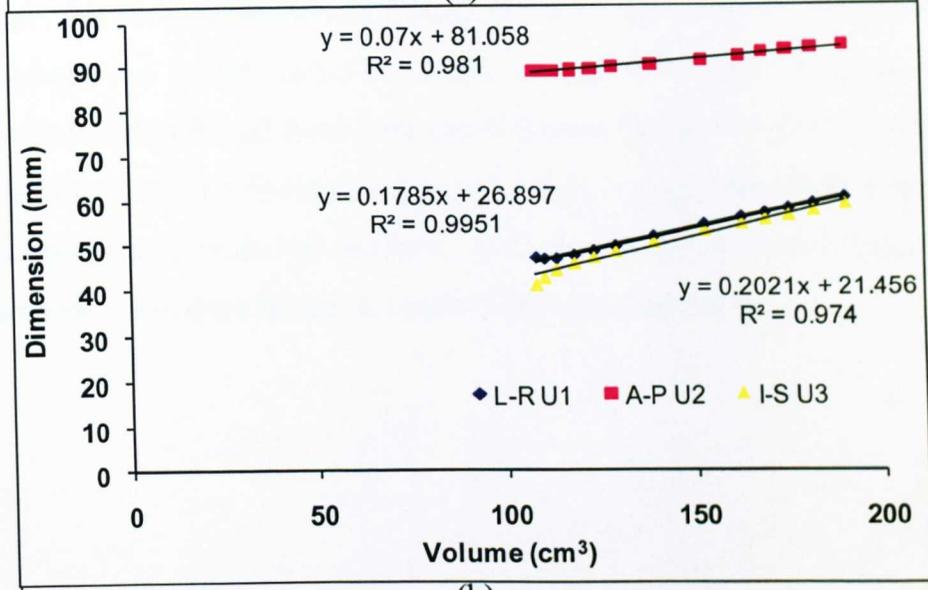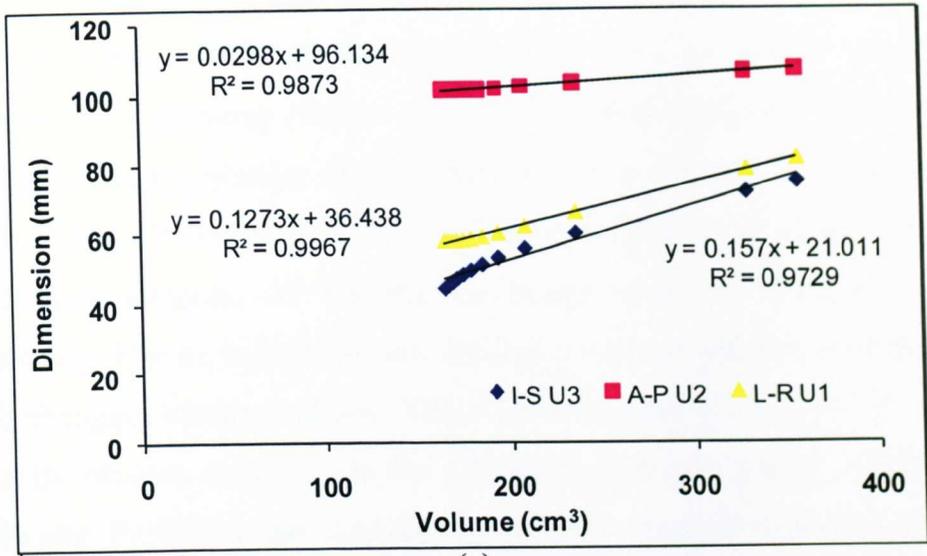
Figure 4.21 Deformation of the bladder at the three principal directions (AP, SI and LR) with volume change during filling; (a) Subject One, (b) Subject two and (c) Subject three.

129

Figure 4.22 is the recorded results of the three subject's aspect ratio with different bladder volume. Figure 4.22 (a) shows the aspect ratio of anterior-posterior *vs* inferior-superior, with changing bladder volume. The relationship for all three of the subjects indicates that the bladder displacement in the IS direction is displacing at a faster rate than the AP direction. This trend is applicable to all three subjects as anatomical features suppress AP bladder movement while the bladder can easily displace superiorly. Figure 4.22 (b) shows the aspect ratio of anterior posterior *vs* left – right, with changing bladder volume. The relationship for all three of the subjects indicates that the bladder dimension in the AP and the LR direction tend to change at a comparable rate. Published data also agrees with this trend the AP and LR bladder movement is similar for a given volume change (Pinkawa *et al*, 2007). Figure 4.22 (c) shows the aspect ratio of left right *vs* inferior – superior, with changing bladder volume. The relationship for all three subjects indicates that the bladder dimension in the IS direction increases at a faster rate then the LR direction. This trend is applicable to all three subjects as anatomical features, such as the pelvic bones, suppress LR bladder movement while the bladder can easily displace superiorly.
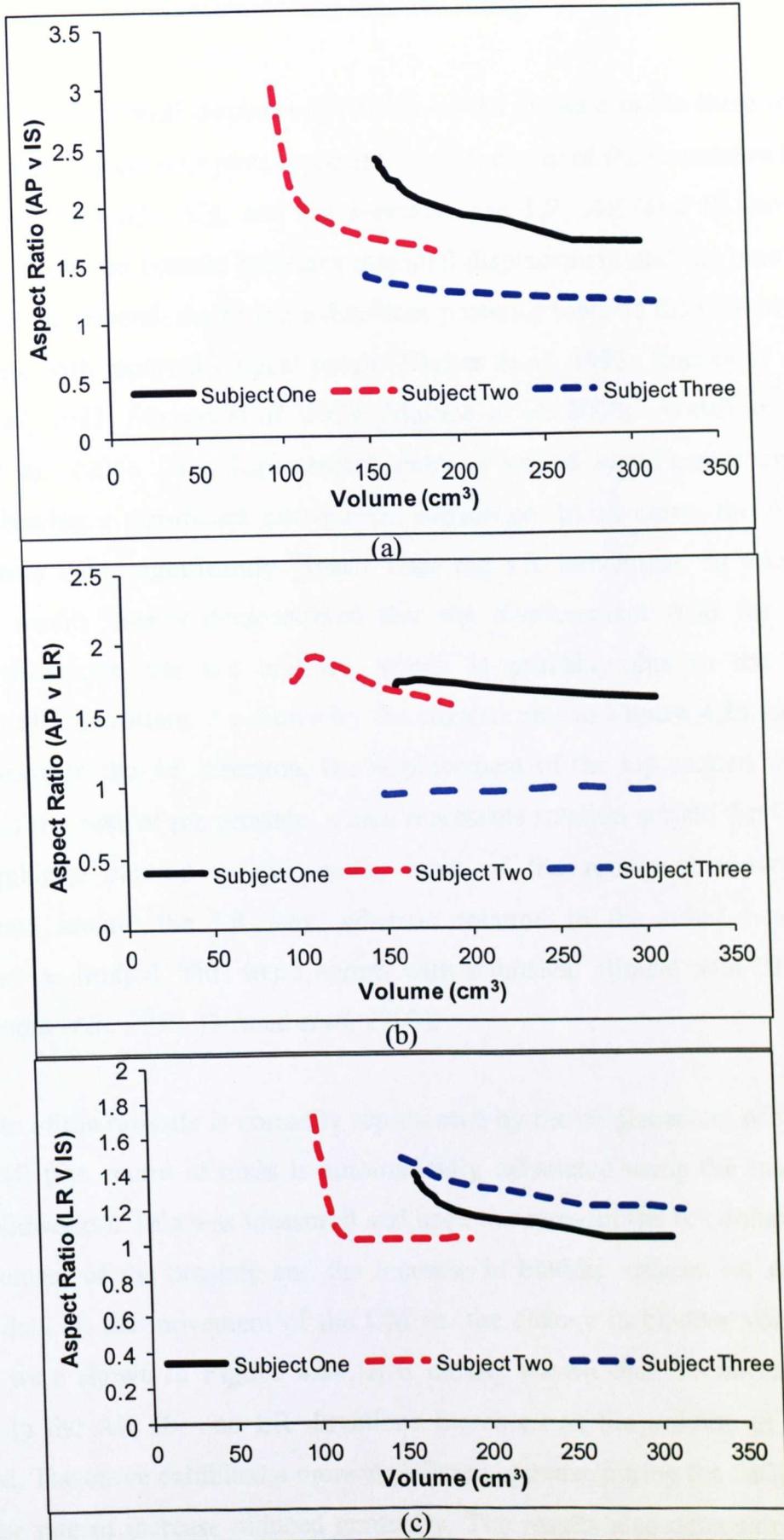
Figure 4.22 Changing aspect ratio (ratio of the wall distances in different directions, AP v IS (a), AP v LR (b), LR v IS (c)) during bladder filling increase for all three subjects.

4.4.5 Movement of the prostate during bladder filling

Figure 4.23 shows typical displacement fields of the prostate in the three directions for the subjects. The contour plots represent the movement of the prostate in the three principal directions (U1, U2, and U3 represent the LR, AP, and IS movements, respectively). The red contour indicates maximal displacement and the blue minimal displacement. In general, the prostate displaces posterior towards the rectum which is in agreement with reported clinical results (Balter *et al*, 1995; Roeske *et al*, 1995; Melian *et al*, 1997; Stroom *et al*, 1999; Malone *et al*, 2000; Welsh *et al*, 2004; Villeirs *et al*, 2004). The displacement contour varied significantly among the patients, showing a significant inter-patient difference. In all cases, the AP and IS displacements were significantly greater than the LR movement. In addition, the numerical results clearly demonstrated that the displacement field for the three principal directions was not uniform, which is probably due to the rotational movement of the prostate. As shown by the contour plot in **Figure 4.23 (a, d, g)** for the movement in the AP direction, the displacement of the top section was greater than that of the base of the prostate, which represents rotation around the LR axis. In all the subjects studied in this work, most of the rotational movement was concentrated around the LR axis, whereas rotation in the other two principal directions was limited. This trend agrees with published clinical data (Balter *et al*, 1995; Stroom *et al*, 1999; Dehnad *et al*, 2003).

Movement of the prostate is normally represented by the displacement of its centre of mass (CM) (the centre of mass is automatically calculated using the mass function using Solidworks). This was measured and used to represent the relationship between the movement of the prostate and the increase in bladder volume for each patient. Typical data on the movement of the CM *vs.* the change in bladder volume for the subjects were shown in **Figure 4.24**. It is clearly shown that the movement of the prostate in the AP, IS, and LR directions increased as the volume of the bladder increased. The curve exhibited a more significant increase during the early stage, after which the rate of increase reduced gradually. The results also demonstrated that the movement in the AP and IS directions was much greater than that in the LR direction.

This agreed with several published results that were based on clinical studies and the overall level of prostate movement is also within the average range of some published data, which is reported to be within 2–5 mm (Roeske *et al*,1995; Balter *et al* 1995; Stroom *et al*, 1999; Villeirs *et al*, 2004; Hoogeman *et al*, 2005; Dehnad *et al*, 2006). A detailed comparison between the numerical results and clinically observed data will be presented in the discussion section.
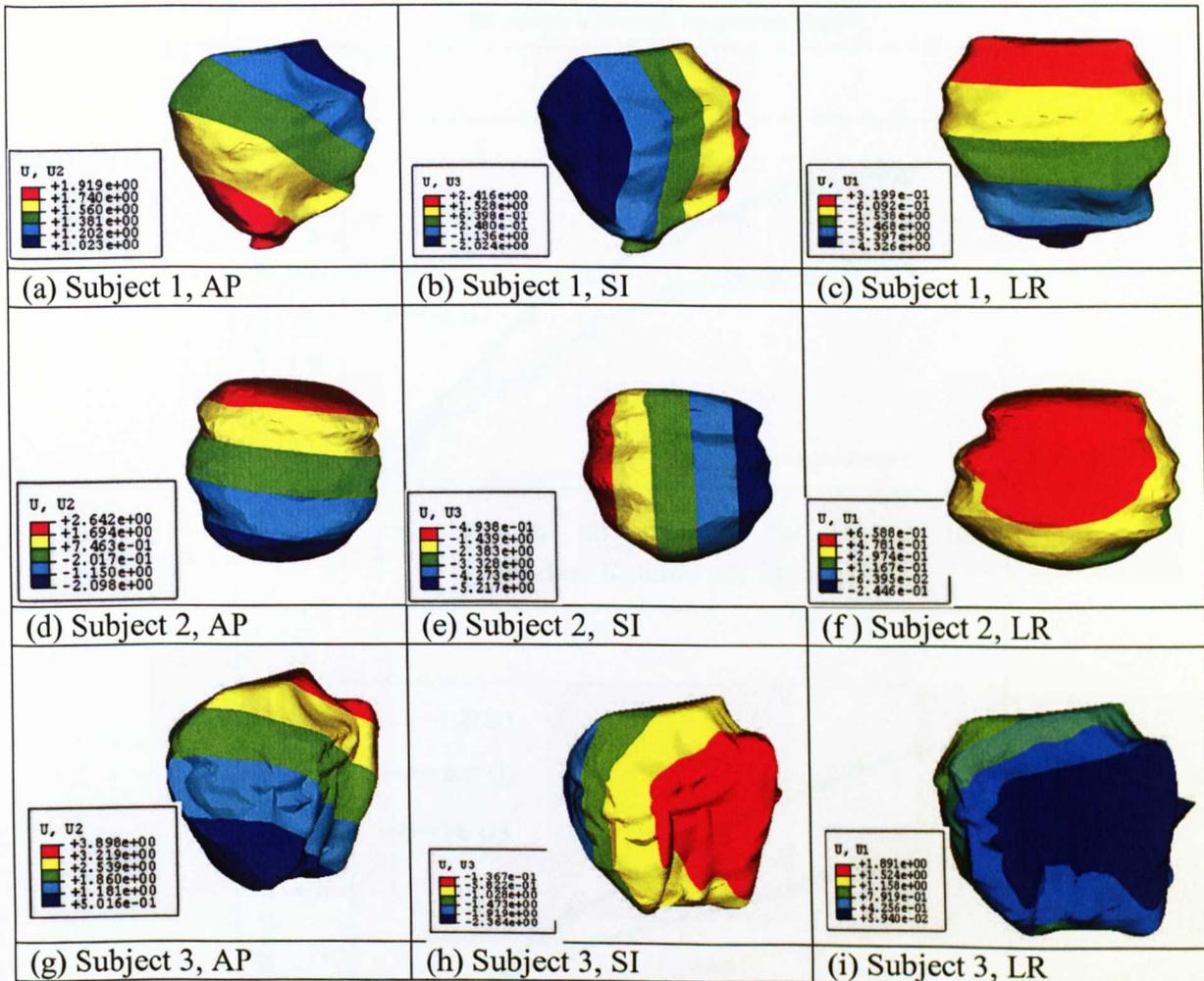
Figure 4.23 Typical displacement contour of the prostate in the three principal orientations (AP, SI and LR).
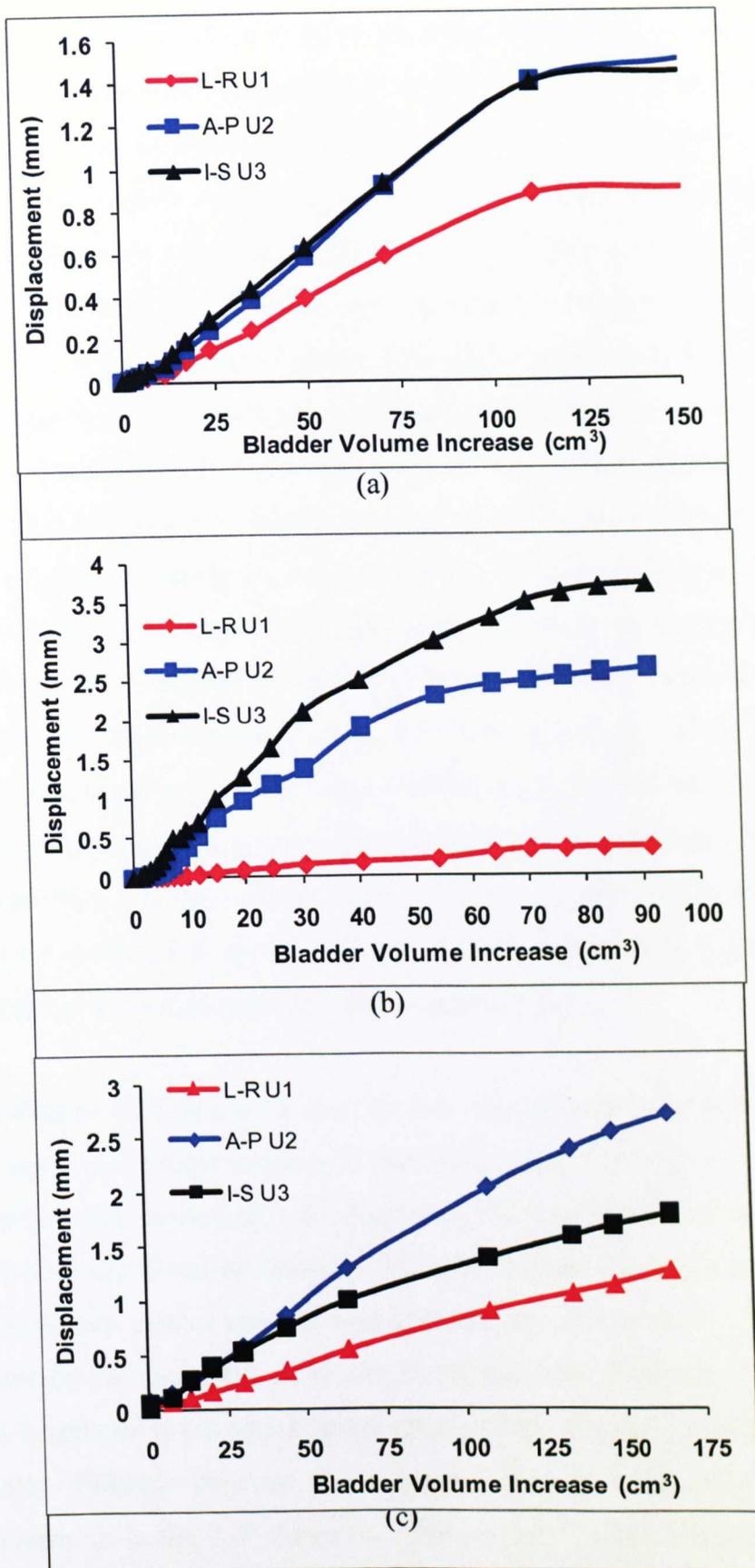
Figure 4.24 Prostate movements *vs.* bladder volume increase for different subjects.
(a) Subject One, (b) Subject Two, (c) Subject Three.

Figure 4.25 plots typical results that show the movement of the prostate against the percentage volume increase for each subject. In this case, the increase in volume was normalised by dividing the volume increase with the original volume of the bladder. In all the cases, the prostate movements increased with the bladder volume and the rate of increase decreased when the bladder volume reaches a higher level. There is still significant inter-subject difference even though the volume increase has been normalised by the original bladder volume. For subject one during the initial bladder filing stage an increase rate of prostate displacement was seen in all directions. After 70% bladder volume increase, there was little or negligible prostatic displacement movement in all directions. For subject two during the initial bladder filing stage an increase rate of prostate displacement was seen in all directions apart from the left right. After 80% bladder volume increase, there was little or negligible on the IS direction, for the AP direction it was 73% of bladder volume increase resulted in negligible prostatic displacement. For the left right direction with a 95% bladder volume increase resulted in only a 0.3 mm displacement. For subject three during the initial bladder filing stage an increase rate of prostate displacement was seen in all directions. After 95% bladder volume increase, there was little displacement on the IS direction as well as the LR direction. For the AP direction a 100% of bladder volume increase resulted in a reduced rate of prostate displacement.

As shown in **Figure 4.24 and 4.25**, there was a clear difference between the subjects, even for the same percentage increase in volume. Apart from the obvious difference in the scale of prostate movement, the relative level of the movement in the IS and AP movement is also significantly different. To establish the trend, the data at different volume increase has been extracted and prostate movement in the AP direct was plotted against the IS movement, as shown in **Figure 4.26**. There are some scatters of the data, but in general it fits into a linear relationship. But the correlation coefficient is significantly different between the subjects; Subject 1 has significantly more profound movement in the A-P direction. This reflects a clear structure effect of the bladder shape on the prostate movement which suggest that subject specific modelling is essential for quantifying prostate movement.

During the course of radiotherapy, the bladder volume may vary significantly on the same subject. As shown in **Figure 4.23 and 4.24**, the numerical model is able to produce a continuous relationship between the bladder volume and the prostate movement. This could provide a mean to estimate the level of prostate movement. **Figure 4.27** (a) plots averaged movement of the prostate at the three directions for a volume increase of 75–100%, which represents a normal upper limit of bladder volume variation among subjects in radiotherapy based clinical studies (Miralbell *et al*, 1998) and the data presented in Chapter 3. The rotation movement were also measured and plotted in **Figure 4.27** (b). The main rotation movement has been concentrated at the LR rotation while rotation movement around the AP and SI rotation is very limited, which is in a general agreement with clinical results (Balter *et al*, 1995; Stroom *et al*, 1999; Dehnad *et al*, 2006). These data also showed reasonable agreement with the clinical observed data presented in Chapter 3, which is to be discussed in details in the next section.
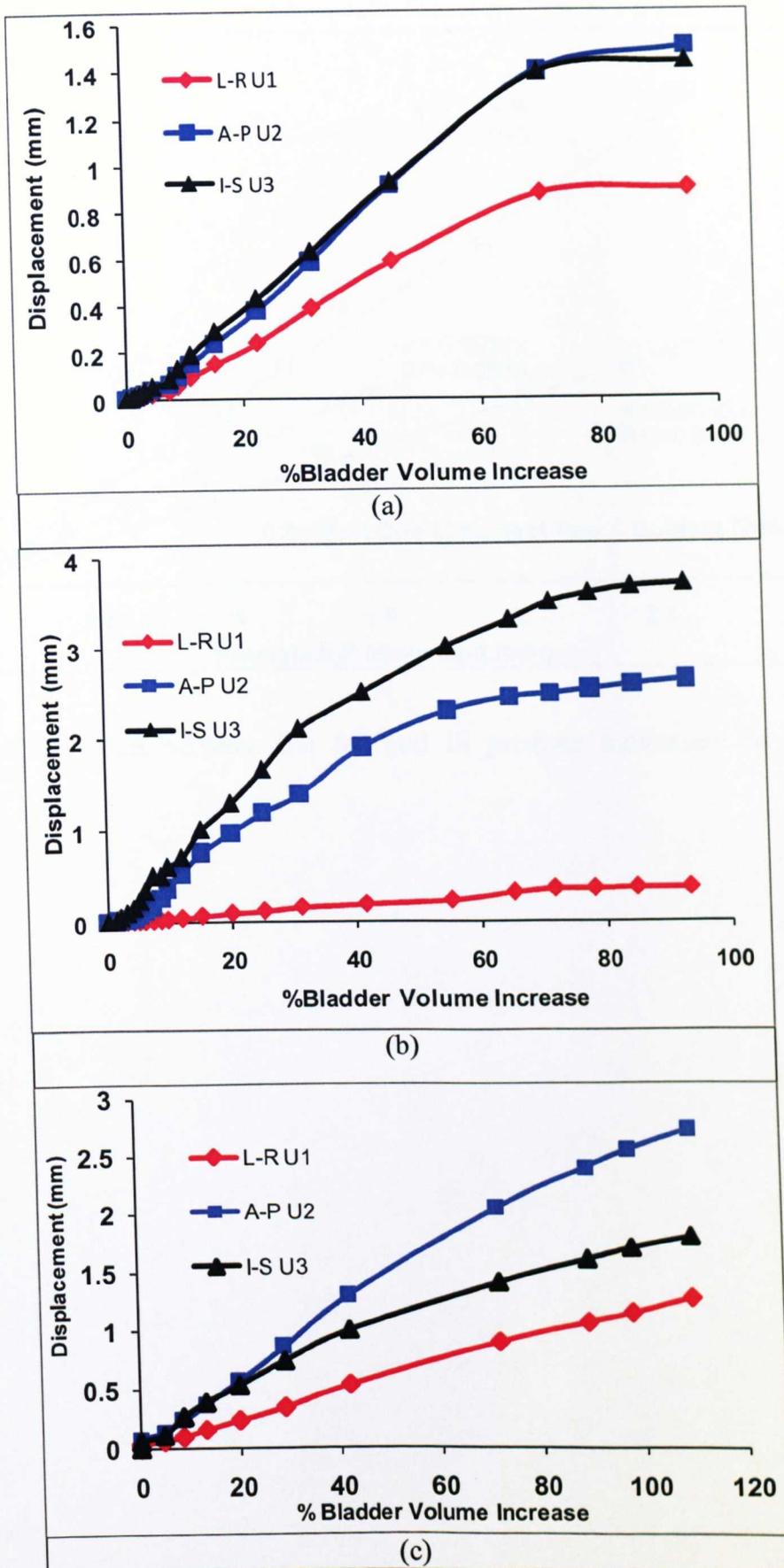
Figure 4.25 Prostate movements vs. percentage (%) bladder volume increase. (a) Subject One, (b) Subject Two, (c) Subject Three.
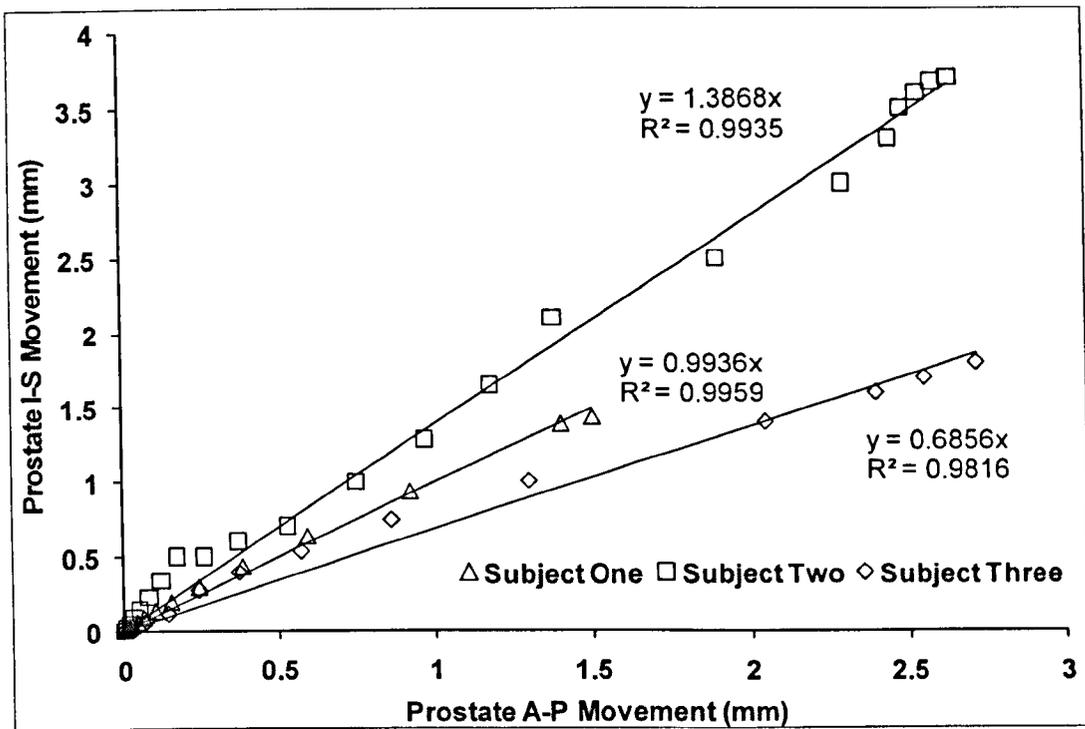
Figure 4.26 Correlation between the AP and IS prostate movement of the three subjects.
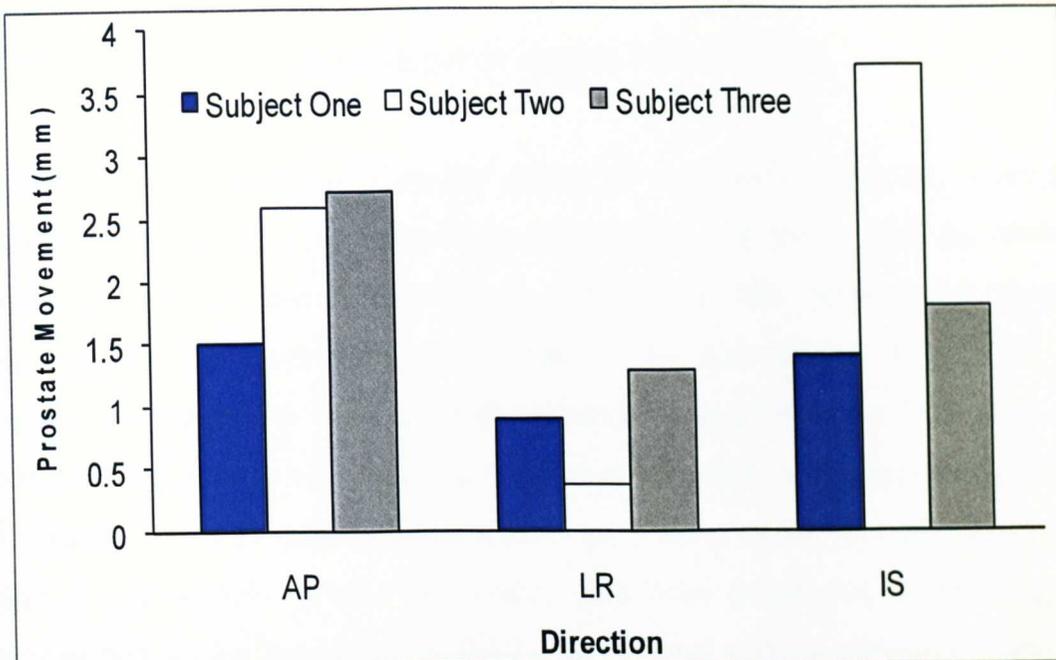
(a) Average transitional movement of the prostate at a 75-100% volume increase.
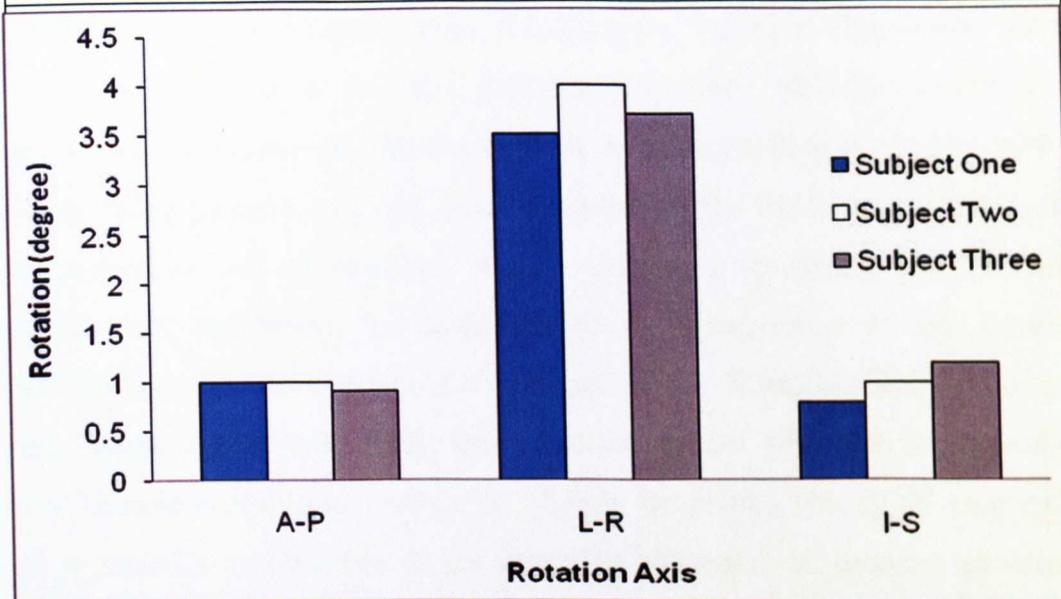
(b) Rotational movement of the prostate at a 100% volume increase

Figure 4.27 (a) Transitional and (b) rotational movement of the prostate (Centre of Mass) at a volume increase of 100% representing the upper limit of the prostate movement.

4.5 Discussion

4.5.1 Comparison of the numerical prediction and clinical data

The deformation of the bladder during filling is a complex process, a detailed understand of this process has significant importance for many medical areas in particular for prostate cancer radiotherapy. This work has developed a detailed numerical model and methodology to establish the deformation of bladder and prostate movements due to bladder filling based on patient specific MRI data. The approach involved a complex imaging process that was used to produce a detailed FE model specific to each patient. As shown in **Figure 4.14**, a new method of constructing full models for the key organs has been developed by merging the images obtained in the transaxial, sagittal, and coronal planes providing important details for the creation of a geometrically accurate model. This approach has resolved the drawbacks due to the incompleteness of images (as shown in **Figure 4.6**) taken at different planes which is an intrinsic problem associated with the nature of the scanning process. As shown in **Figures 4.14 & 4.15**, a detailed procedure with the optimal assembling process, meshing scheme, boundary and loading condition and the materials properties was established, this is important to ensure the FE model represent the real condition. As demonstrated by comparison of the simulated deformed bladder and the repeated CT images of the filled bladder of the same participant **(Figures 4.19 and 4.20)**, the numerical model was able to simulate the process of bladder filling and predict its change in shape. The slight discrepancy observed is probably attributable to the nature of the repeated imaging process for such a complex system; however the margin of error is acceptable for clinical applications. This has laid an important framework for future studies of large group cohorts in clinical conditions.

Due to the limitation on the experimental design direct comparison between the data of movement of the prostate on the subject is not possible. However, the data of the prostate movement showed reasonable agreement with some clinical observations on a similar group of subjects who have gone through the same imaging protocol. As shown in **Figure 3.18**, the maximum displacement of the prostate is in the range of 3–

5 mm. This is in a good agreement of the FE prediction. Similar agreement has been found in some clinical observation based on Gold Seed Studies (Fenwick et al, 2006). In the Gold Seed Study, the displacement of the prostate was monitored by implanting a small gold seed in the prostate. The movement of the prostate was subsequently measured using the gold seed. Four subject preparation protocols in terms of assessing prostate positioning reproducibility were used. The protocols were full bladder, relaxit. Full bladder, no relaxit. Empty bladder relaxit and Empty bladder no relaxit. There were 45 patients that received radical radiotherapy for early prostate cancer. Fortnightly CT scans assessed and provided the data for geometric analysis of rectal control measures and bladder filling. Subjects showed the variation of the prostate, under the conditions used in the FE simulation is in the range of 1.5 mm – 4 mm, which is in close agreement of the work.

Figure 4.28 plots the numerical results from this work in comparison with some published data under similar conditions (Balter et al, 1995; Crook et al, 1995; Lebesque et al, 1995; Roeske et al, 1995; Althof et al, 1996; Stroom et al, 1999; Villeirs et al, 2004; Hoogeman et al, 2005). The scale bar represents the uncertainty with a 20% uncertainty with the bladder materials properties in vivo based on a detailed materials property sensitivity study. Details analysis of the material properties effect is to be presented at the next section **(4.5.2).** Due to the nature of the FE simulation and clinical works, direct comparison between the results of modelling and clinical observation is often difficult. In a radiotherapy process, the major concern is the maximum displacement for setting the treatment margins. As shown in the figure, the predicted prostate movement is well within the range of the published data on the movement of the prostate. Please note the clinical data were obtained with different imaging method (i.e. CT or MRI), which may cause some discrepancy. For example, (Roeske et al, 1995) used CT images to evaluate the changes in the location of the prostate, bladder, and rectum during a course of external beam radiation therapy. Quantification of the CM motion was found to be less than 1 mm in the LR direction, whereas motion that ranged from 0–5 mm was observed in the AP and SI directions. In another study, (Villeirs et al, 2004) used MRI to assess the variability in the location of the prostate during intensity-modulated radiotherapy (IMRT) for prostate

cancer. They measured the position of the prostatic midpoint (PMP) relative to the bony pelvis and found that the greatest variability occurred in the posterior (2.6 mm), superior (2.4 mm), and inferior (1.0 mm) directions. The agreement between the numerical data and clinical data suggests that the modelling is a feasible approach for the prediction of prostate movements during radiotherapy. In current clinical medical practice, the normal margin used could be up to 7 mm which ensures the whole prostate is covered. The results indicate that the current practice is sufficient for the potential variation of prostate position due to bladder filling; however it also suggests that potential reduction of this margin is possible for some patients with the aid of subject specific modelling method. The effect of which will be investigated further with a larger group of cohorts to establish the medical benefits.
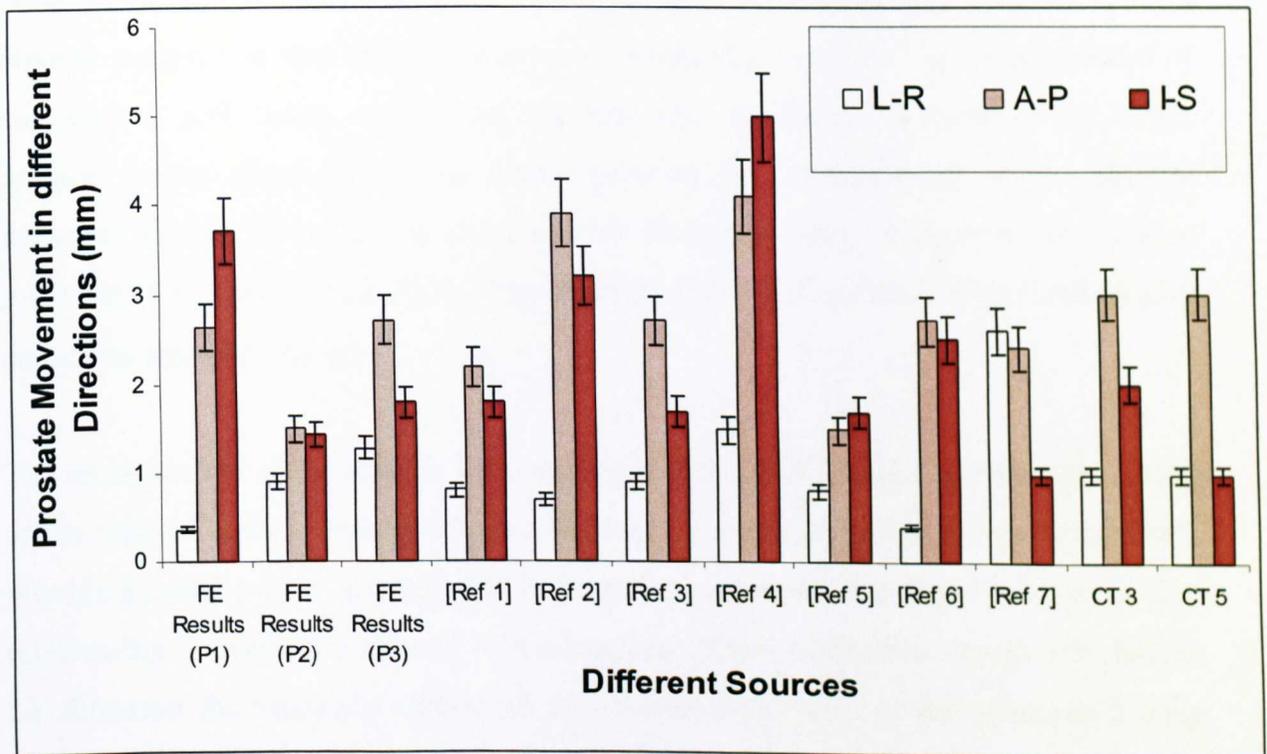
Figure 4.28 Comparison of the results (average over 100% volume change) and the published data. (The error bar of the FE data represents the uncertainty of material change).

Ref [1] Balter *et al*, 1995.
Ref [2] Roeske *et al*, 1995.
Ref [3] Van Herk *et al*, 1995.
Ref [4] Crook *et al*, 1995.
Ref [5] Althof *et al*, 1996.
Ref [6] Stroom *et al*, 1999.
Ref [7] Villeirs *et al*, 2004.

4.5.2 The deformation of the bladder in the filling process

As the bladder fills, it is stretched like a balloon to accommodate a greater volume of urine. This has been mainly characterised qualitatively by clinical observation of the bladder shape and wall movement during the filling process (Roeske *et al*, 1995; Villeirs *et al*, 2004; Kristiansen *et al*, 2004). As shown in **Figure 4.18 & 4.19**, the numerical results showed that the shape of the bladder changed from irregular to a more regular oval shape. This is reflected by the analysis of the aspect of the bladder. As shown **Figure 4.22**, the aspect ratio (ratio between the wall distances at different direction) increases as the bladder volume increases. The shape of the bladder is known to be the main factor to determine the compactness of the bladder that is a dimensionless factor that describes how much the object resembles a circle. From a clinical perspective this shape change can potentially result in the displacement of surrounding soft tissue, which can increase the likelihood of missing the target volume during treatment. It has been observed that compactness of the bladder increases during filling as its cross section becomes more circular as its volume increases (Kristiansen *et al*, 2004). The findings showed that filling of the bladder also caused its shape to change.

The cross-section of the bladder becomes more circular as its volume increases. Most of the clinical studies were qualitative in nature, the numerical model developed will provide a useful tool to quantify this important parameters. The numerically predicted relationship between the volume of the bladder and its dimensions in the AP, SI and LR direction showed good agreement with semi-quantitative observations on a large number of patients that were reported by (Miralbell *et al*, 1998). Due to the uncertainty in the measurements, and the nature of the medical imaging techniques used, it is difficult to make quantitative conclusions using results obtained from only three participants. However, the slope of the data presented here is comparable to that of the clinical data reported by (Miralbell *et al*, 1998). In their work, based on the data obtained from a large group of patients, the slopes obtained from the S-I, A-P, and L-R data were 0.016, 0.01 and 0.009, respectively. This suggests that the FE modelling method described herein could potentially be used to predict the patient specific relationship between bladder dimensions and volume. However, a statistically robust

trial based on the methodology developed in this pilot study and using a much larger group of patients is required. One significant advantage of the FE model is that the modelling bladder deformation is able to capture the changes in volume, bladder shape, and wall movement during different stages of filling. This will offer significant advantages over pure clinical observation, where the bladder can only be measured under a limited number of conditions (e.g. empty, half full, full) (Pinkawa, *et al* 2006).

4.5.3 Use of subject specific FE modelling in radiotherapy during radiotherapy

It has been well documented in clinical works that the bladder filling has significant effect on the movement of the prostate, but it is difficult to be quantified based on pure clinical studies due to the complex structure of the system and the influence of other organs such as the rectum. Analysis of the rectum for the cases selected in this work shows they have a small diameter; this is normally regarded as having less effect on the prostate movements during filling of the bladder. For example, Melian *et al* (1997) showed that there was no significant displacement of the prostate position when 30 cc of rectal contrast was injected. Villeirs *et al* (2004) has studied the effect of rectum volume on the prostate positions and motion of the prostate was only found to occur above a rectal volume of 56.1 ml and the rectum did not significantly affect the prostate position below this critical volume. The rectum volume in the cases of this work is well below these critical values, so it is reasonable to assume that the numerical results presented mainly by the effect of bladder filling.

The numerical results clearly showed that the relationship between the bladder volume and prostate movement could potentially be treated as a two-phased process. In the first phase, with a smaller bladder, the prostate movement is much more profound with increasing bladder volume. Once the volume of the bladder reaches a certain value, the movement of the prostate becomes rather limited (second phase). This finding could have significant implications during clinical medical practise. It provides a direct physical explanation behind the widely observed limit (~5mm as shown in **Figure 4.28**) for prostate movement (Balter *et al*, 1995; Crook *et al*, 1995; Roeske *et al*, 1995; van Herk *et al* 1995; Althof *et al*, 1996; Stroom *et al*, 1999;

Villeirs *et al*, 2004; Hoogeman *et al*, 2005). This finding could be used to establish the optimal initial scanning conditions. There has been much effort to establish the best condition for the initial scan (i.e. whether the scan should be made with an empty or full bladder/rectum). It has been normally agreed that a smaller rectum will be beneficial to stabilise the prostate but no agreement has been made on the effect of the bladder. As shown in **Figures 4.24 and 4.25**, the movement of the prostate became much less significant with increasing bladder volume at the later stage, this indicates that a fuller bladder may potentially minimise the uncertainty of the prostate position due to the bladder filling under the same patient setup. In addition, a fuller state is also preferable to an empty state for keeping small loops outside the radiation field (Villeirs *et al*, 2004). Future work will study this systematically using data obtained from more subjects to establish the influence of these factors and link this directly with the treatment planning program. As shown by the simulation result, there is a clear inter-patient difference in the volume-displacement relationship (**Figure 4.23 – 4.25**) and the relationship of the movement at I-S and A-P directions (**Figure 4.26**). This is probably the reason behind the difficulty in clinical studies to establish direct correlation between the prostate movement and bladder filling based on data from different subjects (Balter *et al* 1995; Melian *et al*, 1997; Stroom *et al*, 1999; Zellars *et al* 2000; Villeirs *et al*, 2004). For the studies in which the patients were scanned in a supine position, Zeller *et al* (2000) observed a significant correlation, while Roeske *et al* (1995) observed a weak correlation between prostate motion and bladder volume changes. This work demonstrated that MRI based FE modelling technique could be used to establish the relationship for each individual patient and provide guideline to improve the estimate of the prostate position or to define a patient specific CTV-to-PTV margin that is optimized to data with the unique characteristics of the treated patient. The gain in geometrical accuracy can either be used to irradiate the prostate to a higher dose, while the risk of complications remains at an acceptable level or to decrease the risk of complications while the target volume dose is not affected (Hoogeman *et al*, 2005). This demonstrate that the technique potentially can be used to obtain more quantitative data of the influence of the filling of the bladder on the position of the prostate or other structures of interest. One future research direction is to directly link this with the treatment planning program based on more subjects' data.

In current clinical medical practice, the normal margin used could be up to 7 mm to ensure that the whole prostate is covered. The results indicate that the current practice is sufficient for the potential variation of prostate position due to bladder filling; however it also suggests that potential reduction of this margin is possible for some patients with the aid of patient specific modelling method. The effect of which will be investigated further with a larger group of cohorts to establish the medical benefits.

4.6 Summary

In this work, 3D FE models of the human pelvic system was developed, using MR images that were specific to each patient, to study the bladder filling process and the interactions between the bladder, prostate, and rectum during bladder filling. A new method of constructing complete models of the key organs has been developed by merging the images obtained in the transaxial, sagittal, and coronal planes to provide important details for the creation of a geometrically accurate model. The overall model of bladder deformation was found to be comparable to repeated CT images of the same subject, thus validated the FE models and the approach used in this work. The optimum mesh and materials were also established based on parametric studies. The relationship between bladder deformation and its volume increase has been established. The numerical results showed that the bladder dimensions increased linearly with its volume and the predicted coefficients is comparable to some published clinical results. The displacement of the prostate of each patient in the AP, SI and LR directions during filling of the bladder was predicted. The results showed that there were clear inter- subject differences in the relationship between the movement of the prostate and the increase in the volume of the bladder. The amount of prostate movement showed good agreement with published clinical data and the analysis of CT data. The work showed that the effect of bladder filling on the prostate movement treatment can be analysed as a two stage process. In the first stage, with a smaller bladder, the prostate movement is much more profound with increasing bladder volume, while the movement of the prostate become rather limited after the bladder volume has reached a critical value in the second stage. This has provided a

146

direct physical explanation for the widely observed upper limit of prostate movement (~5mm) widely reported in clinical studies. Another direct clinical implication of the results showed that initial patient scan based on a fuller bladder would minimise the uncertainty of the prostate position due to variation of the bladder filling. This potentially can be used to establish more quantitative data on the influence of bladder and rectum filling on the prostate positions or other structures of interest

CHAPTER FIVE

CONCLUSIONS AND FUTURE WORKS

5.1 Summary and conclusions

In this work, the variation of the bladder volume/shape and prostate movement during the prostate radiotherapy treatment process has been systematically studied. From this resulting data, a methodology to develop detailed subject specific Finite Element models using MR images to simulate the bladder filling process and its effect on the prostate position has been established. The bladder dimensions were studied based on measurement from Computed Tomography (CT) images of a group of 10 patients with prostate cancer following the same preparation protocol over the course of radiotherapy treatment. The bladder wall distance in the anterior-posterior (AP), superior-inferior (SI) and left-right (LR) directions is measured using scanned images taken on the transaxial, sagittal and coronal planes. The results showed that the dimensional data of the bladder taken from images at the three directions (transaxial, coronal and sagittal) were comparable and consistent. This proved that the multi-orientation scanning approach can be used to develop complete images. The variation of the bladder dimensions, volume and shape were analysed between different arms for the same subject and the upper limit of bladder volume variation were determined. The data showed that, despite all the patients have followed the same preparation protocol before each scan, there are significant variation in the bladder volume during the course of radiotherapy treatment. In most cases, the increase of the bladder wall distance in the superior inferior and anterior posterior direction during bladder filling was much greater than the wall displacement in the left right direction. The volume of the bladder among the subjects studied is ranged between 178000 to 327000 mm^3, 92000 to 189000 mm^3 and 159000 to 315000 mm^3 respectively, and the bladder volume variation is 83, 105 and 98%. These data were comparable with previously published clinical study data. The prostate movement was successfully measured by using the apex of the pubic bone as a point of origin and centre of prostate. The results showed that there is more displacement in the AP and SI direction than the LR direction, the average movement is in the range of 1.5 mm – 2.7 mm, 1.4 mm – 3.7 mm and 0.3 mm – 1.2 mm in the AP, SI and LR direction respectively. Analysis of the relationship between the bladder dimensional change and the

prostate movement showed that both the bladder volume variation and the prostate movement exhibited strong subject dependence that would directly influence on the diagnosis and treatment planning process. These results suggest that it is important to develop subject specific models to reproduce the effect of bladder volume/shape change to be able to accurately predict the prostate position during radiotherapy treatment planning.

Based on the analysis of the variation of the bladder shape and volume during the course of the prostate radiotherapy, a systematic numerical modelling method based on MR images has been developed to simulate the mechanics of bladder filling and its effects on the position of the prostate A new approach for constructing detailed three dimensional (3D) Finite Element (FE) models that were specific to each patient were developed using multiple magnetic resonance (MR) images taken in three different planes (sagittal, transaxial, and coronal). This multi direction scanning approach is able to provide full dimensional data of the bladder that is important for building a complete realistic model and fine tuning of the model by cross comparison of the models between different image sets. Detailed sensitivity studies have been performed on the mesh size, materials models and parameters to establish an optimum modelling scheme balancing the accuracy and the requirement on the computational resources. The overall model of bladder deformation was compared with repeated images of the filled bladder that were obtained using computed tomography (CT) to validate the FE models. The overall model of bladder deformation was found to be comparable to repeated CT images of the same patient, thus validated the FE models and the approach used in this work.

The relationship between bladder deformation and its volume change has been established. The numerical results showed that the bladder dimensions increased linearly with its volume and the predicted coefficients are comparable to some published clinical results. The movement of the prostate in the anterior-posterior (AP), superior-inferior (SI) and left-right (LR) directions, as well as its rotational movement, that was associated with changes in bladder volume was predicted. The

numerical results showed that the movement of the prostate in the AP and SI directions was much greater than that in the LR direction. The scale of the movement of the prostate with the increase in bladder volume varied considerably among subjects.

The work showed that the effect of bladder filling on the prostate movement treatment can be analysed as a two stage process. In the first stage, with a smaller bladder, the prostate movement is much more profound with increasing bladder volume, while the movement of the prostate becomes rather limited after the bladder volume has reached a critical value in the second stage. This has provided a direct physical explanation for the widely observed upper limit (~5mm) of the uncertainty of prostate position based statistic data from clinical studies. Another direct clinical implication of the results showed that initial patient scan based on a fuller bladder would potentially minimise the uncertainty of the prostate position due to variation of the bladder filling. This can be used to establish more quantitative data on the influence of bladder and rectum filling on the prostate positions or other structures of interest. The work showed that subject specific Finite Element modelling could potentially provide crucial guidance for the medical practice on the treatment planning process of the prostate cancer.

5.2 Recommendations for future works

This work has developed a framework for predicting biomechanical changes during bladder filling based on CT and MR images. The analysis of organ motion and the results achieved using Finite Element analysis have laid a solid platform for future works within the following areas:

1. Use the approach to study a greater number of patients which could provide key statistical data to be used for clinical applications whilst treating prostate cancer.

2. Use the approach to accurately recreate geometrically accurate bladder, prostate and rectum phantoms. To be able to study the interactions of the phantoms when simulating bladder volume increase. Material characterisation of the bladder wall using indentation testing will be an important contribution to characterise the bladder material parameters.

3. The methodology developed represents a viable approach which could potentially be adapted for many other biological systems (e.g lung, breast cancer).

4. The work can be used to establish more quantitative data on the influence of bladder and rectum filling, on the prostate positions or other structures of interest. This can be of benefit whilst treating other bladder diseases such as bladder cancer, incontinence, etc, where quantification of bladder size is an important factor due to the reduction of patient bladder capacity.

References

ABAQUS, User's Manual, version 6.4, Hibbitt, Karlsson & Sorensen.Inc.

Abbott D.J., 2009, 'CT Scan, Temporal Bone'. Otolaryngology and Facial Plastic Surgery medline.

Alagna M., 2001, *Everything you need to know about Chemotherapy.* ISBN 0-823-93394-6. The Rosen Publishing Group. New York.

Al-Azab R., Toi A., Lockwood G., Kulkarni G.S., Fleshner N., 2007, 'Prostate Volume Is Strongest Predictor of Cancer Diagnosis at Transrectal Ultrasound-Guided Prostate Biopsy with Prostate-Specific Antigen Values Between 2.0 and 9.0 ng/mL'. Urology. Vol. 69, No 1, pp.103-107.

Alberts B., Johnson A., Lewis J., Raff M., Roberts K., Walter P., 2002, *Molecular Biology of the Cell.* ISBN 0-8153-1619-4. Garland Science. New York and London.

Alberts B., 2004, *Essential Cell Biology.* ISBN 0-8153-3481-8. Taylor Francis. New York.

Alterovitz R., Goldberg K., Pouliot J., 2005, 'Registration of MR prostate images with biomechanical modelling and nonlinear parameter estimation and nonlinear parameter estimation'. Medical Physics. Vol. 33, No 2, pp. 446-453.

Applewhite J.C., Matlaga B.R., McCullough D.L., Hall M.C., 2001, 'Transrectal ultrasound and biopsy in the early diagnosis of prostate cancer'. Cancer Control. Vol. 8, No 2, pp.141-50.

Atkin R.J., Fox N., 1980, *An Introduction to the Theory of Elasticity.* ISBN: 0-582-44283-4. Longman Inc. New York.

Balter J. M., Sandler H. M., Lam K., 1995, 'Measurement of prostate movement over the course of routine radiotherapy using implanted markers'. International Journal Radiation Oncology Biolgical Physics. Vol. 31, No.1, pp. 113-8.

Beyer D.C., 2001, 'The evolving role of prostate brachytherapy'. Cancer Control. Vol.8, No.2, pp.163-70.

Bharatha A., Hirose M., Hata N., 2001, 'Evaluation of Three-Dimensional Finite Element-Based Deformable Registration of Pre- and Intra-Operative Prostate Imaging'. Medical Physics. Vol.28, No.12, pp. 2551-2560.

Blatt A. H., Titus J., Chan L., 2008, ' Ultrasound measurement of bladder wall thickness in the assessment of voiding dysfunction'. Journal of Urology. Vol. 179, No. 6, pp. 2275 – 2279.

Boubaker M., Haboussi M., Ganghoffer J., Aletti P., 2009, 'Finite Element simulation of interactions between pelvic organs: Predictive model of the prostate motion in the context of radiotherapy'. Journal of Biomechanics. Vol.42, No.12, pp. 1862-1868.

Brenner D., Elliston C., 2004, 'Estimated Radiation Risks Potentially Associated with Full-Body CT Screening'. Radiology. pp. 735-738.

Cancer Research UK., 2006, *UK Mortality Rates*, September 2010, http://info.cancerresearchuk.org/cancerstats/mortality/.

Cancer Research UK., 2009, *How many different types of cancer are there?*, September 2010, http://www.cancerhelp.org.uk/about-cancer/cancer-questions/how-many-different-types-of-cancer-are-there.

Carelle N., Piotto E., Pharm. A. B., Germanaud .J., Thuillier A., Khayat D., 2002, 'Changing patient perceptions of the side effects of cancer chemotherapy'. American Cancer Society. Vol. 95, No. 1, pp. 155-163.

Carter T. J., Sermesant M., Cash D. M., Barratt D. C., Tanner C., Hawkes D. J., 2005, 'Application of soft tissue modelling to image-guided surgery'. Medical Engineering & Physics. Vol.27, pp. 893–909.

Cheung J.T., Zhang M., An K. N., 2004, 'Effects of plantar fascia stiffness on the biomechanical responses of the ankle-foot complex'. Clinical Biomechanics. Vol. 19, No.8, pp. 839-46.

Chi K. N., Gleave M. E., Klasa R., 2001, 'A Phase I Dose-finding Study of Combined Treatment with an Antisense Bcl-2 Oligonucleotide (Genasense) and Mitoxantrone in Patients with Metastatic Hormone-refractory Prostate Cancer'. Clinical Cancer Research. Vol.7, pp. 3920 – 3927.

Cilingir A.C., Ucara V., Kazan R., 2007, 'Three-Dimensional Anatomic Finite Element Modelling of Hemi-Arthroplasty of Human Hip Joint'. Trends Biomaterials Artificial. Organs. Vol.21, No.1, pp. 63-72.

Constantinou C., Damaser M., Perkash I., 2002, 'Displacement sequence and elastic properties of anterior prostate/urethral interface during micturition of spinal cord injured men'. Ultrasound in Medicine & Biology. Vol. 28, No. 9, pp. 1157-1163.

Crawford E. D., 2003, 'Epidemiology of prostate cancer'. Urology. Vol. 62, (suppl6A), pp. 3–12.

Crook J. M., Raymond Y., Salhani D., Yang H., Esche B., 1995, 'Prostate motion during standard radiotherapy as assessed by fiducial markers'. Radiotherapy and Oncology. Vol. 37, pp. 35-42.

Crouch J. R., Pizer S. M., Chaney E. L., Hu Y. C., Mageras S., Zaider M., 2007, 'Automated Finite Element Analysis for Deformable Registration of Prostate Images'. Ieee transactions on Medical Imaging. Vol. 26, No. 10, pp. 1-13.

Dahms S.E., Piechota H.J., Dahiya R., Lue T.F., Tanagho E.A., 1998, 'Composition and Biomechanical Properties of the Bladder Acellular Matrix Graft: Comparative Analysis in Rat, Pig and Human'. British Journal of Urology. Vol. 82, pp. 411-419.

Damaser M., Lehman S., 1995, 'The effect of urinary bladder shape on its mechanics during filling'. Journal of Biomechanics. Vol. 28, No. 6, pp. 125-132.

Dehnad H., Nederveen A. J., van der Heide U. A., 2003, 'Clinical feasibility study for the use of implanted gold seeds in the prostate as reliable positioning markers during megavoltage irradiation'. Radiotherapy and Oncology. Vol. 67, pp. 295–302.

Deurloo K. E.I., Steenbakkers J.H.M., Zijp L. J., de Bois J. A., Nowak P.J.C.M., Rasch C.R.N., Van Herk M., 2005, 'Quantification of shape variation of prostate and seminal vesicles during external beam radiotherapy'. International Journal of Radiation Oncology Biology Physics. Vol.61, No.1, pp. 228-238.

Diridollou S., Patat F., Gens F., Vaillant L., Black D., Lagarde J.M., Gall Y., Berson M., 2000, 'In vivo model of the mechanical properties of the human skin under suction'. Skin Research and Technology. Vol.6, pp. 214–221.

Elkut F., Krywonos J., Fenwick J., Jenkinson I., Ren X. J., 2010, 'An Experimental and Numerical Program to Study the Properties of Thin Biological Membranes and Water Filling Process'. IFMBE Proceedings World Congress on Medical Physics and Biomedical Engineering. Vol. 25, No.4, pp. 2178-2180.

Ellis R.J., Kaminsky D.A., 2006, 'Fused Radioimmunoscintigraphy for Treatment Planning'. Reviews in Urology. Vol. 8, No. 1, pp. s11-s19.

Enmark M., Korreman S., Nystrom S., 2006, 'IGRT of prostate cancer; is the margin reduction gained from daily IG time-dependent?'. Acta Oncologica. Vol. 45, No. 7, pp. 907- 914.

Elsner P., Berardesca E., Wilhelm K.P., Maibach H.I., (eds). 2002, Bioengineerinng of the Skin: Skin Biomechanics. ISBN: 0-8493-7521-5. London, CRC Press LLC.

Egorov V., Ayrapetyan S., Sarvazyan A. P., 2006, 'Prostate Mechanical Imaging: 3-D Image Composition and Feature Calculations'. IEEE Trans Medical Imaging. Vol. 25, No.10, pp. 1329–1340.

Fagan M., 1992, *Finite Element Analysis: Theory and Practice*. ISBN: 9780582022478. Prentice-Hall. London.

Fenwick J., Syndikus I., Heaton A., Mayles P., 2006, 'Reduction of Prostate Movements During Radiotherapy'. Clatterbridge Centre of Oncology, UK.

Fink K. G., Hutarew G., Pytel A., Esterbauer B., Jungwirth A., Dietze O., Schmeller N. T., 2003, 'One 10-core prostate biopsy is superior to two sets of sextant prostate biopsies'. BJU International. Vol. 92, No. 4, pp. 385–388.

Firat M., 2007, 'Computer aided analysis and design of sheet metal forming processes: Part I – The Finite Element modeling concepts'. Materials and Design. Vol. 28, pp. 1298–1303.

Fu K. K., Pajak T. F., Trotti A., Jones C. U., Spencer S. A., Phillips T. L., Ridge J. A., Cooper J. S, Ang K. K., 2000, 'A radiation therapy oncology group (RTOG) phase III randomized study to compare hyperfractionation and two variants of accelerated fractionation to standard fractionation radiotherapy for head and neck squamous cell carcinomas: first report of RTOG 9003'.International Journal of Radiation Oncology Biology Physics.Vol. 48, No.1, pp. 7-16.

Fuller C.D., Scarbrough T. J., 2006, 'Fiducial Markers in Image-guided Radiotherapy of the Prostate'. US Oncological Disease.

Galvin J. M., 2006, 'Alternative Methods for Intensity-Modulated Radiation Therapy Inverse Planning and Dose Delivery'. Seminars in Radiation Oncology. Vol.16, pp. 218-223.

Gamble G., Simmons C., Freedman M., 1986, 'The Symphysis Pubis: Anatomic and Pathological Considerations and Feature Calculations'. IEEE Trans Medical Imaging. Vol.25, No. 10, pp. 1329 – 1340.

Ganz E.L., Shabshin N., Itzchak Y., Gefen A., 2006, 'Assessment of mechanical conditions in sub-dermal tissues during sitting: A combined experimental-MRI and Finite Element approach'. Journal of Biomechanics. Vol. 40, No. 7, pp. 1443-1454.

Gerber D. E., Chan T., 2008, 'Recent Advances in Radiation Therapy'. American Family Physician. Vol. 78, No. 11, pp. 1254-1262.

Grimm P., Heaney C., Sylvester J., Blasko J., 2003, 'Prostate Seed Implantation for Prostate Cancer PCRI Insights'. Vol. 6, No.4.

Grönberg H., 2003, 'Prostate cancer epidemiology'. The Lancet. Vol.361, No. 9360,pp.859-864.

Gu Y. D., Ren X. J., Li J. S., Lake M. J., Zhang Q. Y., Zeng Y. J., 2010, 'Computer simulation of stress distribution in the metatarsals at different inversion landing angles using the Finite Element method'. International Orthopaedics. Vol. 34, No. 5, pp. 669-676.

Haberstroh K. M., Kaefer M., Retik A., Freeman M.R., Bizios R., 1999, 'The Effects of Sustained Hydrostatic Pressure on Select Bladder Smooth Muscle Cell Functions'. The Journal of Urology. Vol.162, No. 6, pp. 2114-2118.

Hamidian H., Soltanian-Zadeh H., Faraji-Dana R., Gity M., 2010, 'Data-guide for brain deformation in surgery: comparison of linear and nonlinear models'. BioMedical Engineering OnLine. Vol. 9, No. 51, pp. 1-19.

Hardman A.E., Stensel D.J., 2003, 'Physical Activity and Health: the evidence explained'. Routledge. pp.149.

Hellerstedt B., Pienta K., 2002, 'The Current State of Hormonal Therapy for Prostate Cancer'. A Cancer Journal for Clinicians. Vol. 52, No. 3, pp. 154 – 179.

Hensel J., Menard C., Chung P., Milosevic F., Kirilova A., Moseley J., Haider A., Brock K., 2007, 'Development of multi organ Finite Element- based prostate deformation model enabling registration of endorectal coil magnetic resonance imaging for radiotherapy planning'. International Journal of Radiation Oncology Biology Physics. Vol. 68, pp. 1522–1528.

Hedriana H.L., Moore T.R., 1994, 'Ultrasonographic evaluation of human fetal urinary flow rate: accuracy limits of bladder volume estimations.' American Journal Obstet Gynecol. Vol. 170, No. 5, pp. 1250 – 1254.

Hing J.T., Brooks A.D., Desai J.P., 2006, 'Reality-based needle insertion simulation for haptic feedback in prostate brachytherapy'. ICRA 2006 Proceedings 2006 IEEE International Conference on Robotics and Automation. Vol.15, No.19, pp. 619 – 624.

Hoogeman M., van Herk M., de Bois J., Lebesque J., 2005, 'Strategies to reduce the systematic error due to tumor and rectum motion in radiotherapy of prostate cancer'. Radiotherapy and Oncology. Vol. 74, No. 2, pp. 177-185.

Horwitz E., Hanks G., 2000, 'External Beam Radiation Therapy for Prostate Cancer'. A Cancer Journal for Clinicians. Vol. 50, No. 6, pp. 349-375.

Jaillet F., Amrani M., Beuve M., Shariat B., 2004, 'Tracking of target motion using physically based modelling of organs'. Radiotherapy and Oncology. Vol. 73, No. 2, pp. S73-S76.

Jiang S., 2006, 'Radiotherapy of Mobile Tumors'. Seminar Radiation Oncology. Vol.16, pp. 239-248.

Keeve E., Girod S., Pfeifle P., Girod B., 1996, 'Anatomy-Based Facial Tissue Modeling Using the Finite Element Method'. Proceedings of the 7th conference on Visualization '96. IEEE Computer Society Press. pp. 21-31.

Kemper J., Sinkus R., Lorenzen J., Nolte – Ernsting C., Stork A., Adam G., 2004, 'MR Elastography of the Prostate: Initial in-vivo application'. Rofo. Vol.176, No.8, pp. 1094-1099.

Knight L.R., Smeathers J.E., Isdale A.H., Helliwell P.S., 2001, 'Evaluating the cutaneous involvement in scleroderma: torsional stiffness revisited'. Rheumatology. Vol.40, pp. 128-132.

Korkmaz I., Rogg B., 2007, 'A simple fluid-mechanical model for the prediction of the stress–strain relation of the male urinary bladder'. Journal of Biomechanics. Vol. 40, pp. 663-668.

Korossis S., Bolland F., Ingham E., Fisher J., Kearney J., Southgate J., 2006, 'Review: Tissue Engineering of the Urinary Bladder: Considering Structure-Function Relationships and the Role of Mechanotransduction'. Tissue Engineering. Vol.12, No. 4, pp. 635-644.

Kristiansen N., Ringgaard S., Nygaard H., Djurhuus J., 2004, 'Effect of Bladder volume, gender and body position on the shape and position of the urinary bladder'. Scandinavian Journal of Urology and Nephrology. Vol. 38, No.6, pp. 462-468.

Kumar R. J., Barqawi A., Crawford E. D., 2005, 'Preventing and treating the complications of hormone therapy'. Current Urology Reports. Vol.6, No.3, pp. 217-223.

Laforet J., Azevedo-Coste C., Andreu, D., Guiraud D., 2010, 'Modeling and simulation of bladder artificial control'. Biomedical Robotics and Biomechatronics (BioRob), 2010 3rd IEEE RAS and EMBS International Conference. No 26 -29, pp. 265 – 269.

Langen K., Pouliot J., Anezinos C., Aubin M., Gottschalk A., Hsu I., Lowther D., Liu Y., Shinohara L., Verhey K., 2003, 'Evaluation of ultrasound-based prostate localization for image-guided radiotherapy'. International Journal of Radiation Oncology Biology Physics. Vol. 57, No. 3, pp. 635-644.

Lebesque J., Bruce M., Kroes G., Touw A., Shouman T., Van Herk M., 1995, 'Variation in volumes, dose-volume histograms, and estimated normal tissue complication probabilities of rectum and bladder during conformal radiotherapy of T3 prostate cancer'. International Journal of Radiation Oncology, Biology, Physics. Vol. 33, No. 5, pp. 1109-1119.

Lee H., Lin M., Foskey M., 2008, 'Physically-Based Validation of Deformable Medical Image Registration'. Medical Image Computing and Computer-Assisted Intervention – MICCAI 2008. Springer Berlin / Heidelberg. Vol. 5242, No. 2008, pp. 830-838.

Lehman C. D., Gatsonis C., Kuhl C. K., Hendrick R. E., Pisano E. D., Hanna L., Peacock S., Smazal S. F., Maki D. D., Julian T. B., DePeri E. R., Bluemke D. A., Schnall M. D., 2007,'MRI Evaluation of the Contralateral Breast in Women with Recently Diagnosed Breast Cancer'. The New England Journal of Medicine. Vol. 356, pp. 1295-1303.

Liang P., Averboukh L., Keyomarsi K., Sager R., Pardee A., 1992, 'Differential Display and Cloning of Messenger RNAs from Human Breast Cancer versus Mammary Epithelial CeUs'. Cancer Research. Vol. 52, pp. 6966-6968.

Ling C., Yorke E., Fuks Z., 2006, 'From IMRT to IGRT: Frontierland or Neverland?' Radiotherapy and Oncology. Vol. 78, No. 2, pp. 119-122.

Lotz H.T., van Herk M., Betgen A., Pos F., Lebesque J.V., Remeijer P., 2005, 'Reproducibility of the bladder shape and bladder shape changes during filling'. Medical Physics. Vol. 32, No.8, pp. 2590 – 2597.

Madsen B., Berit L., Hsi A., Pham H., Presser J., Esagui L., Corman J., Myers L., Jones D., 2003, 'Interfractional stability of the prostate using a stereotactic radiotherapy technique'. International Journal Radiation Oncology Biology Physics. Vol. 57, No. 5, pp. 1285–1291.

Malone S., Crook J., Kendal W., Zanto J., 2000, 'Respiratory-induced prostate motion: quantification and characterization'. International Journal of Radiation Oncology Biology Physics. Vol. 48, No. 1, pp. 105-109.

Marchal M., Promayon E., Troccaz J., 2005, 'Simulating Complex Organ Interactions: Evaluation of a Soft Tissue Discrete Model'. Proceedings of International Symposium on Visual Computing. Lecture Notes in Computer Science. Vol. 38, No. 4, pp. 175-182.

Mattei C.P., Zahouani H., 2004, 'Study of adhesion forces and mechanical properties of human skin in vivo'. Journal of Adhesion Science and Technology. Vol.18, No.15-16, pp. 1739-1758.

Meier U., Lopez O., Monserrat C., Juan M., Alcaniz M., 2005, 'Real-time deformable models for surgery simulation: a survey'. Computer Methods and Programs in Biomedicine. Vol. 77, pp. 183-19.

Meijer G., Rasch C., Remeijer P., Lebesque J., 2003, 'Three-dimensional analysis of delineation errors, setup errors, and organ motion during radiotherapy of bladder cancer'. International Journal of Radiation Oncology Biology Physics. Vol. 55, No. 5, pp. 1277-1287.

Melian E., Mageras G., Fuks Z., Leibel S., Niehaus A., Zelefsky M., Baldwin B., Kutcher G., 1997, 'Variation in prostate position quantitation and implications for three-dimensional conformal treatment planning'. International Journal of Radiation Oncology Biology Physics. Vol. 38, No. 1, pp. 73-81.

Mills N.J., Fitzgerald C., Gilchrist A., Verdejo R., 2003, 'Polymer foams for personal protection: cushions, shoes and helmets'. Composites Science and Technology. Vol.63, pp. 2389–2400.

Mills N., Zhu H., 1999, 'The high strain compression of closed cell polymer foam'. Journal of the Mechanics and Physics of Solids. Vol.47, pp. 669-695.

Miralbell R., Nouet P., Rouzaud M., 1998, 'Radiotherapy of bladder cancer: relevance of bladder volume changes in planning boost treatment'. International Journal of Radiation Oncology Biology Physics. Vol. 41, No. 4, pp. 741-746.

Misra S., Macura K., Ramesh K., Okamura A., 2009, 'The importance of organ geometry and boundary constraints for planning of medical interventions'. Medical Engineering & Physics. Vol. 31, No 2, pp. 195-206.

Mohamed A., Davatzikos C., Taylor R., 2002, 'A combined statistical and biomechanical model for estimation of intra-operative prostate deformation'. In: MICCAI 2002 Proceedings. pp. 452–460.

Mooney M., 1940, 'A theory of large elastic deformation'. Journal of Applied Physics. Vol. 11, No. 9, pp. 582.

Moran M., Elshaikh A., Lawrence S., 2005, 'Radiotherapy: what can be achieved by technical improvements in dose delivery?'. Lancet Oncology. Vol. 6, No. 1, pp. 51-58.

Moreu Y. M., Mills N.J., 2004, 'Test Method-Rapid hydrostatic compression of low density polymeric foams'. Polymer Testing. Vol.23, pp. 313-322.

Muren L., Smaaland R., Dahl O., 2003, 'Organ motion, set-up variation and treatment margins in radical radiotherapy of urinary bladder cancer'. Radiotherapy and Oncology. Vol. 69, No. 3, pp. 291-304.

Netter F.H., 2006, *Atlas of human anatomy.* 4th ed. Philadelphia, USA: W.B. Saunders Company.

Nielsen O., Munro A.J., Tannock I. F., 1991, 'Bone metastases: Pathophysiology and management policy'. Journal of Clinical Oncology. Vol. 9, pp. 509-524.

O'Connell M. J., Martenson J. A., Wieand H. S., Krook J. E., Macdonald J. S., Haller D. G., Mayer R. J., Gunderson L. L., Rich T. A., 1994, 'Improving Adjuvant Therapy for Rectal Cancer by Combining Protracted-Infusion Fluorouracil with Radiation Therapy after Curative Surgery'. New England Journal of Medicine. Vol. 331, pp. 502-507.

O'Doherty U., McNair H., Norman A., Miles E., Hooper S., Davies M., Lincoln N., Balyckyi J., Childs ., Dearnaley D., Huddart R., 2006, 'Variability of bladder filling in patients receiving radical radiotherapy to the prostate'. Radiotherapy and Oncology. Vol. 79, pp. 335–340.

Ogden R.W., 1972b, 'Large deformation isotropic elasticity-on the correlation of theory and experiment for compressible rubberlike solids'. Proceedings of the Royal Society Lond. Vol.A328, pp. 567-83.

Papademetris X., Shi P., Dione D. P., Sinusas A. J., Constable R. T., Duncan J. S., 1999, 'Recovery of Soft Tissue Object Deformation from 3D Image Sequences Using Biomechanical Models'. Lecture Notes in Computer Science. Vol. 1613/1999, pp. 352-357.

Pathmanathan P., Gavaghan D., Whiteley J., Brady M., Nash M., Nielsen P., Rajagopal V., 2004, 'Predicting Tumour Location by Simulating Large Deformations of the Breast Using a 3D Finite Element Model and Nonlinear Elasticity'. Medical Image Computing and Computer-Assisted Intervention Lecture Notes in Computer Science. Vol. 3217, No.2004, pp. 217-224.

Paulsen K. D., Miga M. I., Kennedy F. E., Hoopes P. J., Hartov A., Roberts D. W., 1999, 'A Computational Model for Tracking Subsurface Tissue Deformation During Stereotactic Neurosurgery'. Ieee Transactions on Biomedical Engineering. Vol.46, No. 2, pp. 213-255.

Petre M.T., Erdemir A., Cavanagh P.R., 2007, 'Determination of elastomeric foam parameters for simulations of complex loading'. Computer Methods in Biomechanics and Biomedical Engineering. Vol.9, No.4, pp. 231-242.

Pinkawa M., Asadpour B., Gagel B., Piroth M.D., Holy R., Eble M.J., 2006, 'Prostate position variability and dose-volume histograms in radiotherapy for prostate cancer with full and empty bladder'. International Journal of Radiation Oncology Biology Physics. Vol.64, No. 3, pp. 856-61.

Pinkawa M., Asadpour B., Siluschek J., 2007, 'Bladder extension variability during pevic external beam radiotherapy with a full or empty bladder'. Radiotherapy and Oncology. Vol. 83, pp. 163-167.

Podder T., Clark D., Sherman J., Fuller D., Brasacchio R., 2006, '*In vivo* motion and force measurement of surgical needle intervention during prostate brachytherapy'. Medical Physics. Vol. 33, No 8, pp. 2915- 2923.

Poggi M. M., Gant D. A., Sewchand W., Warlick W. B., 2003, 'Marker seed migration in prostate localization'. International Journal of Radiation Oncology Biology Physics. Vol. 56, No.5, pp. 1248-1251.

Ragaz J,. Jackson S. M., Le N., Plenderleith I. H., Spinelli J. J., Basco V. E., Wilson K. S., Knowling M. A., Coppin C. M., Paradis M., Coldman A. J., Olivotto I. A., 1997, 'Adjuvant Radiotherapy and Chemotherapy in Node-Positive Premenopausal Women with Breast Cancer'. The New England Journal of Medicine. Vol. 337, pp. 956-962.

Roeske J. C., Forman J. D., Mesina C. F., 1995, 'Evaluation of changes in the size and location of the prostate, seminal vesicles, bladder and rectum during a course of external beam radiation therapy'. International Journal of Radiation Oncology Biology Physics. Vol. 33, No. 5, pp. 1321-1329.

Saad F., Clarke N., Colombel M., 2006, 'Natural History and Treatment of Bone Complications in Prostate Cancer'. European Urology. Vol.49, No. 3, pp. 429 – 440.

Seiwert T. Y., Salama J. K., Everett E., Vokes E. E., 2007, 'The concurrent chemoradiation paradigm general principles'. Nature Clinical Practice Oncology. Vol.4, pp. 86-100.

Shepard D. M., Ferris M. C., Olivera G. H., Mackie T. R., 1999, ' Optimizing the Delivery of Radiation Therapy to Cancer Patients'. Society for Industrial and Applied Mathematics. Vol. 41, No. 4, pp. 721–744.

Sikora K., Hynd S., Pettingell J., 2009, 'Precision radiotherapy: A guide to commissioning IMRT and IGRT'. Journal of Management & Marketing in Healthcare. Vol. 2, No. 4, pp. 401–409.

Stollman N., Raskin P. J. B., 2004, 'Diverticular disease of the colon'. The Lancet. Vol. 363, No.9409, pp. 631-639.

Stroom J., Koper M., Korevaaar G., 1999, 'Internal organ motion in prostate cancer patients treated in prone and supine treatment position'. Radiotherapy and Oncology. Vol.51, No. 3, pp. 237-248.

Theodorescu D., 2004, 'Cancer Cryotherapy: Evolution and Biology'. Reviews in Urology. Vol. 6, No. 4, pp. S9–S19.

Tsai C. L., Wu . K., Wang C.W., Hsu F.M., Lai M.K., Cheng C. H., 2009, 'Using Cone-Beam Computed Tomography to Evaluate the Impact of Bladder Filling Status on Target Position in Prostate Radiotherapy'. Strahlentherapie und Onkologie .Vol.185, No. 9, pp. 588-595.

Tsap L.V., Goldof D.B., Sarkar S., 2000, 'Nonrigid motion analysis based on dynamic refinement of Finite Element models'. Pattern Analysis and Machine Intelligence. Vol. 22, No.5, pp. 526-543.

van Herk M., Bruce A., Kroes A., Shouman T., Touw A., Lebesque J., 1995, 'Quantification of organ motion during conformal radiotherapy of the prostate by three dimensional image registration'. International Journal Radiation Oncology Biology Physics. Vol.33, No.5, pp. 1311-1320.

Vannah W.M., Childress D.S., 1996, 'Indenter tests and Finite Element modeling of bulk muscular tissue *in vivo*'. Journal of Rehabilitation Research and Development. Vol.33 No. 3, pp. 239-252.

Vescovo P., Varchon D., Humbert P., 2002, 'In vivo tensile tests on human skin: the extensometers'. in *Bioengineering of the Skin: Skin* Biomechanics. (Elsner, P., Berardesca E., Wilhelm K.P. Maibach H. I., eds) London, CRS Press LLC.

Villeirs G. M., Meerleer G., Verstraete K., Neve W., 2004, 'Magnetic resonance assessment of prostate localization variability in intensity-modulated radiotherapy for prostate cancer'. International Journal of Radiation Oncology Biology Physics. Vol.60, No. 5, pp. 1611-1621.

Watanabe T., Omata S., Lee J., Constantinou C., 1997, 'Comparative Analysis of Bladder Wall Compliance Based on Cystometry and Biosensor Measurements During the Micturition Cycle of the Rat'. Neurourology and Urodynamics. Vol.16, pp. 567–581.

Weiss J.A., Gardiner J.C., 2001, 'Computational Modeling of Ligament Mechanics'. Critical Reviews in Biomedical Engineering. Vol.29, No. 4, pp. 1-70.

Welsh J., Berta C., Borzillary S., Sam C., Shickell D., Nobile L., Greenberg M., Weiss S., Detorie N., 2004, 'Fiducial markers implanted during prostate brachytherapy for guiding conformal external beam radiation therapy'. Technol Cancer Res Treat. Vol. 3, No. 4, pp. 359-64.

Yuen, J., Ngiap J., Cheng C., Foo K., 2002, 'Effects of bladder volume on transabdominal ultrasound measurements of intravesical prostatic protrusion and volume'. International Jounral of Urology. Vol.9, No. 4, pp. 225-299.

Zelefsky M. J., Fuks Z., Hunt M., Yamada Y., Marion C., Ling C., Amols H., Venkatraman E. S., Leibel S. A., 2002, 'High-dose intensity modulated radiation therapy for prostate cancer: early toxicity and biochemical outcome in 772 patients' .International Journal of Radiation Oncology Biology Physics. Vol. 53, No. 5, pp. 1111-1116.

Zellars R.C., Roberson P.L., Strawderman M., Zhang D., Sandler H.M., Ten Haken R.K., Osher D., McLaughlin P.W., 2000, 'Prostate position late in the course of external beam therapy: patterns and predictors'. International Journal of Radiation Oncology Biology Physics Vol.47, No. 3, pp. 655-60.

Zhang M., Castaned B., Wu Z., Nigwekar P., Joseph J. V., Rubens D. J., Parker., 2007,'Congruence of Imaging Estimators and Mechanical Measurements of Viscoelastic Properties of Soft Tissues'. Ultrasound Med Biol.Vol.33, No.10, pp. 1617-1631.

Publications List

Krywonos J., Fenwick J., Elkut F., Jenkinson I., Liu Y. H., Brunt J. N. H., Scott A., Malik Z., Eswar C., Ren X. J., 2010, 'MRI image-based FE modelling of the pelvis system and bladder filling'. Computer Methods in Biomechanics and Biomedical Engineering. Vol. 13, No. 6, pp 669 – 676.

Krywonos J., Elkut F., Brunt J. N. H., Malik Z., Eswar C., Fenwick J., Ren X. J., 2009, 'Numerical Study of Effects of Bladder Filling on Prostate Positioning In Radiotherapy'. 4th European Conference of the International Federation for Medical and Biological Engineering IFMBE Proceedings. Vol 22, No. 22, pp 2655-2658.

Elkut F., Krywonos J., Fenwick J., Jenkinson I., Ren X. J., (abstract), 2009, 'An experimental and numerical program to study the properties of thin biological membranes and Water filling process'. Medical Engineering Conference, Germany.

Brunt J.N., Krywonos J., Elkut F., Malik Z., Eswar C., Fenwick J., Ren X.J, 2009, MRI-derived computational modelling of bladder filling mechanics to investigate prostate displacement effects relevant to radiotherapy. The British Institute of Radiology. UK Radiological Congress. pp 25.